Forschungszentrum Karlsruhe
in der Helmholtz-Gemeinschaft

Wissenschaftliche Berichte

FZKA 7448

Behavior of AgInCd Absorber Material in Zry/UO_2 Fuel Rod Simulator Bundles Tested at High Temperatures in the CORA Facility

L. Sepold, S. Hagen, P. Hofmann, G. Schanz

Institut für Materialforschung
Programm Nukleare Sicherheitsforschung

Januar 2009

Forschungszentrum Karlsruhe

in der Helmholtz-Gemeinschaft

Wissenschaftliche Berichte

FZKA 7448

Behavior of AgInCd Absorber Material in Zry/UO_2 Fuel Rod Simulator Bundles Tested at High Temperatures in the CORA Facility

L. Sepold, S. Hagen, P. Hofmann, G. Schanz

Institut für Materialforschung
Programm Nukleare Sicherheitsforschung

Forschungszentrum Karlsruhe GmbH, Karlsruhe

2008

Note: This document was prepared in 1994 for publication as KfK report 4419 but was not released then. Due to timeliness of the topics and in context with the follow-up research program “QUENCH” it is published in 2008 as report FZKA 7448.

Für diesen Bericht behalten wir uns alle Rechte vor

Forschungszentrum Karlsruhe GmbH
Postfach 3640, 76021 Karlsruhe

Mitglied der Hermann von Helmholtz-Gemeinschaft
Deutscher Forschungszentren (HGF)

ISSN 0947-8620

urn:nbn:de:0005-074489

Abstract

The CORA experiments carried out in an out-of-pile facility at the Kernforschungszentrum Karlsruhe (KfK), Federal Republic of Germany, are part of the "Severe Fuel Damage" (SFD) program.

The experimental program is to provide information on the failure mechanisms of Light Water Reactor (LWR) fuel elements in a temperature range from 1200°C to 2000°C and in a few cases up to 2400°C.

In the CORA experiments two different bundle configurations are tested: PWR (Pressurized Water Reactor) and BWR (Boiling Water Reactor) bundles. The PWR-type assemblies usually consist of 25 rods with 16 electrically heated fuel rod simulators and nine unheated rods (full-pellet and absorber rods). Bundle CORA-5 contained one Ag/In/Cd - steel absorber rod whereas two absorber rods were used in CORA-12, CORA-15, and CORA-9. The larger bundle CORA-7 contained 5 absorber rods. CORA-12 was terminated by quenching with water from the bottom. In CORA-15 the heated and unheated rods were pressurized to achieve pronounced clad ballooning. Bundle CORA-9 was tested with a system pressure of 1.0 MPa instead of 0.22 MPa.

The test bundles were subjected to temperature transients of a slow heatup rate in a steam environment. Thus, an accident sequence is simulated, which may develop from a small-break loss-of-coolant accident of a LWR.

The transient phases of the tests were initiated with a temperature ramp rate of 1 K/s. The temperature escalation due to the exothermal zircaloy (Zry)-steam reaction started at about 1100°C, leading the bundles to maximum temperatures of approximately 2000°C.

Rod destruction started with the failure of the absorber rod cladding at about 1200°C, i. e. about 250 K below the melting regime of steel. Penetration of the steel cladding was presumably caused by a eutectic interaction between steel and the zircaloy guide tube.

The test bundles resulted in severe oxidation and partial melting of the cladding, fuel dissolution by Zry/UO_2 interaction, complete Inconel spacer destruction, and

relocation of melts and fragments to lower elevations in the bundle, where extended blockages have formed.

There was no difference in the behavior of the large bundle CORA-7 compared to the test bundles of regular size.

Verhalten von Ag/In/Cd - Absorbermaterial in Zirkaloy/UO2 -Brennstäben bei hohen Temperaturen
(Nachuntersuchungsergebnisse der Experimente CORA-5, -12, -15, -9 u. CORA-7)

Kurzfassung

Die CORA-Experimente, die in einer Out-of-pile Versuchsanlage des Kernforschungszentrums Karlsruhe (KfK) durchgeführt werden, sind Teil des sog. Severe-Fuel-Damage-Programms (SFD) zur Untersuchung schwerer Kernschäden in Leichtwasserreaktoren (LWR).

Mit Hilfe der CORA-Versuche sollen die Versagensmechanismen von LWR-Brennelementen im Temperaturbereich bis 2000°C und in einigen Fällen bis 2400°C ermittelt werden.

In diesen Versuchen werden zwei unterschiedliche Typen von Brennstabbündeln getestet: DWR (Druckwasserreaktor)- und SWR (Siedewasserreaktor)-Bündel. Die DWR-Bündel bestehen aus 25 Stäben, davon sind 16 elektrisch beheizte Brennstabsimulatoren. Der Rest setzt sich aus unbeheizten Stäben und aus Ag/In/Cd - Absorberstäben mit Stahlhülle zusammen. In Test CORA-5 war ein Absorberstab, in den Bündeln CORA-12, CORA-15 und CORA-9 waren zwei Absorberstäbe, im Bündel CORA-7 waren fünf Absorberstäbe eingesetzt. Die Testbündel waren Temperaturtransienten mit langsamer Aufheizrate und in Dampfatmosphäre ausgesetzt. Damit wird ein Unfallablauf für einen LWR simuliert, der sich aus einem Kühlmittelverluststörfall durch Auftreten eines sogenannten kleinen Lecks entwickeln kann.

Die anfänglichen Aufheizraten für alle Versuche betrugen wie geplant 1 K/s, bis die Temperatureskalation aufgrund der exothermen Zircaloy (Zry)-Wasserdampf-reaktion ab ca. 1100°C einsetzte. Die Höchsttemperaturen betrugen 2000°C.

In beiden Versuchen begann die Stabzerstörung mit dem Versagen der Absorberstabhülle bei etwa 1200°C, d. h. etwa 250 K unterhalb des Schmelz-bereichs von Stahl. Die Stahlhülle wurde vermutlich durch den Kontakt mit dem Zry-Führungsrohr (eutektische Wechselwirkung zwischen Stahl und Zirkaloy) beschädigt.

Nach den Versuchen zeigten die Versuchsbündel starke Oxidation und teilweises Schmelzen des Hüllmaterials, chemische Auflösung von Brennstoff durch die Wechselwirkung Zry/UO_2, vollständige Zerstörung des Inconel Abstandshalters sowie Umverlagerung von Schmelzmassen und Bruchstücken in den unteren Teil des Bündels unter Bildung ausgedehnter Blockaden.

Inhaltsverzeichnis

1. Introduction

Safety studies have demonstrated that so-called small break loss-of-coolant accidents in Light-Water Reactors (LWR), in combination with failure of the required safety systems, can lead to overheating of the core and thus result in severe fuel damage (SFD) and fission product release.

In such an accident the nuclear fuel rods may be subjected to temperatures beyond the present design basis accident limit of 1200°C. The temperature transient, however, will not necessarily escalate to an uncontrolled core meltdown accident, as was learned from the TMI accident in 1979.

The transient of a SFD-type accident is initiated by a slow temperature rise in the order of 0.5 - 1.0 K/s, followed by a rapid temperature escalation (several tens of degrees Kelvin per second) due to the exothermal heat produced by the cladding oxidation in steam environment. Besides oxidation and embrittlement of the fuel rod cladding, local melting of the cladding and an interaction between molten zircaloy and uranium oxide pellets will occur, leading to destruction of fuel rod elements and other core structure far below the melting point of the fuel. The concern with melting of fuel rod materials in a SFD accident is relocation, solidification, and therefore the formation of coolant channel blockages.

To investigate the relevant damage mechanisms acting with increasing temperature on an uncovered core, and to develop models for estimating core damage initiation and propagation, research programs have been defined in various countries. In these programs in-pile and out-of-pile experiments are being performed under severe fuel damage conditions, i.e. temperature escalation to about 2000°C with termination of the transient before complete core meltdown.

At the Kernforschungszentrum Karlsruhe (KfK) a series of out-of-pile experiments on SFD research is being performed in the CORA facility. The entire experimental program is provided with Table 1 (CORA test matrix). All CORA experiments are performed with UO_2 as pellet material and with absorber material (except for CORA-2 and -3 /2/). Two different absorber materials are used within different bundle configurations, i.e. (Ag, In, Cd) rods are to PWR (Pressurized Water Reactor) conditions whereas boron carbide refers to the experiments simulating BWR (Boiling Water Reactor) fuel elements. Pellets, claddings, and grid spacers

are typical for those of commercial PWRs with respect to their chemical compositions and dimensions.

This report describes the results of the first SFD experiments designated CORA-5, CORA-12, CORA-15, CORA-9, and CORA-7.

2. Test Description

2.1 Description of the Test Facility

A detailed description of the CORA facility is given in reference /1/. In the axial cross section of Figure 1 the main components of the CORA facility are shown schematically. The test bundle is surrounded by a high-temperature shield which is insulated by ZrO_2 and Al_2O_3/SiO_2 fiber ceramics (Fig. 2). The fiber ceramics are proven to be excellent insulators with a low heat capacity due to the low density of the material.

The high-temperature shield is located within the pressure tube. Through a number of holes in the shield, the test bundle is being inspected during the test by several video and still cameras. The holes are also used for temperature measurements by two-color pyrometers complementing the thermocouple readings at elevated temperatures.

Steam generator and steam superheater are placed inside the CORA containment. Using the total electric power of the steam generator, a maximum steam temperature of more than 800°C can be reached. The maximum steam flow rate amounts to 33 g/s. A typical temperature history of the gas exiting the steam superheater and entering the test section is provided with Fig. 4.

Two different condensers are installed in the CORA facility: A vent condenser and a surge condenser. Under normal operating conditions the steam which is not consumed by oxidation of the bundle, is condensed in two vent condenser units. The surge condenser is physically separated from the high pressure system by four rupture disks. In case of emergency, e.g. due to an extremely high evaporation rate caused by quenching of the bundle, the void volume of the surge condenser serves as a pressure suppression system.

The condensate from the vent condensers and -in the case of emergency- the excess spray water of the surge condenser are collected in the condensate tank. After each test the amount of water in the condensate tank is determined to perform a water mass balance.

To avoid any hazard of hydrogen formed during the zircaloy oxidation, the non-condensable gases are expanded and diluted in a mixing chamber (see Fig. 3). In particular the hydrogen is diluted to a concentration below explosion limits by adding compressed air to the gas.

The test facility has a quench capability which is activated by raising a water-filled quench cylinder into the test section at a controlled speed. After the test the high-temperature shield can be lowered into the quench unit without moving the bundle. So, the tested bundle can be inspected and photographed posttest in its original condition that existed at the termination of the transient.

2.2 Test Train Design

The test bundles CORA-5, CORA-12, CORA-15, and CORA-9 consisted of 25 fuel rod simulators, test bundle CORA-7 was built of 57 rods. The test rods were arranged within the bundle as shown in the schematic cross section of Fig. 5. 16 of the 25 fuel rods and 32 of the 57 rods, respectively were electrically heated by using tungsten pins as heater elements. The heated rods (fuel rod simulators) were filled with annular UO_2 pellets whereas the unheated rods contained full UO_2 pellets of the same outer diameter.

The design of the heated and unheated types of rods used in the CORA test bundle is given with Fig. 6.

A schematic of the absorber rod arrangement is provided with Fig. 7. The rods are surrounded by a shroud made of Zircaloy-4. The dimensions of the shroud can be taken from the cross section in Fig. 8. In this figure the grid spacer is shown as well. The shroud itself is insulated with a 20 mm-thick layer of ZrO_2 fiber material to guarantee a uniform radial temperature distribution.

Three grid spacers of approximately 40 mm length were mounted below the heated region, in its center, and in the upper zone. The lower and upper grid spacers were made of Zircaloy-4 whereas the central spacer was of Inconel 718.

Details on the location of the spacers and the fuel rod simulator design characteristics are given in Tables 2 through 5.

The test train instrumentation comprised thermocouples and two-color pyrometers for the various temperature measurements. The test section was instrumented with thermocouples (W/Re and NiCr/Ni type thermoelements) and two-color pyrometers to measure steam temperature, rod cladding temperature, shroud temperature, and insulation temperature. The high-temperature thermocouples were made of W5Re/W26Re wires, insulated with HfO_2 and sheathed in Ta/Zry duplex tubing. For the measurements inside the absorber rods tantalum-sheathed thermocouples and for the positions at lower maximum temperatures K-type thermocouples with inconel sheath were installed. The positions of the thermocouples can be taken from Tables 6 through 9b and Figs. 8a through 8e.

Ten videoscopes were used in both tests to observe the materials behavior and the relocation of material during transient testing. A schematic of the videoscope system with video camera and 35-mm still camera is given with Fig. 9, the positions in the individual tests with Figs. 9a and 9b.

The operational data, e.g. voltage, current, electric power, pressure, and temperatures were recorded by a data acquisition system as were the temperatures of the test section.

The hydrogen produced during the test by the steam/Zr reaction is usually measured at two different positions, i.e. above the test section and in the mixing chamber (see Fig. 3).

A schematic of the probes, gas lines, and gas analysis system is provided with Fig. 10. To dilute the gas taken at the location above the test section a dilution chamber with flow meters is installed. The off-gas mixture which contains hydrogen among other gases is being transported to the spectrometer via capillary tubes. It is analyzed by two quadrupole mass spectrometers of the type Leybold PQ 100. The ion currents representing the concentrations of the respective gases are determined. From these data the mass production rate of hydrogen as well as of the other gases is calculated with the ratio of the partial pressure of the particular gas and that one of argon (carrier gas) and multiplied by the argon flow rate through the test bundle.

2.3 Test Conduct and Results

In the CORA experiments the test sequence can be distinguished in the following phases:

- Pre-heating 0000 - 3000 s (argon only)
- Heat-up 3000 - 3900 s (argon + steam)
- Escalation 3900 - 4900 s (argon + steam)
- Cool-down ˆ 4900 s (argon only).

During the preheating phase argon of about 500°C enters the test bundle with a flow rate of 6 - 8 g/s. Between 3000 s and 4700 s the electric power is increased from 6 kW to 28 kW to achieve the initial heatup rate of 1 K/s. At 3300 s within the test a constant flow of superheated steam of 6 g/s and 12 g/s (for the large bundle CORA-7), respectively, is established in addition to the argon flow. In the escalation phase, i.e. starting from about 1100°C the slow temperature rise is followed by a rapid increase caused by the increased electric power input and the additional energy from the exothermal zirconium - steam reaction. The contribution of this exothermal heat to the total energy input is generally between 30 and 40 %.

The tests are terminated by power reduction (slow cooldown) or power reduction and quenching with water (fast cooldown). In both cases the steam supply is turned off with the shutoff of the electric power.

The power input history for tests CORA-12, CORA-15, CORA-9, and CORA-7 is provided together with the coolant data as argon flow, steam flow (provided as mass flow of the injected water into the evaporator), and coolant pressure is depicted in Figs. 11 through 14. Test CORA-5 was run with an identical power input and steam flow as test CORA-12. Test CORA-12, however, was terminated by quenching.

The response of the rod temperatures during the CORA transients at different elevations is provided with Figs. 15 through 19. The maximum temperature reached in the CORA tests amounts to about 2000°C, except for test CORA-7 where the turnaround occurred below 2000°C due to the shutoff of the steam supply at 4080 s.

The temperatures of absorber rod and pertinent guide tube show basically the same behavior as the unheated or heated rods as is demonstrated with Fig. 20 (CORA-5).

The conduct of tests CORA-5, CORA-12, and CORA-7 resulted in a behavior typical for CORA experiments. Tests CORA-15 (internal rod pressure) and CORA-9 (high system pressure) exhibited a different performance. A difference in CORA-15 compared to experiments without internal rod pressure can be found for the temperature escalation process. In CORA-15 the escalation developed in the upper half of the bundle only. Usually the escalation also takes place in the lower half of the bundle, down to about 150 mm. In CORA-15 the temperature in the lower part was insufficient to trigger a temperature escalation.

Test CORA-9 demonstrated a similar behavior.

The onset of the temperature escalation was reached at a later time and at a higher power in case of the high system pressure. At 4800 s (The time at which a CORA transient is usually finished) only about 1000°C were reached with a power input of 27 kW. (In CORA-5 the identical temperature was obtained at about 4100°C with a power input of 20 kW only). Higher heat losses in case of the high system pressure required a larger power input to start the temperature escalation. In test CORA-9 the energy release was concentrated in the upper half of the bundle.

In CORA-15 the fuel rod simulators (heated and unheated) were pressurized to 6.0 MPa at temperature. So, all rods underwent ballooning and rupture. Bursting occurred within 150 s in the temperature regime of 650 to 750 °C. The sequence of the rupture for the individual rods is presented with Fig. 21.

To "freeze" the damage propagation in the large bundle CORA-7 the steam supply was stopped at 4080 s and the electric power was turned off at 4200 s. However, the temperature responded with a decrease only at the lower section, i.e. up to 350 mm. Temperatures at locations from 450 mm upward continued to rise due to the zirconium-steam reaction with the strongest heatup at 750 mm. At this location the maximum temperature amounts to 1900 °C.

The steam supply during cooldown of test CORA-12 was quite different to the typical transient phase. The steam supply rate during quenching by evaporation

from the quench cylinder is in the order of ten times the feed during the transient phase.

The quenching of the test bundle CORA-12 has an impact on temperature behavior and hydrogen release. In Fig. 22 the hydrogen production is plotted together with the temperature recordings of the full-pellet rods. At the upmost part of the bundle, i.e. at 1250 mm the temperature shows a temporary increase which coincides with the additional peak in the hydrogen production. This peak is due to an extremely strong reaction between saturated steam of the quench water and the zirconium that was not yet completely consumed during the first part of the transient /3, 4/. It is a remarkable amount of hydrogen that was generated during the flooding phase.

The amount of hydrogen produced during tests CORA-5 and CORA-12 cannot be given quantitatively. Quantitative data from other quench experiments indicate that up to 80 % of the total hydrogen can be produced during the flooding phase /3/.

The measured data for tests CORA-15, CORA-9, and CORA-7 including the total values are given in Figs. 23 through 25. They are derived from the ion current obtained from the gas probes at the outlet of the test section. The peak production rate of hydrogen in test CORA-7 was evaluated to be 0.19 g/s.

Based on the accumulated H_2 productions of tests CORA-15, CORA-9, and CORA-7 the oxidation energy is determined. Its percentage amounts to 30 - 45 % of the total energy input (electric supply plus exothermal energy), as is given in Table 6.

Also on the basis of the total H_2 generation the percentage of zirconium oxidation was calculated. This percentage, provided as well in Table 6, is an integral value and does not reflect local differences.

The fraction of steam consumed during the transient (heatup) phase, was calculated. The result, too, is an integral (average) value that is based on the total amount of H_2, the steam flow rate, and the time at temperature above 1400 °C.

3. Posttest Appearance of the Bundles

Overall views of the test bundles CORA-5, CORA-12, CORA-15, CORA-9, and CORA-7 at different orientations are given in Figs. 26 through 30.

Detailed views of the bundles at different orientations and elevations are provided for

CORA-5: Figs. 31 and 32

CORA-12: Figs. 33 and 34

CORA-15: Figs. 35 and 36

CORA-9: Figs. 37, 38, and 39

CORA-7: Figs. 40, 41, and 42.

The following description of the posttest appearances of the individual test bundles was made possible with help of cross sections. The sections were obtained as follows.

After visual inspection, photographic documentation, and collecting of fragments the test bundles were encapsulated in epoxy resin and sectioned according to the lists provided in the Appendix. The locations of the sections are illustrated in figures of the Appendix.

For encapsulation of the bundle the epoxy system Rütapox 0273 with the hardener designated LC (Epoxy resin and hardener manufactured by Bakelite GmbH, D-5860 Iserlohn 7) was chosen. For this a mold of plastic ("plexiglas") was set up around the bundle. Then the bundle was filled from the bottom, through the steam inlet line, to avoid air entrainment in the encapsulant (see Fig. 43). The mould was filled to an elevation above the top of the shroud. The epoxy showed some heating during the curing stage but the shrinkage effect was negligible. After epoxying the bundle the resin was allowed to harden for one week.

A saw with a 2.3 mm-thick diamond blade (mean diamond size 138 μm) of 500 mm OD was used to do the cutting of the slab at 3200 rpm. The thickness of a slice from the epoxied bundle resulted in 13 mm corresponding to the distance of the marks of 15 mm.

As the behavior of bundle CORA-5 is typical for most of the test bundles containing (Ag/In/Cd) absorber material the description of bundle CORA-5 is given in more detail than that for the other specimens.

3.1 Appearance after Test CORA-5

Prior to removal the shroud was found strongly deformed and embrittled. The attack of the absorber melt is visible along the entire test section. An extended blockage has developed above 400 mm. The final state of the cross-sectional geometry is provided with Fig. 44 a /7/.

In general, claddings still present above 400 mm were radially deformed by the process called "flowering". Also in the upper part of the bundle the claddings were completely oxidized. At the location of the upper grid spacer made of zircaloy no zirconium remained. Due to the concentration of zirconium an intensive interaction between spacer and claddings on one side and UO_2 on the other side took place at this elevation.

Not such an interaction was detected between 250 mm and 400 mm, i.e. below the blockage zone. The blockage itself mainly contains resolidified melt of cladding and fuel and its formation at this position was influenced by the central spacer made of Inconel. The video film of the test reveals that the relocation of melt from upper positions was held up by the spacer and continued after the spacer had molten away (due to the interaction with zirconium).

In the blockage section the oxidation of the cladding was inhibited because the claddings in this region were protected from exposure of steam by "refrozen" melt.

The vertical cross sections (Fig. 45) show that the absorber rod has disappeared above 250 mm. Above this elevation only the ZrO_2 skin formed on the outer side of the guide tube is left. This thin ZrO_2 shell is well to be seen in the vertical section between 495 mm and 985 mm. The absorber material (Ag, In, Cd), the stainless steel cladding, and the inner unoxidized part of the guide tube have relocated from their original positions. Also the claddings of the rods surrounding the absorber rod have relocated to lower positions due to

dissolution by the steel/absorber melt. In addition, some localized attack on fuel pellets can be recognized.

A massive blockage has formed between 400 mm and 470 mm as can be seen in the longitudinal section as well as in the horizontal cross sections of Fig. 46. The horizontal section at 436 mm demonstrates that that nearly all coolant channels inside the bundle are filled with relocated material that is mainly oxidic melt: (U, Zr) O_2.

The lower sections (97 - 290 mm) show that the absorber rod is present up to about 250 mm. The absorber rod melt has filled the gap between stainless sreel cladding and zircaloy guide tube. The relocation in this gap has stopped at about 50 mm. The guide tube has survived the attack of the absorber melt up to about 150 mm. Above this elevation the zircaloy is chemically dissolved by the absorber rod melt. There the oxide layer of the guide tube has kept the molten material in place. However, at two elevations, i.e. at 160 mm and 180 mm holes must have formed in the ZrO_2 layer so that part of the melt has flown out. Outside the guide tube the absorber melt has solidified at an elevation of about 150 mm. According to the thermocouple readings the temperature at this elevation had a maximum of 750°C.

Scenario of absorber rod failure

On the basis of the video observations, temperature measurements, and post-test investigations of test bundle CORA-5 the following scenario of absorber rod failure and its impact on fuel element behavior can be described.

The failure of the stainless steel cladding must have started at about 800 mm. After penetration of the absorber cladding (steel), the (Ag, In, Cd) alloy with a melting point of 800°C has moved into the gap between absorber rod and guide tube and has then started to dissolve the metallic part of the zircaloy guide tube. Only a relatively small amount of absorber melt has flown down within the gap. The major part of it must have penetrated the guide tube approximately 30 to 40 s after failure of stainless steel cladding initiating the radial and axial relocation of the absorber melt. This failure is presumably caused by a eutectic interaction with the zircaloy of the guide tube as a result of contact between both partners due to an eccentricity established in the course of a temperature transient /5, 6/.

From the video observations it can be learned that the distribution of absorber melt takes a time of several minutes.

With the increase of temperature, also in the lower part of the bundle, the stainless steel cladding eventually melted allowing more and more absorber melt to escape from the absorber rod. So, the absorber melt has been distributed in the bundle and has been able to initiate the liquefaction of the zircaloy cladding of the fuel rods. The resulting zirconium-rich melt then started to dissolve the outer part of the UO_2 pellets.

The deposition of melts has been stratified in the way that: A blockage which contains preferentially UO_2 dissolved by molten metallic zircaloy, followed by a relative open region which is eventually succeeded by relocated absorber material. This structure is typical for all tests performed with absorber material /4, 5, 6/.

So, two kinds of melt are formed in the experiments with PWR absorber material. (1) A ceramic melt of (U, Zr, O) and (2) a metallic melt comprising (Ag, In, Zr).

More details on the behavior of the (Ag, In, Cd) absorber material are given in section 5 (post-test examinations).

3.2 Appearance after Test CORA-12

The photographs taken from the outside of bundle CORA-12 demonstrate strong interaction between the various materials, oxidized and embrittled cladding. However, the appearance of test bundle CORA-12 is quite similar to that of CORA-5. The more rapid cooldown by quenching with water has led to a strong fragmentation of the bundle components, even to powdering. Loose rubble is found on top of the central as well as the lower spacer as is illustrated in the schematic of Fig. 47. As can be taken from Fig. 44 b /7/ the claddings are intact below 150 mm. Between 150 mm and the blockage zone which is located between 200 mm and 300 mm a third of the claddings are lost, another third is broken mechanically, and the remainder has reacted with melt.

Above the blockage zone that consists of relocated absorber melt about 80 % of the cladding underwent "flowering". Above the central spacer the UO_2 pellets

exhibit fuel dissolution. In this upper half more than half the claddings are missing, and the remainders are completely oxidized.

The vertical cross section of the bundle in Figs. 48 and 49 and the horizontal cross sections in Fig. 50 show a void in the upper part, i.e between 600 and 700 mm due to fragmentation of the solids rods.

3.3 Appearance after Test CORA-15

In test CORA-15 escalation took place only in the upper half of the bundle. The posttest appearance confirms the result indicated by the temperature recordings. So, melting and relocation of material took place only in the upper half of the bundle as can be seen in the view from outside the bundle as well as from the vertical and horizontal cross sections (Figs. 51 through 56).

In the upper part the claddings are completely oxidized and embrittled. Larger portions are missing. However, the pellet stacks of the full-pellet rods are kept in place.

The behavior of the bundle might be explained by a different response of the heater resistance in the upper and the lower part of the bundle. Once the temperature increases in the upper part an escalation is triggered in this part while the rods stay cool in the lower part where the heater resistance is kept at a constant value. (The total energy fed into the heated rods is constant). In the lower part the temperature reached was too low to start an escalation. The behavior is a consequence of cladding ballooning which changes the heat transfer in the heated rods.

A partial flow channel blockage occurred at the interface of the hot and the "cool" portion of the CORA-15 bundle (Fig. 44c from /8/). This interface lies axially at the elevation of the central grid spacer.

3.4 Appearance after Test CORA-9

Although the onset of melting was delayed in test CORA-9 (first melt formation was observed at 5278 s), no difference in the meltdown behavior could be recognized when compared to the test performed at a low system pressure. Blockage formation in bundle CORA-9 was less compared to the other

experiments. But the general appearance of the bundle is very similar to the low-pressure tests.

The shroud insulation had well survived the transient. The very strong oxidation in the upper part is very conspicuous (white ZrO_2 oxide). The oxidized cladding shows the "flowering" phenomenon in the typical manner, although flowering was not expected to happen in this way because of the rod outer (system) pressure. Bundle CORA-9 has been at temperatures above 800°C for about 10 min longer than other test bundles. So, embrittlement is severe. Quenching of this bundle would probably have led to a very strong fragmentation.

However, only some rubble has collected at the lower end plate resulting mainly from the droplet-type melt movement. As in the other tests this is a relatively small amount of the total once-molten material. Melt has solidified over the entire length of the bundle. Local dissolution of UO_2 by the zircaloy cladding can be recognized as well as absorber rod failure. The failure location, i.e. the position above which the absorber rods are molten away, is lower compared to other tests:

CORA-9	110 - 120 mm
CORA-5	250 mm
CORA-12	250 mm
CORA-15	400 mm.

By help of the cross sections in Figs. 57 and 58 one can recognize that blockage formation is less pronounced than in the other experiments with 2.2 bar system pressure. However, the radial and axial distribution of absorber melt is not less pronounced as was expected due to the constraining effect of the system pressure. The temperature distribution seems to be of importance instead.

3.5 Appearance after Test CORA-7

In the upper half of the bundle, the usual melt relocations occur (Fig. 40 and 41). The (Ag, In, Cd)absorber elements failed as early as between 1250 and 1400°C; the resulting melt subsequently entered into a reaction with the zircaloy cladding material which it liquefied. Also the heavily oxidised zircaloy cladding tubes - some of them breaking apart and causing so-called flowering - can be clearly

seen. During the cooling-down phase parts of the completely embrittled cladding tubes are torn off and uncover the UO_2-pellets.

According to the temperature history a pronounced deformation (reaction zone) of the zircaloy shroud exists between 500 mm and 1050 mm. After removal of the shroud a strong oxidation (white oxide) and destruction of the claddings is found in the same region, i.e. above the axial midplane.

The generation and distribution of melt in this bundle, too, is affected by the behavior of absorber material.

The cross sections of Figs. 59 through 62 demonstrate that the major portion of melt has solidified in the center of the bundle, between 400 mm and 500 mm. As the detailed photographs of Fig. 61 shows that the absorber rod 6.6 is still present in the section at 426 mm. Between 600 mm and 800 mm remnants of the zircaloy guide tube can be recognized. The vertical section of Fig. 62 provides evidence of the attack of absorber melt on the zircaloy claddings of full-pellet rods.

From the cross sections it is visible that the liquid phases formed in the upper zone of the bundle have become relocated and caused a blockage near the Inconel spacer (456-496 mm). The Inconel spacer acted as a material catcher. However, some of the melts had been relocated also downward into to the lower bundle region where they solidified by forming small local blockages. Even in the lower spacer region (-30 mm), rather large amounts of accumulated solidified melts can still be recognised. Figure 61 shows enlarged details of one of the five absorber rods together with the four neighbouring fuel rods. It can be clearly seen that the (Ag, In, Cd)-absorber rod and the related zircaloy guide tube have completely disappeared in the upper half of the bundle, but not in the lower colder half of it. The absorber rod should fail, i.e. melt down, upon attainment of the melting point of the steel cladding tube ($\approx$ 1400°C) at the latest. On account of eutectic interactions of the steel cladding tube and the zircaloy guide tube, liquefaction can take place locally as early as from 1200°C on. The (Ag, In, Cd) absorber melt contributes essentially to the propagation of damage in the bundle which is an unambiguous finding of chemical-analytical studies of the reaction products by means of the scanning electron microscope.

The horizontal sections demonstrate that the central spacer (Inconel) of this bundle has survived because of the lower temperature at this elevation. The upper spacer of zircaloy has reacted with the fuel pellets enhancing the reaction

of the claddings to dissolve the dissolution of UO_2 (see metallographic examination described in section 5).

4. Mass distribution and blockage formation

An axial profile of voids and structure material, respectively, can be obtained by using the epoxying process. As can be seen in Fig. 43 the epoxy resin is filled into the mould from the bottom end. By wheighing the resin left in the supply container after each step, i.e. when the resin level has raised in the bundle by 1 cm, the difference of mass allows the calculation of the void volume of the bundle as a function of axial height. The filling process is slow enough so that the reading at the scale can be taken per cm providing a specific mass in (g/cm). To obtain an axial distribution of the structural material the cut bundle segments were wheighed.

Applying the cross-sectional areas of the mould inside, and the epoxy resin, the area of the structural material is evaluated. The result of bundle CORA-5 is presented with Fig. 44 a that of test CORA-12 with Fig. 44 b, and that of test CORA-15 is presented with Fig. 44c. All three figures are taken from reference /5/.

The blocked area of CORA-5 between 350 and 500 mm can be seen in Fig. 44 a. CORA-12 demonstrates the relocation of material from the upper elevations to the bottom of the test section.

5. Results of the destructive post-test examinations

For the analysis of cross sections and longitudinal sections the selected samples were infiltrated by "Araldit" resin to close up residual pores then grinded and polished.

The procedure of the preparation for the metallographic examination is given with Table A-1 (Appendix). The steps described in the list were performed using a semi-automatic machine with a closed water circuit for grinding and an automatic lubricant feeder for the polishing steps. The cross sections were studied in the as-polished condition.

5.1 Post-test Examinations of the CORA-5 Bundle

Besides the heavy destruction of the cladding tube, caused by oxidation and flowering, respectively, liquid phases formed which lead to the chemical dissolution of the UO_2-fuel. The bundle has been extremely damaged, above all in the zone immediately beneath the spacer. Figure 32 shows this bundle section in an enlarged representation. The various solidified melts are clearly visible, some of them relocated as narrow paths of melt. In the upper part of the figure distinct cracking in the embrittled fuel rod cladding tubes can be detected, too. Therefore, the interactions of the Inconel spacer and the zircaloy cladding tube are very important to initiating and propagating damage.

In Fig. 63 a metallographic longitudinal micro-section is represented. The cut was made through the absorber rod and the two neighbouring unheated fuel rods which contained solid pellets. The badly destroyed absorber rod can be clearly recognised. The (Ag,In,Cd) melt was relocated downwards while chemically reacting with the zircaloy fuel rod cladding tubes and also with some of the UO_2-pellets. At the points of contact of the absorber alloy with the cladding tubes the latter were dissolved chemically. This finding is clearly visible, above all in transverse micro-sections prepared from deeper layers. Figure 64 shows details of the absorber rod and of the neighbouring fuel rods. At the bundle elevation 95 mm (transverse micro-section 5-04) both the zircaloy guide tube and the steel cladding tube are intact. Solidified absorber melt, relocated from overlying regions, can be found between both tubes. Although the steel cladding tube is still intact at the bundle elevation 208 mm (transverse micro-section 5-05), the zircaloy cladding tube has almost completely been dissolved chemically. The (Ag, In, Cd, Zr) melt is retained solely by a thin external oxide layer (Fig. 64, position 2). At the same bundle elevation (208 mm) also the chemical process of zircaloy dissolution by the absorber melt can be well recognised. This causes zircaloy to become liquefied well below its melting point.

At 208 mm there are various examples of relocated melts (Fig. 65). One corner of the cross section is completely blocked by relocated once-molten metallic material. The microstructure indicates that the solidified melts mainly consist of (Ag, In, Cd) absorber rod material which dissolved different amounts of Zry cladding and which contain in addition some oxygen. The relocated melts are oxidized at their surfaces to different extents. The resulting ZrO_2 layers are a clear indication for the Zr content in the melts, which are preferentially oxidized.

The detail of position 1 in Fig. 65 confirms the observation in the macroscopic cross sections: The absorber rod must have failed at higher elevations and the molten (Ag, In, Cd) alloy is relocated within the gap between the stainless steel cladding of the absorber rod and the Zry guide tube. The (Ag, In, Cd) is compatible with stainless steel (Pos. 3) but not with Zry (Pos. 4). The absorber rod melt dissolves the Zry of the guide tube and is kept at place at this elevation only by a thin ZrO_2 layer, which has formed on the external surface of the guide tube during the heatup period by interaction with steam (bottom of Pos. 4). Pos. 5 shows a location, where the ZrO_2 layer has failed and the molten (Ag, In, Cd, Zr) alloy could relocate. Pos. 6 gives a UO_2 fuel / Zry cladding contact region, where chemical interaction took place, resulting in the formation of oxygen-stabilized α-Zr(O) and a (U, Zr) alloy.

5.2 Post-test Examinations of the CORA-7 Bundle

Figure 66 shows the bundle cross-sectional level 7-07 at elevation 863 mm, i.e. in the upper zone of the zircaloy spacer. Residues of the completely oxidised zircaloy spacer can still be recognised. The other part has disappeared through melting and, together with the partially molten zircaloy cladding material, contributed greatly to the chemical dissolution of UO_2. The micrographs show the liquefaction of UO_2 about 1000 K below its melting point, with changing intensity from rod to rod. No absorber material can still be detected at this level of the bundle. Likewise, the cladding material has almost completely disappeared and reappears as an alloy constituent in the solidified metals, which cause bundle blockages. The blockages preferably occur in zones with a spacer installed because the spacers act as material catchers.

Figure 67 shows the bundle cross-sectional level 7-04 at the elevation of the Inconel spacer located in the bundle mid-plane (480 mm). At that elevation of the bundle a considerable portion of the predominantly of metal consisting of melts from the upper zone of the bundle has accumulated and causes substantial bundle blockage. The majority of the Inconel spacer material is still present; locally, melting took place which suggests that the temperatures were around 1400°C. The absorber melt of complex composition (Ag,In,Cd,Zr,Fe,Cr,Ni) chemically dissolved the zircaloy cladding material, i.e. it liquefied the material at about 300 K below its melting point and subsequently attacked also the UO_2-fuel. This frozen intermediate state of damage of the bundle is a clear indication of the chemical aggressiveness of the (Ag,In,Cd) absorber melt with respect to zircaloy and UO_2.

The melt penetrated deeply into the UO_2-pellets which it partially liquefied (Figure 68). In all cases large amounts of Ag, together with Zr, were detected at the very front of reactions by means of the scanning electron microscope.

On the whole, the CORA-7 experiment relating to a large DWR-bundle, on account of the low temperatures provided interesting new findings on damage propagation compared to the experiments involving small BWR-bundles because it was possible to freeze intermediate states of bundle damage. However, no basic differences were found in the physical-chemical behaviour of the various bundle components between the large and the small PWR-bundles. For this reason, it had not been and still is not necessary to carry on the more in-depth PWR-experiments with large bundles.

5.3 ZrO_2 Oxide Layer Thickness

The external oxide layer was evaluated for tests CORA-5 and CORA-12 (Fig. 69, from /8/). The presence of a remarkable ZrO_2 layer found at test bundle CORA-12 could be explained by the additional oxidation during the quenching process when unoxidized regions (cold lower part) were oxidized during the reflooding at the end of test.

6. Summary of the major results

The general behavior of the PWR-type fuel element with Ag/In/Cd absorber rods that were tested under severe accident conditions can be described as follows.

- Temperature escalation due to the zirconium-steam reaction starts in the upper, i.e. hotter bundle half at about 1100 °C and propagates from there downwards and upwards. The maximum temperatures were above 2000 °C.
- Remarkably more molten material had formed in the bundle with absorber rod material (CORA-5) compared to the arrangement without absorber rods (CORA-2, CORA-3 /2/.
- In presence of PWR absorber material (Ag, In, Cd) the sequence of failure starts with the release, relocation and resolidification of the (Ag, In, Cd) melt. The melt formation occurs at about 1250 °C. Most of the melt reacts with the zircaloy cladding and guide tube by liquefying the zirconium components, forming a metallic melt of the type (Ag, In, Zr). Due to its zirconium content

this melt is capable of dissolving UO_2 as low as 1250 °C, i.e. clearly below the melting point of zircaloy (1760 °C).

- The non-oxidized part of the zircaloy cladding first melts in the upper bundle zone because of the higher temperatures prevailing there. Due to the progressing chemical dissolution of UO_2, melts consisting of (Zr, U, O) develop with different contents of uranium and oxygen and relocate into the bottom part of the bundle after the ZrO_2 layer has failed. While the melt solidifies in the colder zone, coolant channel blockages develop which are different in size.
- Only a small amount of the absorber melt is moving down inside the guide tube. The major part is radially and axially distributed within the bundle.
- The relocation of the absorber material in the bundle takes place mainly as rivulets. Only a minor portion is falling down in form of fine droplets.
  Also most of the other melt relocates along the surfaces (candling) and, to a minor extent, in the free fall as droplets, i.e. without contact to the surfaces of the materials (slumping). Film flow type of melt relocation along the rods could not be observed.
- On account of the different solidification temperatures of the melts a stratification develops such that the metallic lumps of melt rich in absorber material are superimposed by metallic and/or ceramic (Zr, U, O) melt formed later within the heatup phase.

  So, the absorber rod stainless steel cladding is destroyed above 250 mm. The metallic part of the Zry guide tube is dissolved by the absorber melt down to 160 mm (based on test CORA-5).

  The resulting melt of the fuel rod interaction, containing mainly U, Zr, O is solidified between 400 mm and 470 mm according to its solidus temperature as a large lump of porous structure. The (Ag, In, Cd) absorber melt with the much lower solidus temperature solidified down to 150 mm (based on test CORA-5).
- Besides the formation of solidified lumps of melts at "cold spots" within the lower part of the bundle, debris of absorber material, cladding, and fuel fragments of various sizes accumulates at the very bottom (below the bundle). The smallest particles consist of UO_2 powder and are of the order of micrometers in size.
- Water quenching (flooding) of the hot degraded fuel rod bundle causes additional fragmentation and an enhanced zircaloy/steam interaction

resulting in a renewed temperature rise, a meltdown of material, and in an additional strong hydrogen generation.

- During a SFD accident scenario, the presence of the (Ag, In, Cd) absorber material in a PWR fuel element results in a significant reduction of the liquefaction temperature which changes remarkably the relocation behavior.

7. References

/1/ S. Hagen, K. Hain, "Out-of-pile Bundle Experiments on Severe Fuel Damage (CORA-Program): Objectives, Test Matrix, and Facility Description", KfK 3677, 1986.

/2/ S. Hagen, P. Hofmann, G. Schanz, L. Sepold, "Interactions in Zry/UO_2 Fuel Rod Bundles with Inconel Spacers at Temperatures above 1200°C; (Post-test Results of Severe Fuel Damage Experiments CORA-2 and CORA-3)", KfK 4378, 1990.

/3/ S. Hagen, F. Seibert, L. Sepold, P. Hofmann, G. Schanz, G. Schumacher, "Influence of Reflood in the CORA Severe Fuel Damage Experiments", Heat Transfer and Fuel Behavior in Nuclear Reactor Accidents, 27th ASME/AIChE/ANS National Heat Transfer Conference, Minneapolis, 28-31 July 1991, AIChE Symposium Series 283, Vol. 87, ISBN-0-8169-0548-7, pp. 120-129.

/4/ S. Hagen, V. Noack, L. Sepold, P. Hofmann, G. Schanz, G. Schumacher, "Results of SFD Experiment CORA-13 (OECD International Standard Problem 31)", KfK 5054, 1993.

/5/ S. Hagen, L. Sepold, P. Hofmann, G. Schanz, "Out-of-pile Experiments on the Meltdown Behavior of LWR Fuel Elements: Influence of (Ag,In,Cd) Absorber Material", Proceedings of the International ENS/ANS Conference on Thermal Reactor Safety "NUCSAFE 88", Avignon (France), 2-7 Oct. 1988, Vol. 1, p. 129.

/6/ S. Hagen, L. Sepold, P. Hofmann, G. Schanz, "CORA Experiments on Severe Fuel Damage with and without Absorber Materials", Heat Transfer and Fuel Behavior in Nuclear Reactor Accidents, 26th ASME/AIChE/ANS National Heat Transfer Conference, Philadelphia, 6-9 August 1989, AIChE Symposium Series 289, Vol. 85, ISBN-0-8169-0466-9, pp. 135-140.

/7/ W. Hering, K. Minato, F. Nagase, "Global Analysis of Bundle Behavior in PWR-specific CORA Experiments", Nuclear Technology, 102, 100-115, 1993.

/8/ W. Hering, unpublished results.

8. Acknowledgements

Various kinds of support for preparation, conduct, and evaluation of the experiment are gratefully acknowledged.

The fuel elements were designed by Mr. H. Junker. The test rods were assembled by Mr. E. Mackert, the test bundles by Messrs. H. Giesmann and R. Röder. The authors would like to thank Messrs. H. Benz, C. Grehl, W. Rötzel, and H.J. Röhling for test preparations and conduct.

Mr. K.P. Wallenfels is acknowledged for arrangement of camera and video systems and for the preparation of temperature measurements. Messrs. R. Huber, H. Malauschek, and Ms. I. Schub prepared and conducted the on-line measurements of the off-gas samples.

Mr. W. Rötzel's effort in the posttest photography is greatly appreciated. The authors would like to thank Mr. L. Anselment for sectioning of the epoxied bundle and for preparation of the metallographic samples, Mr. H. Metzger for investigation of the metallographic samples by optical microscope, and Mr. J. Burbach for the SEM investigations.

9. List of Tables

Appendix

10. List of Figures

Appendix

Table 1: CORA Test Matrix

Test No.	Max. Cladding Tempera-tures	Absorber Material	Other Test Conditions	Date of Test
2	≈ 2000°C	-	UO_2 refer., inconel spacer	Aug. 6, 1987
3	≈ 2400°C	-	UO_2 refer., high temperature	Dec. 3, 1987
5	≈ 2000°C	Ag, In, Cd	PWR-absorber	Febr. 26, 1988
12	≈ 2000°C	Ag, In, Cd	quenching	June 9, 1988
16	≈ 2000°C	B_4C	BWR-absorber	Nov. 24, 1988
15	≈ 2000°C	Ag, In, Cd	rods with internal pressure	March 2, 1989
17	≈ 2000°C	B_4C	quenching	June 29, 1989
9	≈ 2000°C	Ag, In, Cd	10 bar system pressure	Nov. 9, 1989
7	< 2000°C	Ag, In ,Cd	57-rod bundle, slow cooling	Febr. 22, 1990
18	< 2000°C	B_4C	59-rod bundle, slow cooling	June 21, 1990

Table 2 Design characteristics of test bundles CORA-5 and CORA-12

Bundle size:			25 rods
Number of heated rods:			16
Pitch:			14.3 mm
Rod outside diameter:			10.75 mm
Cladding material:			Zircaloy-4
Cladding thickness:			0.725 mm
Rod length:			2175 mm
Heated length:			1000 mm
Fuel pellets	- heated rods:		UO_2 annular pellets
	- unheated rods:		UO_2 full pellets
U-235 enrichment			0.2 %
Pellet outer diameter (nominal)			9.1 mm
Heater material:			Tungsten (W)
Heater diameter:			6 mm
Grid spacer	- material:		Zircaloy-4, Inconel 718
	- length:	Zry	42 mm
		Inc.	38 mm
	- location:	lower (Zry)	- 5 mm (a)
		center (Inc.)	+ 496 mm
		top (Zry)	+ 880 mm
Shroud	- material		Zircaloy-4
	- wall thickness		1.2 mm
	- outside dimensions		86 x 86 mm
	- elevation	CORA-5	36 mm - 1260 mm
		CORA-12	36 mm - 1234 mm
	- insulation material		ZrO_2 fiber
	- insulation thickness		20 mm
Absorber rod	- number of rods	CORA-5	1
		CORA-12	2
	- material and composition		80Ag,15In,5Cd (wt.%)
	- cladding		stainless steel
	- cladding OD		10.2 mm
	- cladding ID		8.85 mm
	- length		1489 mm
	- elevation		- 189 mm to + 1300 mm
Absorber rod guide tube			
	- material		Zircaloy-4
	- OD		13.8 mm
	- wall thickness of tube		0.8 mm

(a) Elevations are meant for the top of the grid spacers and are referred to the bottom of the heated zone (0 mm = EL 5121)

Note: In CORA-12 the lower and the central grid spacer were exchanged by mistake.

Table 3 Design characteristics of test bundles CORA-15

Bundle size:			25 rods
Number of heated rods:			16
Pitch:			14.3 mm
Rod outside diameter:			10.75 mm
Cladding material:			Zircaloy-4
Cladding thickness:			0.725 mm
Rod length:			2175 mm
Heated length:			1000 mm
Fuel pellets	- heated rods:		UO_2 annular pellets
	- unheated rods:		UO_2 full pellets
U-235 enrichment			0.2 %
Pellet outer diameter (nominal)			9.1 mm
Heater material:			Tungsten (W)
Heater diameter:			6 mm
Grid spacer	- material:		Zircaloy-4, Inconel 718
	- length:	Zry	42 mm
		Inc.	38 mm
	- location:	lower (Zry)	- 5 mm (a)
		center (Inc.)	+ 496 mm
		top (Zry)	+ 880 mm
Shroud	- material		Zircaloy-4
	- wall thickness		1.2 mm
	- outside dimensions		86 x 86 mm
	- elevation		36 mm - 1236 mm
	- insulation material		ZrO_2 fiber
	- insulation thickness		20 mm
Absorber rod	- number of rods		2
	- material and composition		80Ag,15In,5Cd (wt.%)
	- cladding		Stainless steel
	- cladding OD		10.2 mm
	- cladding ID		8.85 mm
	- length		1489 mm
	- elevation		- 189 mm to + 1300 mm
Absorber rod guide tube			
	- material		Zircaloy-4
	- OD		13.8 mm
	- wall thickness of tube		0.8 mm

(a) Elevations are meant for the top of the grid spacers and are referred to the bottom of the heated zone (0 mm = EL 5121)

Table 4: Design characteristics of test bundle CORA-9

Bundle type:			PWR
Bundle size:			25 rods
Number of heated rods:			16
Pitch:			14.3 mm
Rod outside diameter			10.75 mm
Cladding material:			Zircaloy-4
Cladding thickness:			0.725 mm
Heated rod length:			1840 mm
Elevation:			- 369 to 1471 mm
Elevation of heated length:			0 to 1000 mm
Unheated rod:			1672 mm
Elevation:			- 201 to 1471 mm
Fuel pellets	- heated rods:		UO_2 annular pellets
	- unheated rods:		UO_2 full pellets
U-235 enrichment			0.2%
Pellet outer diameter (nominal)			9.1 mm
Heater material:			Tungsten (W)
Heater diameter:			6 mm
Grid spacer	- material		Zircaloy-4, Inconel 718
	- length:	Zry	42 mm
		Inc.	38 mm
	- location:	lower (Zry)	- 5 mm
		center (Inc.)	+ 496 mm
		top (Zry)	+ 880 mm
Shroud	- material		Zircaloy-4
	- wall thickness		1.2 mm
	- outside dimensions		86 x 86 mm
	- elevation		36 mm - 1236 mm
	- insulation material		ZrO_2 fiber
	- insulation thickness		20 mm
Absorber rod	- number of rods		2
	- material and composition		80Ag, 15In, 5Cd (wt.%)
	- cladding		stainless steel
	- cladding OD		11.2 mm
	- cladding ID		10.2 mm
	- length		1489 mm
	- elevation		- 189 mm to + 1300 mm
Absorber rod guide tube	- material		Zircaloy-4
	- OD		13.8 mm
	- wall thickness of tube		0.8 mm

Note: Elevations referred to the bottom of the heated zone (0 mm = EL 5121)
The values for the grid spacers refer to the top end

Table 5 Design characteristics of test bundles CORA-7

Bundle type:			PWR
Bundle size:			57 rods
Number of heated rods:			32
Number of unheated rods:			20
Pitch:			14.3 mm
Rod outside diameter:			10.75 mm
Cladding material:			Zircaloy-4
Cladding thickness:			0.725 mm
Rod length	- heated rods:		1840 mm
	(elevation		-369 to 1471 mm)
	- unheated rods:		1672 mm
	(elevation		-201 to 1471 mm)
Heated length:			1000 mm
Heater material:			Tungsten (W)
Heater diameter:			6 mm
Fuel pellets	- heated rods:		UO_2 annular pellet s
	- unheated rods:		UO_2 full pellets
Pellet stack	- heated rods:		0 to 1000 mm
	- unheated rods:		-200 to 1300 mm
U-235 enrichment			0.2 %
Pellet outer diameter (nominal)			9.1 mm
Grid spacer	- material:		Zircaloy-4, Inconel 718
	- length:	Zry	42 mm
		Inc.	38 mm
	- location:	lower (Zry)	-5 mm
		center (Inc.	+496 mm
		top (Zry)	+880 mm
Shroud	- material		Zircaloy-4
	- wall thickness		1.2 mm
	- outside dimensions		143 x 143 mm
	- elevation		36 mm to 1216 mm
	- insulation material		ZrO_2 fiber
	- insulation thickness		20 mm
Absorber rod	- number of rods		5
	- material and composition		80Ag,15In,5Cd (wt.%)
	- cladding		Stainless steel
	- cladding OD		11.2 mm
	- cladding ID		10.2 mm
	- length		1489 mm
	- elevation		-189 mm to +1300 mm
Absorber rod guide tube			
	- material		Zircaloy-4
	- OD		13.8 mm
	- wall thickness of tube		0.8 mm

Note: Elevations are referred to the bottom of the heated zone (0 mm = EL 5121). The values for the grid spacers refer to the top end.

Table 6 Positions of thermocouples (CORA-5)

Positions of thermocouples in unheated rods (CORA-5)			
Slot number	Elevation [mm]	Rod number	Type of TC
11	1200	2.4	WRe *
12	950	4.2	WRe *
13	850	4.6	WRe *
14	750	6.4	WRe *
10	550	2.4	WRe*
15	450	4.2	WRe *
16	350	4.6	WRe *
17	250	6.4	WRe *
18	150	2.2	WRe *
40	50	6.2	WRe *

Positions of thermocouples in the absorber rods (CORA-5)			
Slot number	Elevation [mm]	Rod number	Type of TC
1	750	4.4	WRe**
6	550	4.4	WRe**

Positions of thermocouples at the heated rods (CORA- 5)			
Slot number	Elevation [mm]	Rod number	Type of TC
5	750	5.3	WRe *
44	550	3.3	WRe *
45	350	3.5	WRe *
46	150	5.5	WRe *

Positions of thermocouples at the guide tube (CORA-5)			
Slot number	Elevation [mm]	Rod number	Type of TC
2	950	4.4	WRe*
3	750	4.4	WRe*
7	550	4.4	WRe*
8	350	4.4	WRe*
9	150	4.4	WRe*

*) WRe wires,duplex sheath (Ta/Zr)

**) WRe wires,Ta sheath

Positions of thermocouples at the shroud outer surface (CORA-5)			
Slot number	Elevation [mm]	Orientation of TE	Type of TC
41	950	30°	WRe*
42	750	30°	WRe *
47	550	210°	WRe *
48	350	30°	WRe *
49	150	210°	WRe*
50	50	210°	WRe*

Positions of thermocouples at the shroud insulation (CORA-5).			
Slot number	Elevation [mm]	Orientation of TE	Type of TC
54	950	30°	NiCrNi
55	750	30°	NiCrNi
56	550	210°	NiCrNi
57	550	210°	NiCrNi
58	350	30°	NiCrNi
59	350	30°	NiCrNi
60	150	210°	NiCrNi
61	50	210°	NiCrNi

Positions of thermocouples for gas temperature measurement (CORA-5)			
Slot number	Elevation [mm]	Orientation of TE	Type of TC
79	1450	90°	NiCrNi
52	1270	90°	NiCrNi
53	1270	210°	NiCrNi
43	1200	210°	WRe*

Positions of thermocouples for gas temp. and at steam distribution tube (CORA-5)			
Slot number	Elevation [mm]	Orientation of TE	Type of TC
51	150	210°	WRe*
19	0	180°	NiCrNi
20	0	180°	NiCrNi
62	0	180°	NiCrNi
74	0	300°	NiCrNi
75	0	210°	NiCrNi
76	0	30°	NiCrNi
77	0	180°	NiCrNi

Table 7 Positions of thermocouples (CORA-12)

Positions of thermocouples in unheated rods (CORA-12)			
Slot number	Elevation [mm]	Rod number	Type of TC
1	1250	4.2	WRe *
3	950	6.4	WRe *
2	850	2.4	WRe *
4	750	4.4	WRe *
42	550	4.2	WRe*
43	450	6.4	WRe *
44	350	2.4	WRe *
45	250	4.4	WRe *
46	150	2.2	WRe *
47	50	6.6	WRe *
79	0	2.6	NiCrNi

Positions of thermocouples in the absorber rods (CORA-12)			
Slot number	Elevation [mm]	Rod number	Type of TC
50	1300	4.6	NiCrNi
51	1300	6.2	NiCrNi
5	850	4.6	WRe**
6	850	6.2	WRe**
48	500	4.6	WRe**
49	500	6.2	WRe**

Positions of thermocouples at the heated rods (CORA- 12)			
Slot number	Elevation [mm]	Rod number	Type of TC
11	1250	3.7	WRe *
12	900	7.3	WRe *
13	750	3.3	WRe *
14	350	3.5	WRe *
54	0	5.3	NiCrNi

Positions of thermocouples at the guide tube (CORA-12)			
Slot number	Elevation [mm]	Rod number	Type of TC
7	750	4.6	WRe*
9	750	6.2	WRe*
8	150	4.6	WRe*
10	150	6.2	WRe*
52	0	4.6	NiCrNi
53	0	6.2	NiCrNi

Positions of thermocouples at the shroud outer surface (CORA-12)			
Slot number	Elevation [mm]	Orientation of TE	Type of TC
16	1240	30°	WRe*
17	950	30°	WRe *
18	750	30°	WRe *
40	350	30°	WRe *
41	150	30°	WRe*

Positions of thermocouples at the shroud insulation (CORA-12).			
Slot number	Elevation [mm]	Orientation of TE	Type of TC
24	950	30°	NiCrNi
26	750	30°	NiCrNi
27	550	30°	NiCrNi
62	350	30°	NiCrNi
72	150	30°	NiCrNi
74	50	30°	NiCrNi

Positions of thermocouples for gas temp. betw. shroud + HTS and at steam outlet			
Slot number	Elevation [mm]	Orientation of TE	Type of TC
76	1450	90°	NiCrNi
75	1450	270°	NiCrNi
77	1120	180°	NiCrNi
78	1120	360°	NiCrNi

Positions of thermocouples for gas temp. and at steam distribution tube (CORA-12)			
Slot number	Elevation [mm]	Orientation of TE	Type of TC
80	1270	180°	NiCrNi
19	0	180°	NiCrNi
20	0	180°	NiCrNi
55	0	30°	NiCrNi
56	0	300°	NiCrNi
57	-100	300°	NiCrNi
59	-200	300°	NiCrNi

*) WRe wires,duplex sheath (Ta/Zr)

**) WRe wires,Ta sheath

Table 8 Positions of thermocouples (CORA-9)

Positions of thermocouples in unheated rods (CORA-9)			
Slot number	Elevation [mm]	Rod number	Type of TC
83	1150	6.6	WRe *
82	950	6.4	WRe *
81	750	4.4	WRe *
161	550	2.4	WRe *
162	450	4.2	WRe*
163	350	6.4	WRe *
164	250	4.4	WRe *
165	150	2.6	WRe *
166	50	6.6	WRe *

Positions of thermocouples in the absorber rods (CORA-9)			
Slot number	Elevation [mm]	Rod number	Type of TC
88	1150	4.6	WRe**
87	805	6.2	WRe**
176	550	4.6	WRe**
177	350	6.2	WRe**

Positions of thermocouples at the heated rods (CORA- 9)			
Slot number	Elevation [mm]	Rod number	Type of TC
86	1150	3.7	WRe *
85	950	3.3	WRe *
84	750	3.5	WRe *
167	550	5.3	WRe *
168	350	5.5	WRe*
169	150	5.1	WRe*
170	0	7.3	WRe*

Positions of thermocouples at the guide tube (CORA-9)			
Slot number	Elevation [mm]	Rod number	Type of TC
90	950	6.2	WRe*
89	850	4.6	WRe*
171	450	6.2	WRe*
172	250	4.6	WRe*
173	150	6.2	WRe*
174	50	4.6	WRe*
175	0	6.2	WRe*

Positions of thermocouples at the shroud outer surface (CORA-9)			
Slot number	Elevation [mm]	Orientation of TE	Type of TC
93	1150	30°	WRe*
92	950	30°	WRe *
91	750	30°	WRe *
178	550	30°	WRe *
179	350	30°	WRe*
180	150	30°	WRe *
197	0	30°	NiCrNi

Positions of thermocouples at the shroud insulation (CORA-9).			
Slot number	Elevation [mm]	Orientation of TE	Type of TC
112	950	30°	NiCrNi
191	950	30°	NiCrNi
111	750	30°	NiCrNi
192	750	30°	NiCrNi
193	550	30°	NiCrNi
181	550	30°	WRe*
194	350	30°	NiCrNi
195	150	30°	NiCrNi
196	50	30°	NiCrNi

Positions of thermocouples for gas temp. betw. shroud + bundle and at steam outlet			
Slot number	Elevation [mm]	Orientation of TE	Type of TC
116	1511	180°	NiCrNi
113	1245	120°	NiCrNi
114	1245	300°	NiCrNi
123	1450	90°	NiCrNi

Positions of thermocouples for gas temp. and at steam distribution tube (CORA-9)			
Slot number	Elevation [mm]	Orientation of TE	Type of TC
122	351	360°	NiCrNi
121	351	180°	NiCrNi
199	0	180°	NiCrNi
198	0	180°	NiCrNi

*) WRe wires,duplex sheath (Ta/Zr)

**) WRe wires,Ta sheath

Table 9a Positions of thermocouples (CORA-7)

Positions of thermocouples in unheated rods (CORA-7)			
Slot number	Elevation [mm]	Rod number	Type of TC
111	1250	8.6	NiCrNi
112	1250	8	NiCrNi
113	1250	6	NiCrNi
114	1250	4.2	NiCrNi
115	1250	2.8	NiCrNi
116	1250	2.6	NiCrNi
117	1250	.0.8	NiCrNi
118	1250	0.2	NiCrNi
81	1150	4.6	WRe *
82	1050	2.2	WRe *
83	950	6.4	WRe*
84	950	0	WRe *
85	850	6.2	WRe *
86	750	8.8	WRe *
87	750	4.4	WRe *
161	550	8.8	WRe*
162	550	4.4	WRe *
163	550	0	WRe *
164	450	6.2	WRe *
165	350	2.2	WRe *
166	250	6.4	WRe *
167	150	4.6	WRe*
191	50	8.6	NiCrNi
192	50	8	NiCrNi
193	50	6	NiCrNi
194	50	4.2	NiCrNi
195	50	2.6	NiCrNi
196	50	0.8	NiCrNi
197	50	0.2	NiCrNi
198	50	2.8	NiCrNi

Positions of thermocouples in the absorber rods (CORA-7)			
Slot number	Elevation [mm]	Rod number	Type of TC
96	750	2.4	WRe**
97	750	4	WRe**
98	750	4.8	WRe**
99	750	6.6	WRe**
100	750	8.2	WRe**
176	350	2.4	WRe**
177	350	4	WRe**
178	350	4.8	WRe**
179	350	6.6	WRe**
180	350	8.2	WRe**

Positions of thermocouples at the heated rods (CORA- 7)			
Slot number	Elevation [mm]	Rod number	Type of TC
94	950	5.3	WRe *
93	750	5.5	WRe *

Positions of thermocouples at the guide tube (CORA-7)			
Slot number	Elevation [mm]	Rod number	Type of TC
168	150	2.4	WRe*
169	150	4	WRe*
170	150	4.8	WRe*
171	150	6.6	WRe*
172	150	8.2	WRe*

Positions of thermocouples at the grid spacer (CORA-7)			
Slot number	Elevation [mm]	Orientation of TE	Type of TC
205	475	120°	NiCrNi
206	475	210°	NiCrNi
207	475	300°	NiCrNi
208	475	30°	NiCrNi
209	-26	120°	NiCrNi
210	-26	210°	NiCrNi
211	-26	300°	NiCrNi
212	-26	30°	NiCrNi

Positions of thermocouples at the shroud outer surface (CORA-7)			
Slot number	Elevation [mm]	Orientation of TE	Type of TC
95	950	30°	WRe*
88	750	30°	WRe *
173	550	30°	WRe *
174	350	30°	WRe *
175	150	30°	WRe*

*) WRe wires,duplex sheath (Ta/Zr)

**) WRe wires,Ta sheath

Table 9b Positions of thermocouples (CORA-7), continued

Positions of thermocouples at the shroud insulation (CORA-7).			
Slot number	Elevation [mm]	Orientation of TE	Type of TC
199	950	210°	NiCrNi
201	750	210°	NiCrNi
202	550	210°	NiCrNi
203	350	210°	NiCrNi
204	150	210°	NiCrNi

Positions of thermocouples for gas temp. meas. betw. shroud + HTS (CORA-7)			
Slot number	Elevation [mm]	Orientation of TE	Type of TC
91	950	30°	WRe*
92	950	210°	WRe*
89	750	300°	WRe*
90	750	120°	WRe*

Positions of thermocouples btw.shroud + hts and at steam distribution tube (CORA-7)			
Slot number	Elevation [mm]	Orientation of TE	Type of TC
121	351	180°	NiCrNi
215	0	180°	NiCrNi
216	0	180°	NiCrNi
217	0	15°	NiCrNi
218	0	195°	NiCrNi
213	0	345°	NiCrNi
214	0	165°	NiCrNi

*) WRe wires,duplex sheath (Ta/Zr)

**) WRe wires,Ta sheath

Table 10: Zircaloy oxidation, energy release, and hydrogen production during various CORA tests

Test	Steam flow [g/s]	Total H_2 production [g]	Oxidation energy [MJ]	Percentage of oxidation energy [a] [%]	Total Zr oxidation [b] [%]	Test time at T›1400°C [s]	Fraction of H_2O consumed [%]
CORA-15	6	180	27.4	45	74	~ 1000	27
CORA-9	6	159	24.2	30	48	~ 800	30
CORA-7	12	114	17.3	34	28	~ 500	17

[a] Percentage of total energy, i.e. chemical reaction power and electric power input

[b] Percentage referred to bundle length of 1.2 m;

Table A1: Procedure for the metallographic preparation of the CORA samples

	Horizontal grinding	Grinding	Lapping	Polishing		
Abrasive	Corrundum disc 120 µm Diamond disc 64 µm	Diamond disc 20 µm	Petrodisc-M or DP Net*)	PAW cloth	PAN-W	NAP cloth
Particle size			Diamond spray 6 µm	6 µm	3 µm	1 µm
Lubricant	Water	Water	W. lubric. **)	W. lub.	W. lub.	W. lub.
Revolutions of disc	300 rpm	300 rpm	150 rpm (Net) or 300 rpm (Petrod.)	150 U/min	150 U/min	150 U/min
Pressure	200-400 N	200-300 N	200 N	100 N	100 N	100 N
Time	to level	25 min	30 min	30 min	60 min	60 min

*) Petrodisc-M and DP Net are registered trade marks of Struers company

**) "White lubricant" of Struers; liquid on an oil/alcohol/glycerin basis

Table A2 List of cross sections for test bundle CORA-5

Sample	Sample length	Elevation bottom	Elevation top	Comments
5- a	193 mm	- 223 mm	- 30 mm	
Cut	2 mm			
5-01				Not applicable
5-02				Not applicable
5-b1	74 mm	- 28 mm	+ 46 mm	
Cut	2 mm			Transition round-square
5- b2	17 mm	48 mm	65 mm	
Cut	2 mm			
5-03	13 mm	67 mm	80 mm	
Cut	2 mm			
5-04	13 mm	82 mm	95 mm	
Cut	2 mm			
5- c	161 mm	97 mm	193 mm	Vertical section
Cut	2 mm			
5-05	13 mm	195 mm	208 mm	
Cut	2 mm			
5- d	80 mm	210 mm	290 mm	Vertical section
Cut	2 mm			
5- e	86 mm	292 mm	378 mm	Vertical section
Cut	2 mm			
5-06	13 mm	380 mm	393 mm	
Cut	2 mm			
5-07	13 mm	395 mm	408 mm	
Cut	2 mm			
5- f	53 mm	410 mm	463 mm	Vertical section
Cut	2 mm			

5-08	13 mm	465 mm	478 mm	
Cut	2 mm			
5-09	13 mm	480 mm	493 mm	Central grid spacer
Cut	2 mm			
5- g	153 mm	495 mm	648 mm	Vertical section
Cut	2 mm			
5-10	13 mm	650 mm	663 mm	
Cut	2 mm			
5-11	13 mm	665 mm	678 mm	
Cut	2 mm			
5- h	158 mm	680 mm	838 mm	Vertical section
Cut	2 mm			
5-12	13 mm	840 mm	853 mm	Top grid spacer
Cut	2 mm			
5-13	13 mm	855 mm	868 mm	
Cut	2 mm			
5- i	115 mm	870 mm	985 mm	Vertical section
Cut	2 mm			
5-14	13 mm	987 mm	1000 mm	Upper end of heated zone
Cut	2 mm			
5-15	13 mm	1002 mm	1015 mm	
Cut	2 mm			
5- j	232 mm	1017 mm	1249 mm	Remnant

Table A3 List of cross sections for test bundle CORA-12

Sample	Sample length	Elevation bottom	Elevation top	Comments
12- a			- 23 mm	Remnant
Cut	2 mm			
12-01	13 mm	- 21 mm	- 8 mm	Lower grid spacer (Inc)
Cut	2 mm			
12- b	57 mm	- 6 mm	+ 51 mm	
Cut	2 mm			Transition round-square
12- c	148 mm	53 mm	201 mm	Vertical section
Cut	2 mm			
12-02	13 mm	203 mm	216 mm	
Cut	2 mm			
12- d	148 mm	218 mm	366 mm	Vertical section
Cut	2 mm			
12-03	13 mm	368 mm	381 mm	
Cut	2 mm			
12- e	148 mm	383 mm	531 mm	Vertical section
Cut	2 mm			
12-04	13 mm	533 mm	546 mm	
Cut	2 mm			
12- f	148 mm	548 mm	696 mm	Vertical section
Cut	2 mm			
12-05	13 mm	698 mm	711 mm	
Cut	2 mm			
12- g	148 mm	713 mm	861 mm	Vertical section
Cut	2 mm			
12-06	13 mm	863 mm	876 mm	Top grid spacer (Zry)
Cut	2 mm			
12- h	370 mm	878 mm	1248 mm	Remnant

Table A4 List of metallographic samples of bundles CORA-5 and CORA-12

CORA-5

- Sample	5-04	top 95 mm	Intact absorber rod
- Sample	5-05	top 208 mm	Lowest absorber melt
- Sample	5-06	top 393 mm	Absorber melt and ceramic melt
- Sample	5-07	top 408 mm	Metallic inclusions in melt
- Sample	5-12	top 853 mm	Top grid spacer (Zry)
- Sample	5-d	210 - 290 mm	Absorber rod failure
- Sample	5-e	292 - 378 mm	Max. shroud deformation, porous melt
- Sample	5-f	410 - 463 mm	Porous melt

CORA-12

- Sample	12-02	top 216 mm	Absorber melt
- Sample	12-04	top 533 mm	Pellet fragments
- Sample	12-c-L	53 mm-201 mm	Vertical section with absorber melt

Table A5 Fragments taken from bundle CORA-5

Probe Nr.	Höhe[a]	Umfangsl.[b]	Bemerkung
5-101	270 mm	210°	Schwarzer, glänzender Schmelzklumpen (glatt, wenig spröde) am Fenster festgeklebt).
5-102	665 mm	180°	Schmelzklumpen dunkelgrau, bestehend aus verschiedenen Tropfen, die miteinander verbacken sind.
5-103	910 mm	160°	Gelbgrüne Schmelznase am Hüllrohr, beim Entfernen zerfallen (äußerst spröde, evtl. ohne Uran-Phase).
5-104	840 mm	75°	Stück des oberen Zry-Abstandshalters (sehr spröde), Reaktion mit Eckstab.
5-105	610 mm	60°	Schwarz glänzende Schmelze (sehr spröde) am UO_2 bzw. am Hüllrohr erstarrt.

a Abst. von Unterkante Heizzone
b Zur Orientierung: Winkel 180°= Dampfeinlaßstutzen

Table A6 Fragments taken from bundle CORA-12

Probe Nr.	Höhe[a]	Umfangsl.[b]	Bemerkung
12-101	230 mm - 400 mm	120°	Lange Schmelznase aus Absorbermaterial (zur quantitativen Elementanalyse an drei verschiedenen Höhen zu H. Oschinski).
12-102	770 mm	120°	Zur Kugel erstarrte Absorberschmelze aus dem Fenster H38 (zur Untersuchung im IMF).
12-103	900 mm	120°	Auswuchs am Halteband der Shroudisolation (Untersuchung wird zurückgestellt).
12-104	400 mm	120°	Pulver und Hüllrohrbruchstücke aus der Fensternische (Untersuchung wird zurückgestellt).
12-105	200 mm	120°	Pulver bis größere Bruchstücke aus der Fensternische (Untersuchung wird zurückgestellt).
12-106	300 mm	210°	Mehrere lange Schmelznasen aus Absorbermaterial, das aus dem Fenster 300 mm/210° herausgelaufen ist (zur Unters. ins IMF).
12-107	1280 mm	210°	Poröser Niederschlag (?) an der Shroudoberkante (zur Untersuchung der Zusammensetzung zu H. Oschinski).
12-108		210°	Verschiedener "Rubble" unterhalb der Heiz zone (Untersuchung wird zurückgestellt).
12-109	50 mm - 150 mm	300°	Großer Schmelzklumpen aus Absorbermaterial, das aus einer Spalte des Isolationsmaterials herausgelaufen ist (wird fotografiert).
12-110	870 mm - 1050 mm	30°	Shroudstück (zur Untersuchung im IMF).
12-111	470 mm	210°	Mittlerer Abstandshalter (zu H. Oschinski zur Prüfung, ob Zirkaloy).

a Abst. von Unterkante Heizzone
b Zur Winkellage: 180°= Dampfeinlaßstutzen

Table A 7: **Analysis of some fragments of bundle CORA-12**

Sample	Elements in [Wt.%]														
	Ag	Cd	In	Zr	Sn	Fe	Cr	Ni	Cu	Zn	U	Mn	Mg	Mo	W
12-101 top	36.7	0.64	6.67	42.2	2.05	3.84	1.58	2.27	- 0.01	‹ 0.1	0.61	0.13	‹ 0.1	0.07	‹ 0.1
12-101 center	36.1	0.81	5.27	43.1	2.11	4.51	1.66	2.59	- 0.01	‹ 0.1	0.62	0.11	‹ 0.1	0.08	‹ 0.1
12-101 bottom	34.3	0.67	5.75	43.6	2.41	4.95	1.60	2.04	‹ 0.01	‹ 0.1	0.92	0.07	‹ 0.1	0.07	‹ 0.1
12-107	2.19	‹ 0.01	0.27	46.9	0.48	0.10	‹ 0.1	0.08	39.0	‹ 0.1	‹ 0.2	‹ 0.01	‹ 0.1	0.05	‹ 0.1
12-111	0.22	‹ 0.01	‹ 0.01	61.2	0.05	0.12	‹ 0.1	0.29	0.01	‹ 0.1	1.11	‹ 0.01	‹ 0.1	‹ 0.01	‹ 0.1

Table A8 List of cross sections for test bundle CORA-15

Sample	Sample length	Elevation bottom	Elevation top	Comments
15- a	mm		60 mm	Lower remnant
Cut	2 mm			Transition round - square
15- b	141 mm	62 mm	204 mm	
Cut	2 mm			
15- c	120 mm	206 mm	326 mm	
Cut	2 mm			
15-04	13 mm	328 mm	341 mm	Horizontal cross section
Cut	2 mm			
15- d	135 mm	343 mm	478 mm	Add. vertical section
Cut	2 mm			
15-01	13 mm	480 mm	493 mm	Horizontal cross section
Cut	2 mm			
15-02	13 mm	495 mm	508 mm	Horizontal cross section
Cut	2 mm			
15- e	105 mm	510 mm	615 mm	Add. vertical section
Cut	2 mm			
15- f	135 mm	617 mm	752 mm	Add. vertical section
Cut	2 mm			
15- g	135 mm	754 mm	889 mm	Add. vertical section
Cut	2 mm			
15-03	13 mm	891 mm	904 mm	Horizontal cross section
Cut	2 mm			
15- h	120 mm	906 mm	1026 mm	
Cut	2 mm			
15- i	139 mm	1028 mm	1167 mm	
Cut	2 mm			
15- j	mm	1169 mm	mm	Upper remnant

Table A9 Fragments taken from bundle CORA-15

Probe Nr.	Höhe[a]	Umfangsl.[b]	Bemerkung
15-101	150-400 mm	120°	Aus Fenster H28 ausgelaufene Schmelze in Form von langer schwarzer Nase (zur chem. Analyse an drei Stellen durch H. Oschinski)
15-102	360 mm	210°	Schwarze Schmelze m. glänzender Oberfläche am Halteblech der Isolation (zur Untersuchung durch H. Oschinski, HIT).
15-103	-	-	Stück des "inneren" Shrouds mit Goldglanz (Untersuchung wird zurückgestellt).

a Abst. von Unterkante Heizzone
b Zur Winkellage: 180°= Dampfeinlaßstutzen

Table A10: **Analysis of fragments taken from bundle CORA-15**

Elements	Wt % in Sample			
	15-101 top	15-101 center	15-101 bottom	15-102
Zr	54	54	54	53
Ag	28	29	28	30
Fe	5.8	5.7	5.5	5.7
Ni	2.5	2.3	2.5	2.9
Cr	1.6	1.5	1.5	1.6
In	4.2	4.5	4.4	4.1
Cd	0.3	0.3	0.3	0.3
Mo	0.1	0.1	0.1	0.1
Sn	1.1	1.1	1.2	1.0
W	1.0	0.3	1.8	1.0
UO_2	< 1 %	< 1 %	< 1 %	< 1 %

Table A11 List of cross sections for test bundle CORA-9

Sample	Sample length	Elevation bottom	Elevation top	Comments
9-a1	145 mm	-177 mm	-32 mm	Add. vertical section
Cut	2 mm			
9-06	13 mm	-30 mm	-17 mm	Horiz. cross sect., lower spacer
Cut	2 mm			
9-a2	53 mm	-15 mm	38 mm	
Cut	2 mm			Transition round - square
9-b	140 mm	40 mm	180 mm	Add. 2 vertical sections
Cut	2 mm			
9-01	13 mm	182 mm	195 mm	Horizontal cross section
Cut	2 mm			
9-c	140 mm	197 mm	337 mm	
Cut	2 mm			
9-02	13 mm	339 mm	352 mm	Horizontal cross section
Cut	2 mm			
9-d	140 mm	354 mm	494 mm	
Cut	2 mm			
9-03	13 mm	496 mm	509 mm	Horizontal cross section
Cut	2 mm			
9-e	140 mm	511 mm	651 mm	
Cut	2 mm			
9-04	13 mm	653 mm	666 mm	Horizontal cross section
Cut	2 mm			
9-f	140 mm	668 mm	808 mm	
Cut	2 mm			
9-g	30 mm	810 mm	848 mm	
Cut	2 mm			

9-05	13 mm	850 mm	863 mm	Horiz. cross sect., Upper spacer
Cut	2 mm			
9-h	140 mm	865 mm	1005 mm	
Cut	2 mm			
9-i	140 mm	1007 mm	1147 mm	
Cut	2 mm			Above Shroud
9-j	xx mm	1149 mm	xxxx mm	Upper remnant

Table A12 List of cross sections for test bundle CORA-7

Sample	Sample length	Elevation bottom	top	Comments
7-a	xxx mm	-xxx mm	-60 mm	Lower remnant
Cut	2 mm			
7-01a	13 mm	-58 mm	-45 mm	Horizontal cross section
Cut	2 mm			
7-01	13 mm	-43 mm	-30 mm	Horiz. cross sect., lower spacer
Cut	2 mm			
7-01b	13 mm	-28 mm	-15 mm	Horizontal cross section
Cut	2 mm			
7-b	125 mm	-13 mm	112 mm	
Cut	2 mm			
7-02	13 mm	114 mm	127 mm	Horizontal cross section
Cut	2 mm			
7-c	140 mm	129 mm	269 mm	
Cut	2 mm			
7-03	13 mm	271 mm	284 mm	Horizontal cross section
Cut	2 mm			
7-d	140 mm	286 mm	426 mm	With 2 add. vert. sections (7-d-L)
Cut	2 mm			
7-e	37 mm	428 mm	465 mm	With additional vertical section
Cut	2 mm			
7-04	13 mm	467 mm	480 mm	Horiz. cross sect., central spacer
Cut	2 mm			
7-f1	34 mm	482 mm	516 mm	With 2 add. vert. sect. (7-f1-R)
Cut	2 mm			
7-f2	104 mm	518 mm	622 mm	With additional vertical section
Cut	2 mm			

7-05	13 mm	624 mm	637 mm	Horizontal cross section
Cut	2 mm			
7-g	140 mm	639 mm	779 mm	
Cut	2 mm			
7-06	13 mm	781 mm	794 mm	Horizontal cross section
Cut	2 mm			
7-h	54 mm	796 mm	848 mm	
Cut	2 mm			
7-07	13 mm	850 mm	863 mm	Horiz. cross sect., upper spacer
Cut	2 mm			
7-i	140 mm	865 mm	1005 mm	
Cut	2 mm			Above heated zone
7-j	140 mm	1007 mm	1147 mm	
Cut	2 mm			
7-k	81 mm	1149 mm	1230 mm	
Cut	2 mm			
7-l	xx mm	1232 mm	xxxx mm	Upper remnant

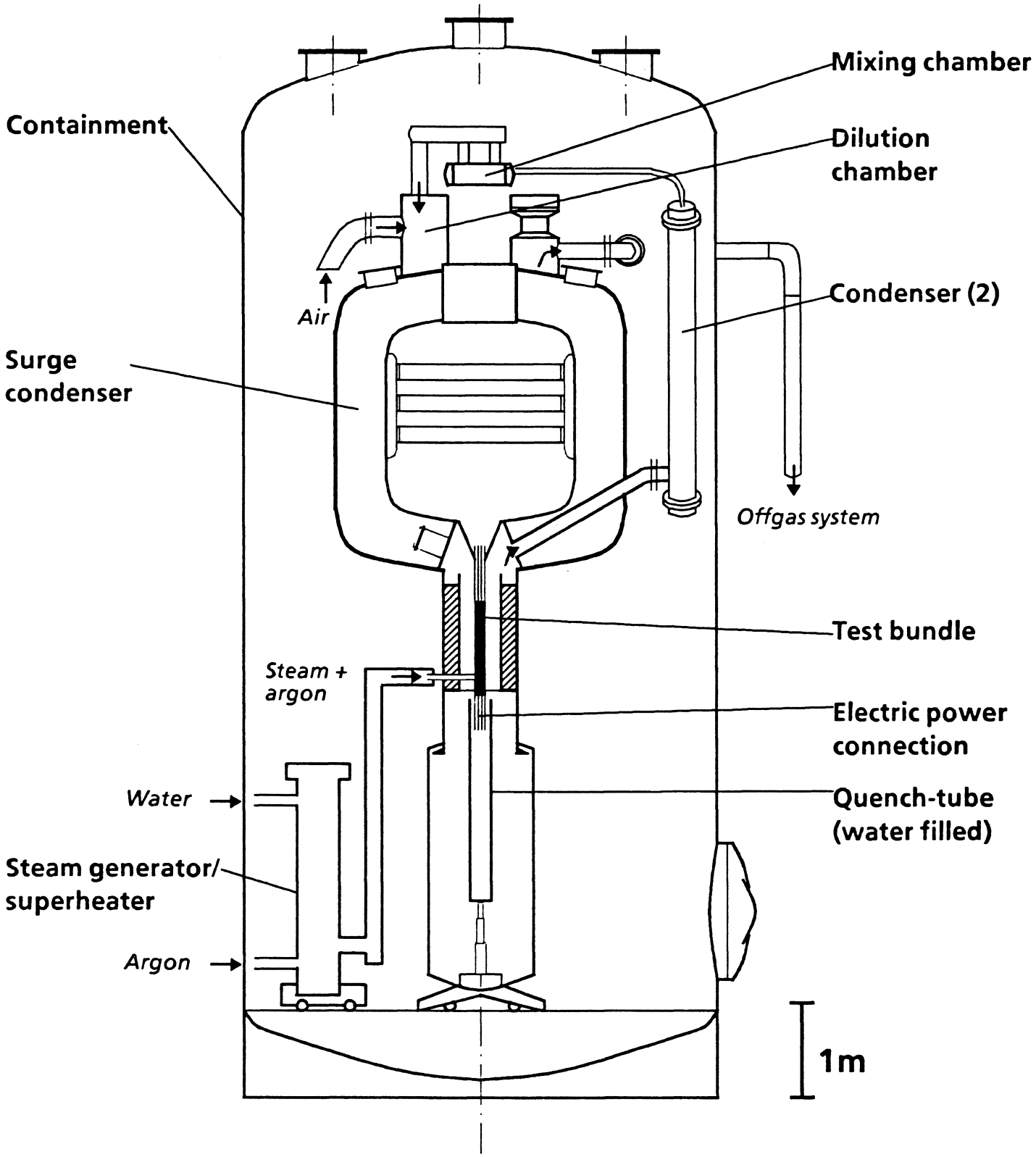

Fig.1: SFD test facility CORA, main components

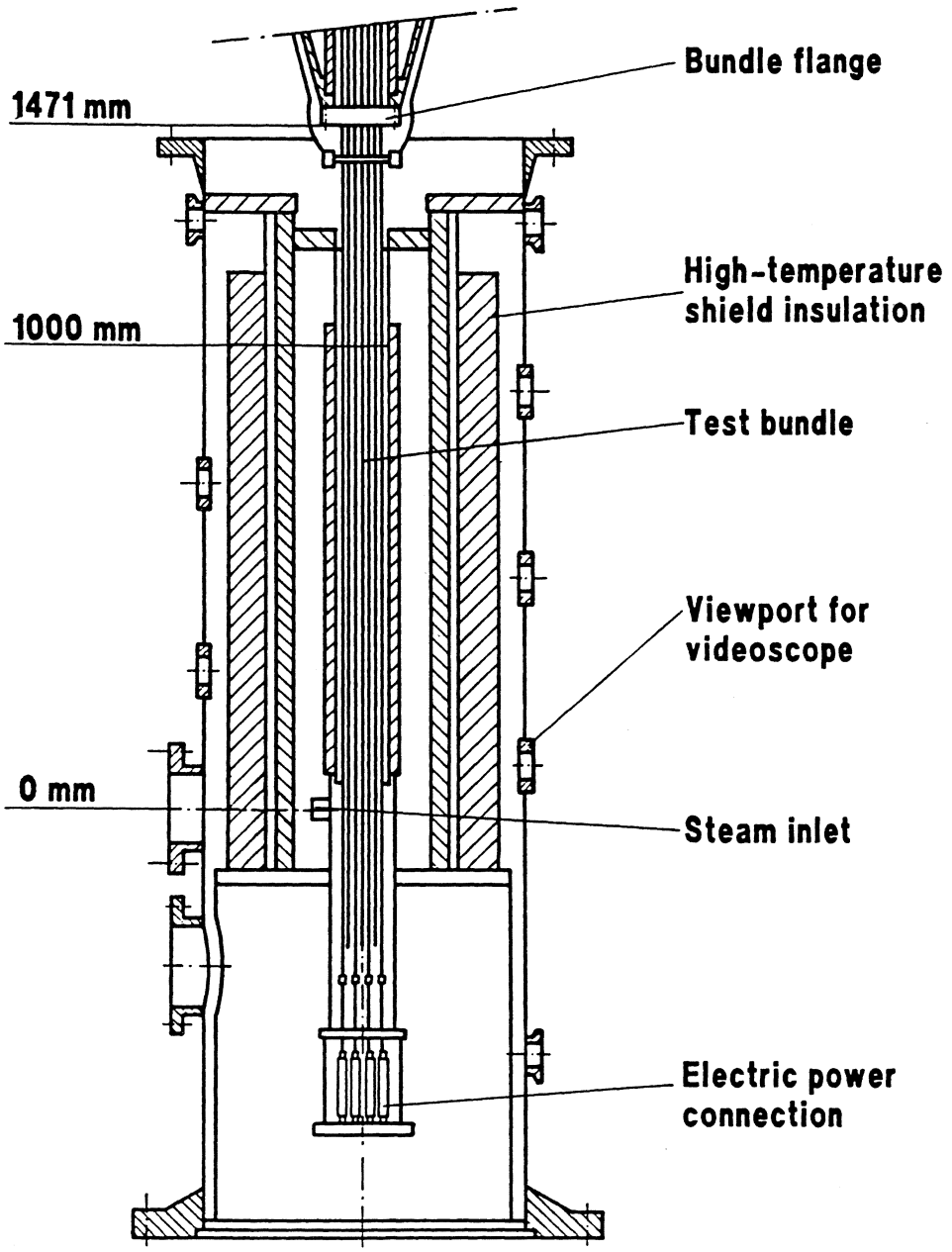

Fig. 2: CORA test section

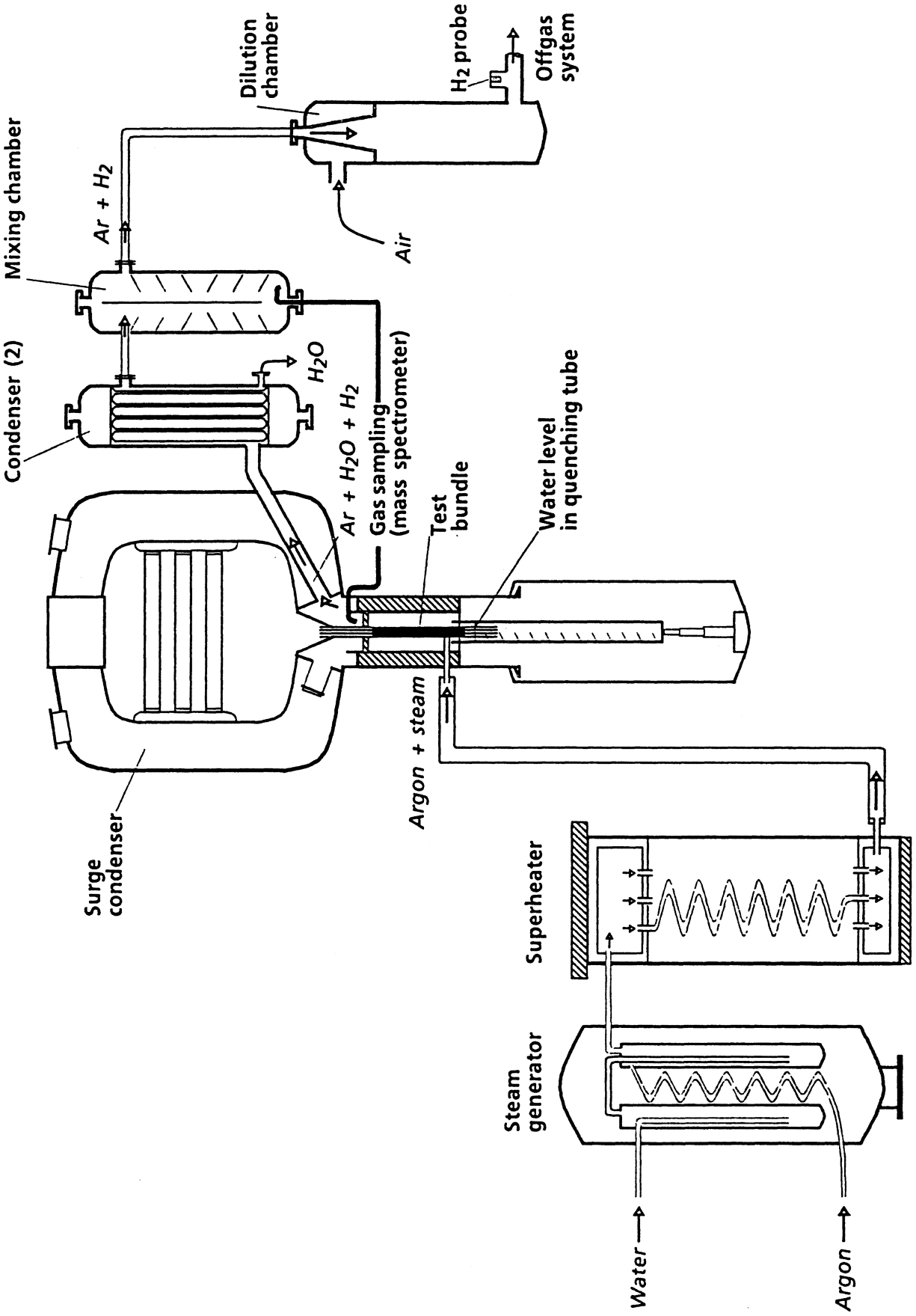

Fig.3: Simplified flow diagram of the CORA test facility

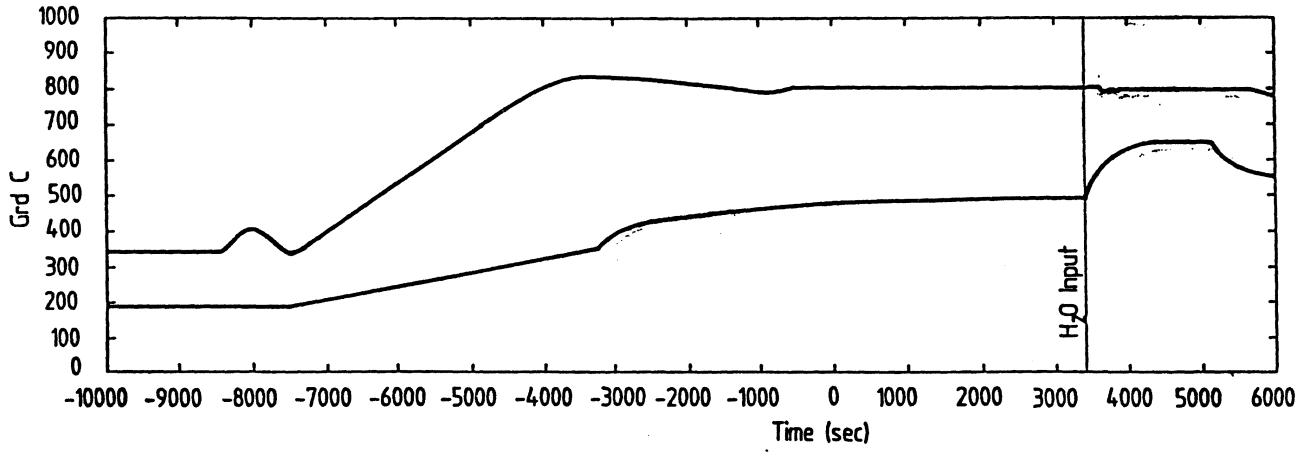

Fig. 4: "Gas temperature" at the exit of the steam superheater and at the entrance of the test train (CORA-5)

CORA - 5

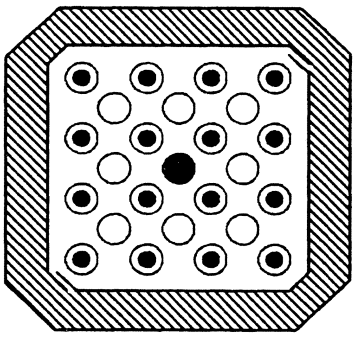

16 heated rods
8 unheated rods
1 absorber rod

CORA - 12
CORA - 15
CORA - 9

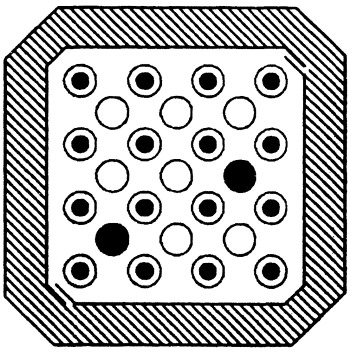

16 heated rods
7 unheated rods
2 absorber rods

CORA - 7

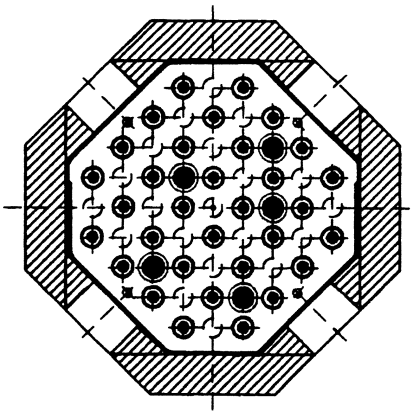

32 heated rods
20 unheated rods
5 absorber rods

Fig. 5: Test rod arrangement for bundles CORA-5, CORA-12, CORA-15, CORA-9 and CORA-7

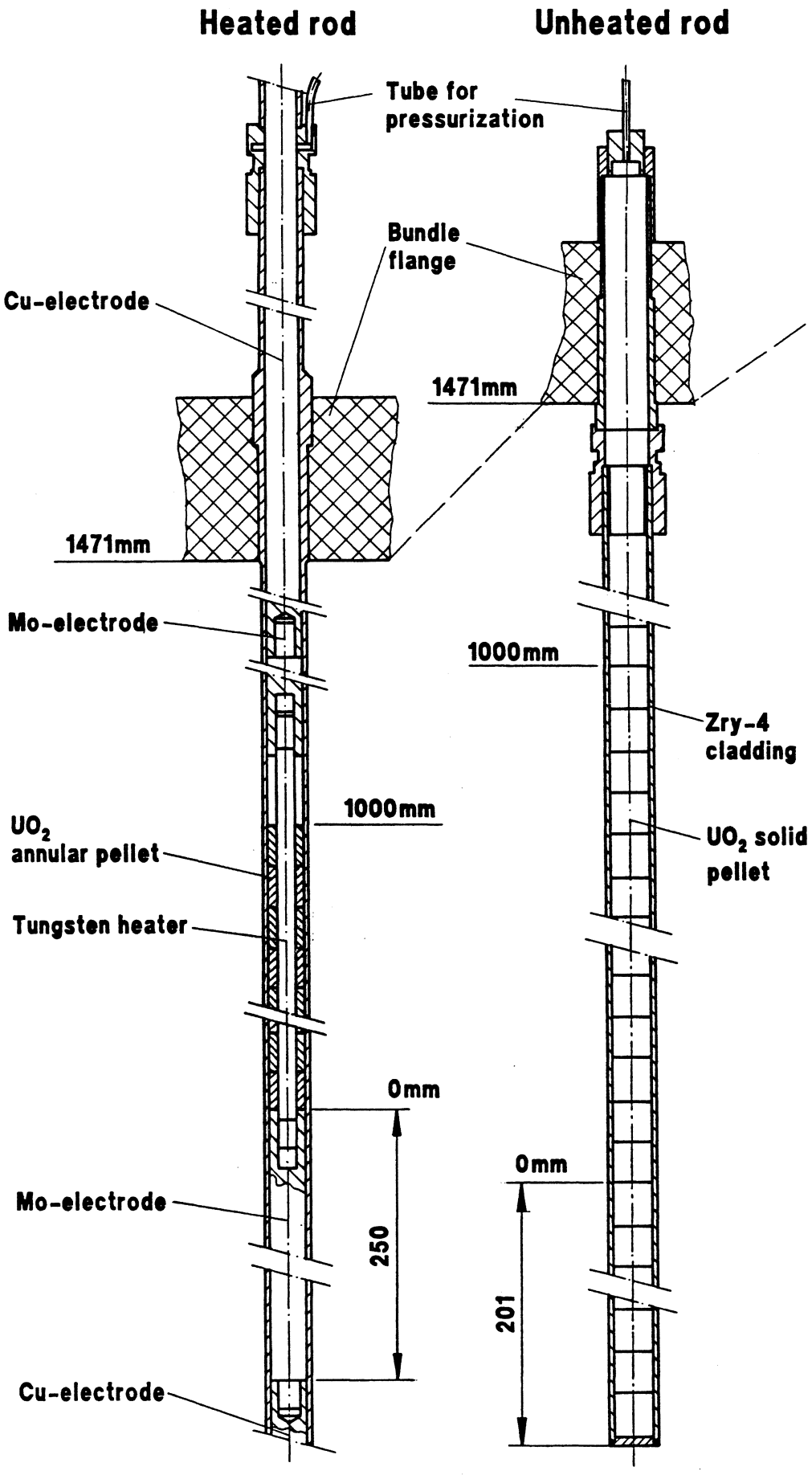

Fig. 6a: Test rod design, schematic

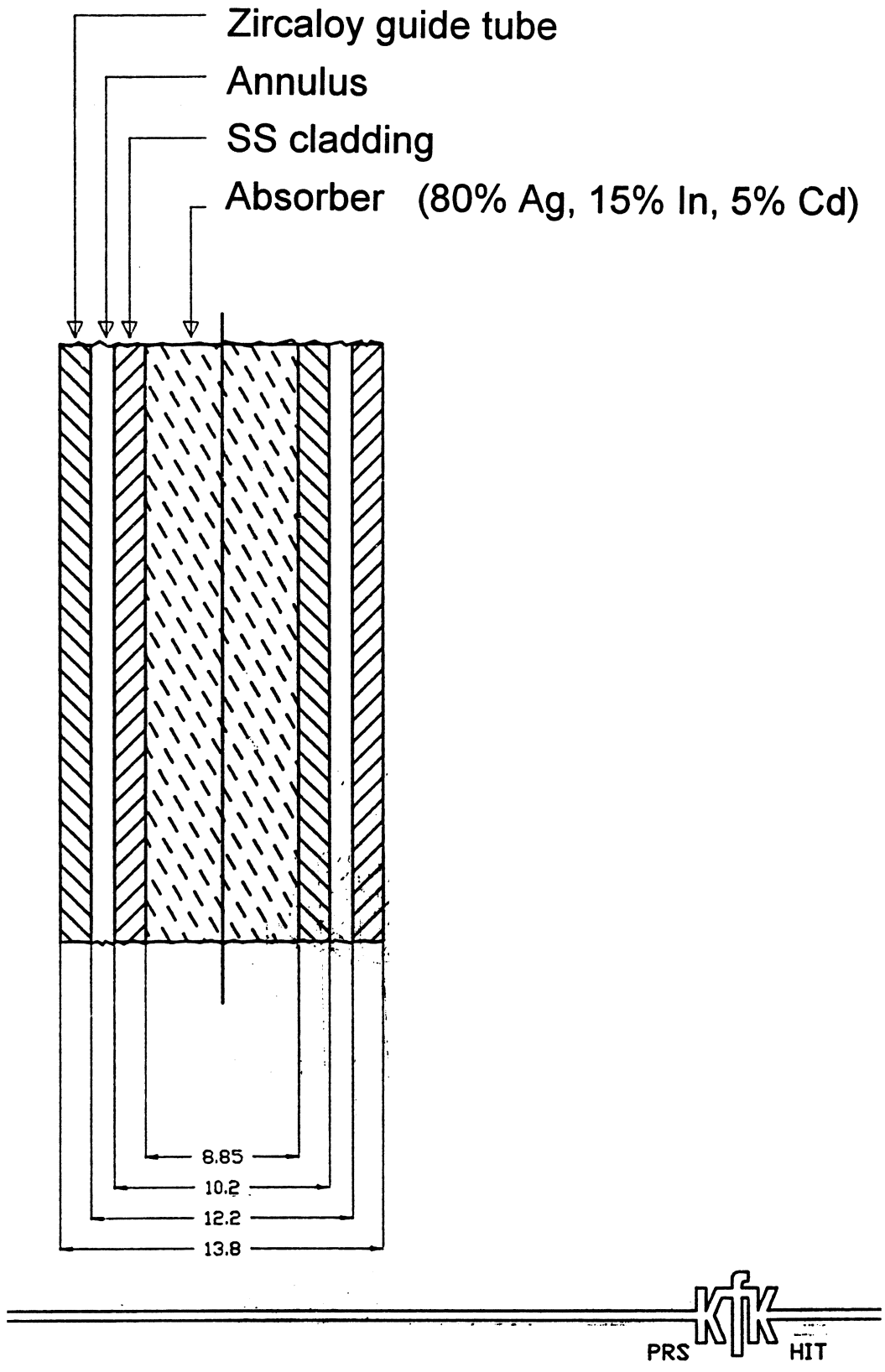

Fig. 6b: Design of the PWR-type absorber rod

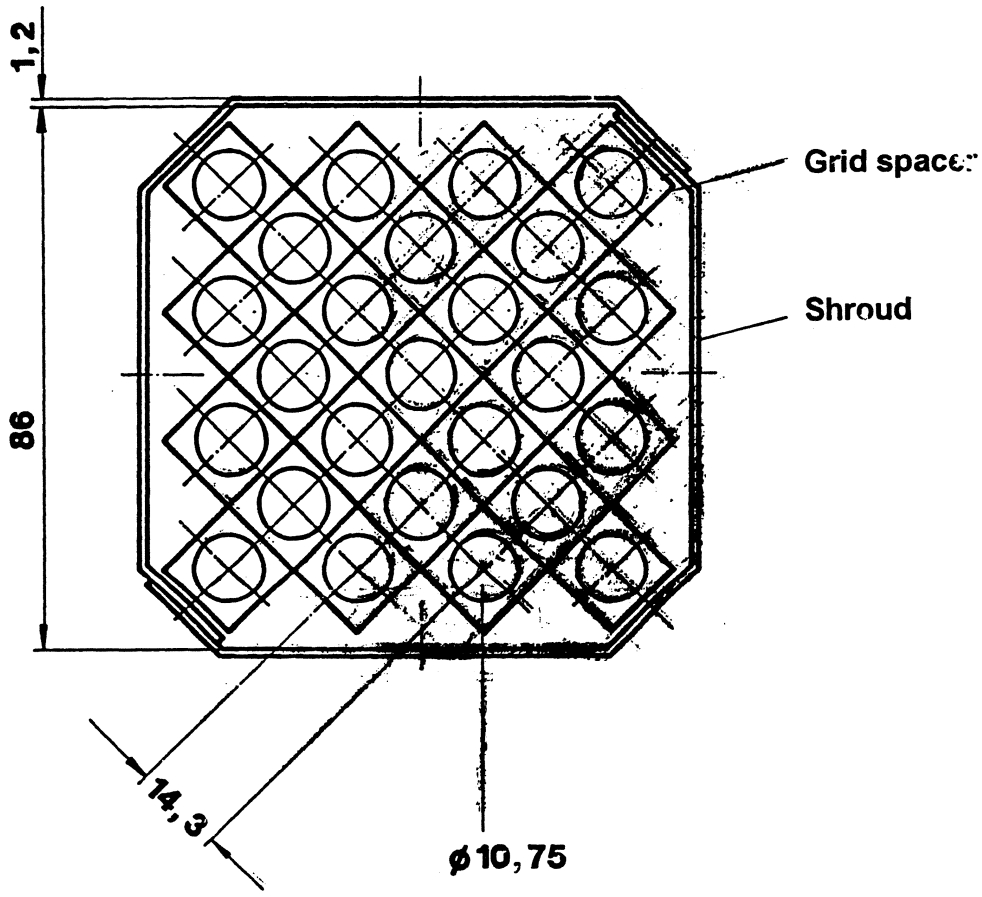

Fig. 7: Cross section of a typical CORA PWR-type bundle with shroud and grid spacer

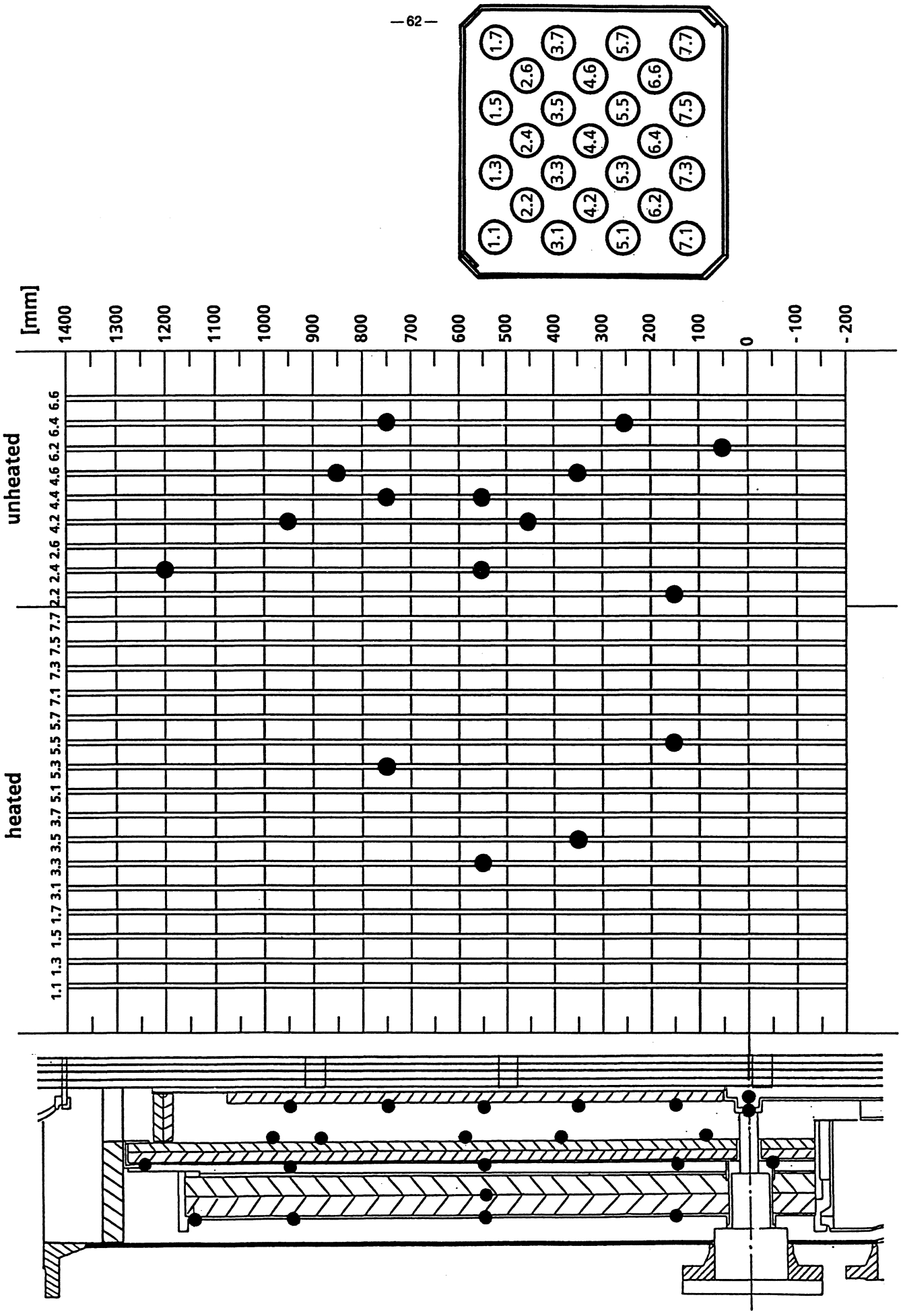

Fig. 8a: Positions of thermocouples (CORA-5)

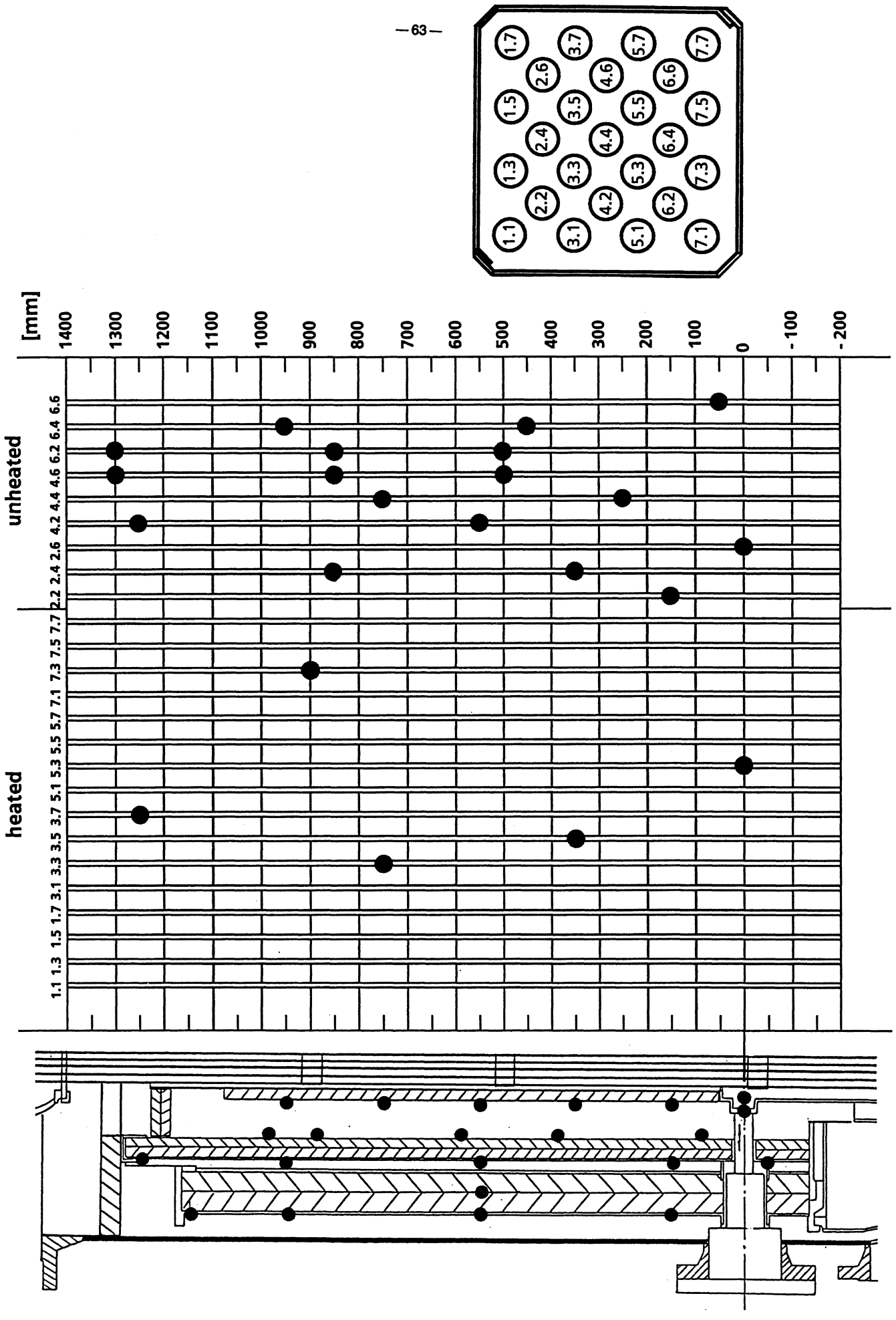

Fig. 8b: Positions of thermocouples (CORA-12)

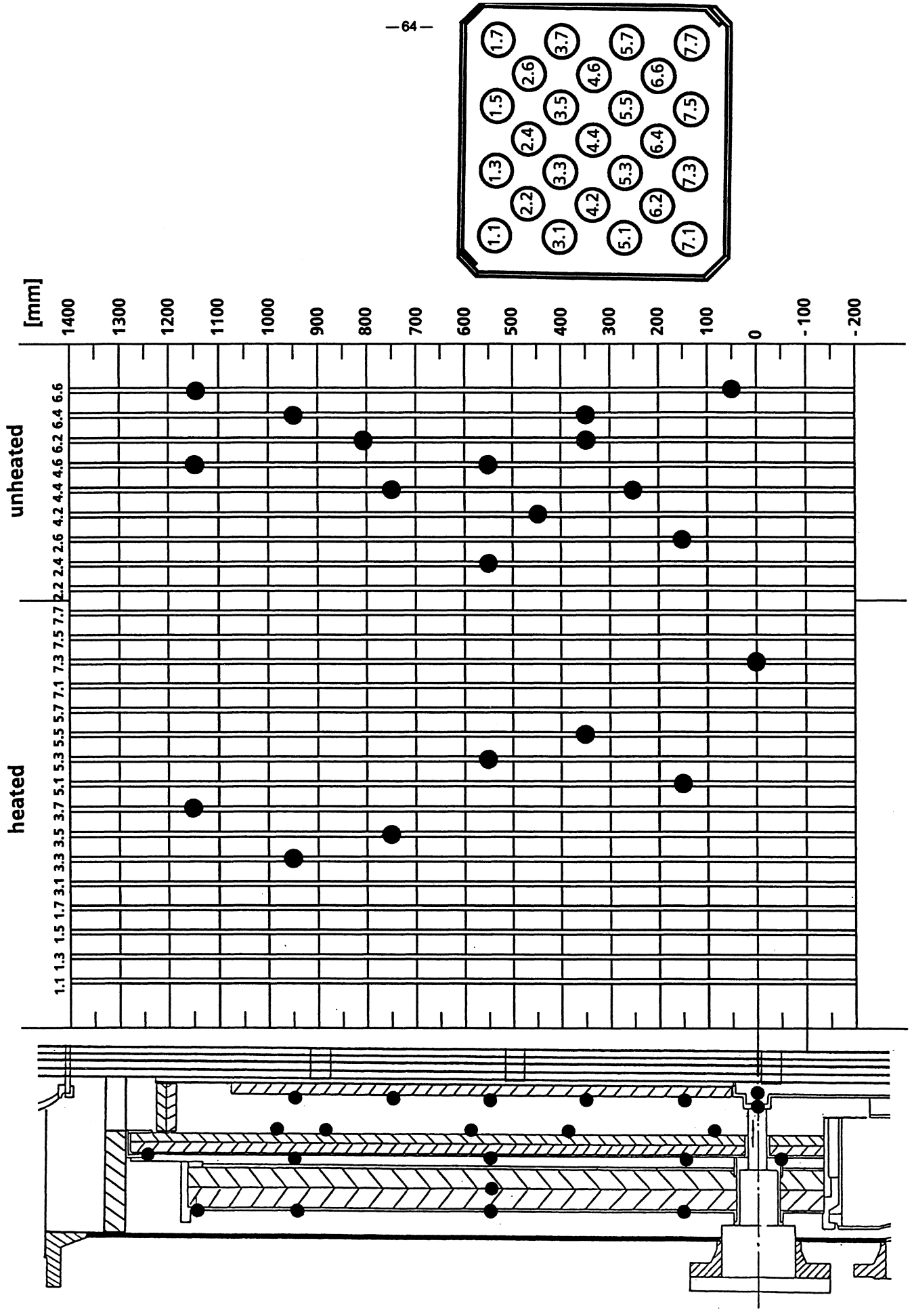

Fig. 8c: Positions of thermocouples (CORA-9)

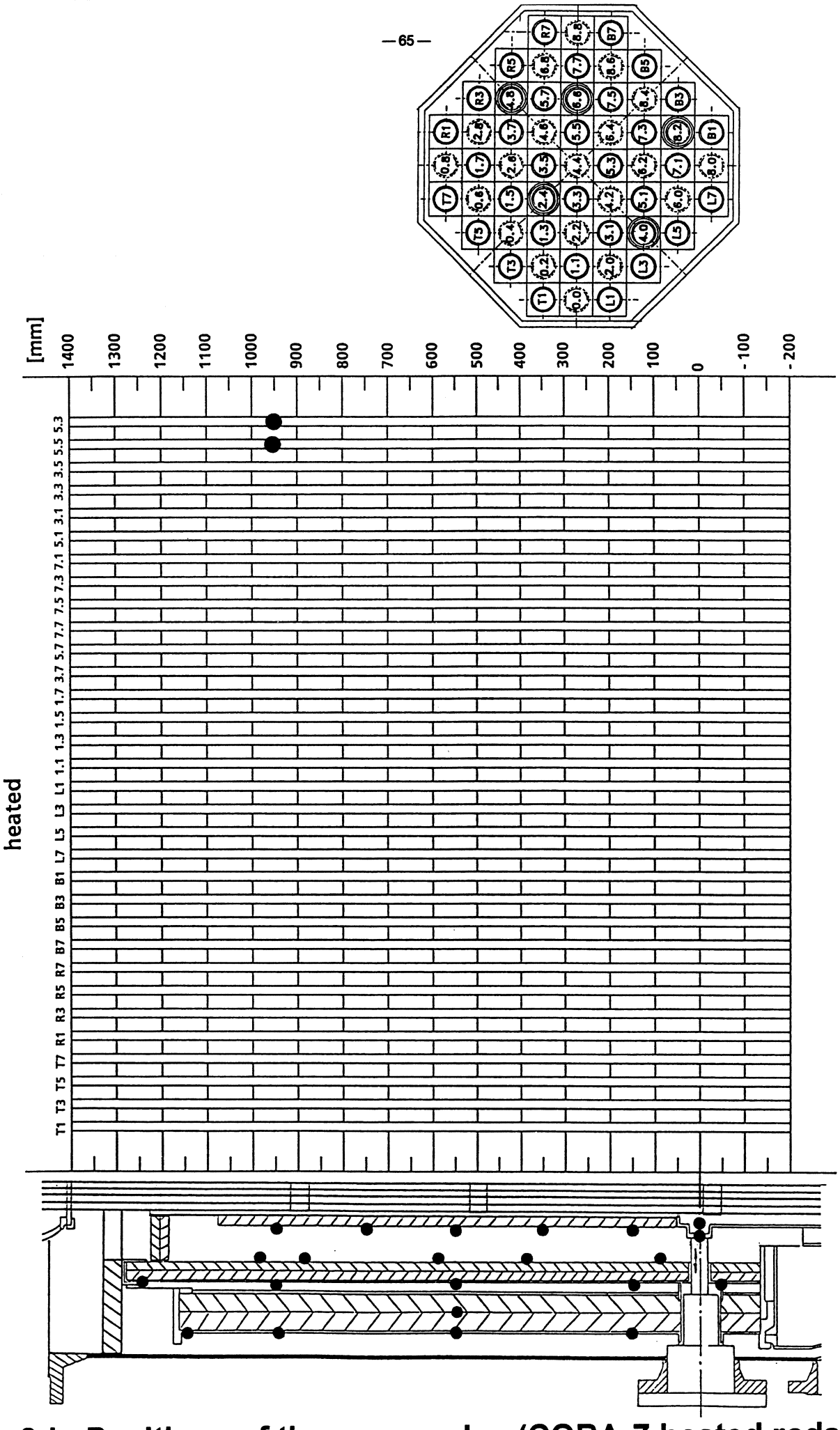

Fig. 8d: Positions of thermocouples (CORA-7 heated rods)

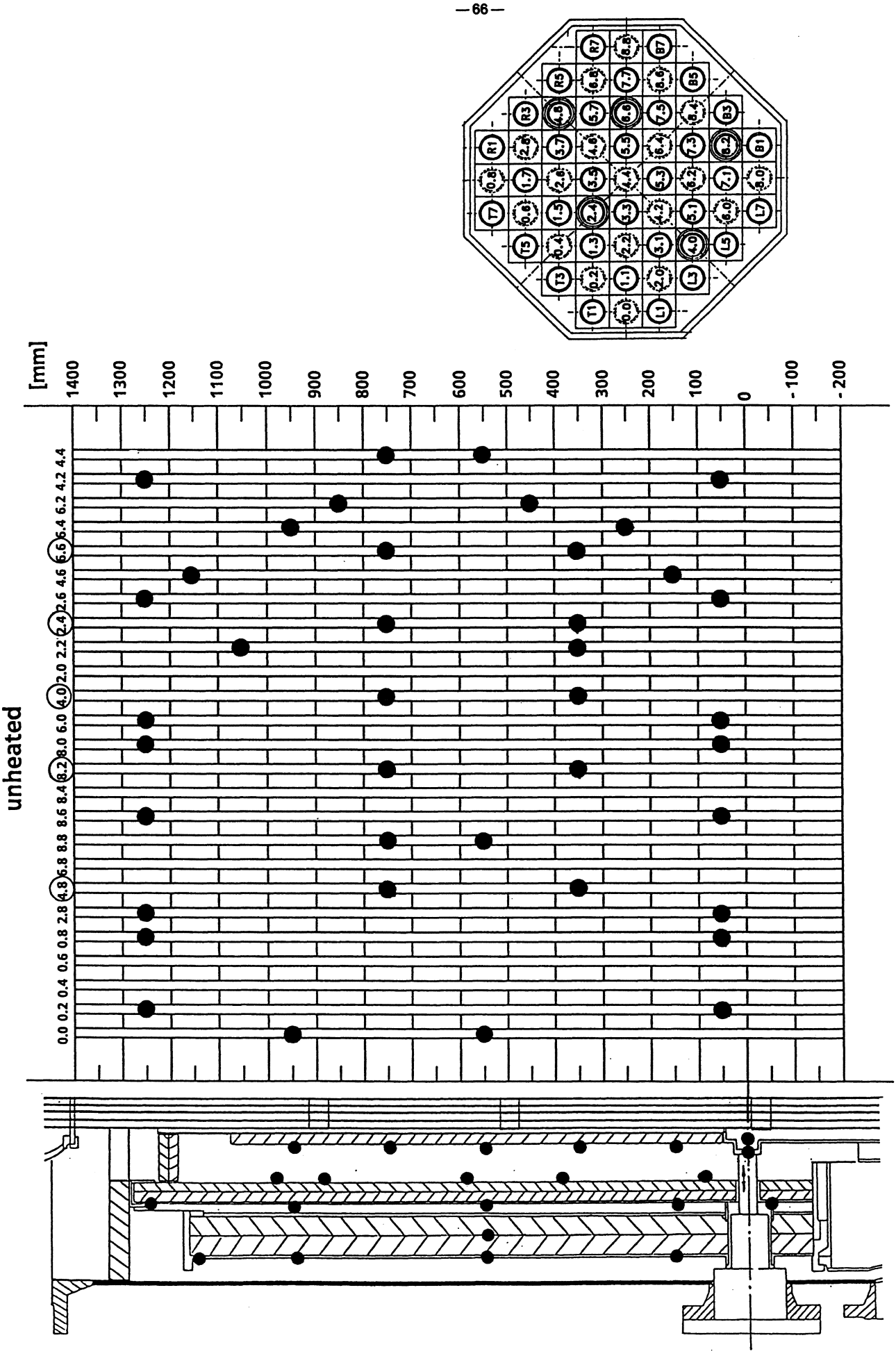

Fig. 8e: Positions of thermocouples (CORA-7 unheated rods)

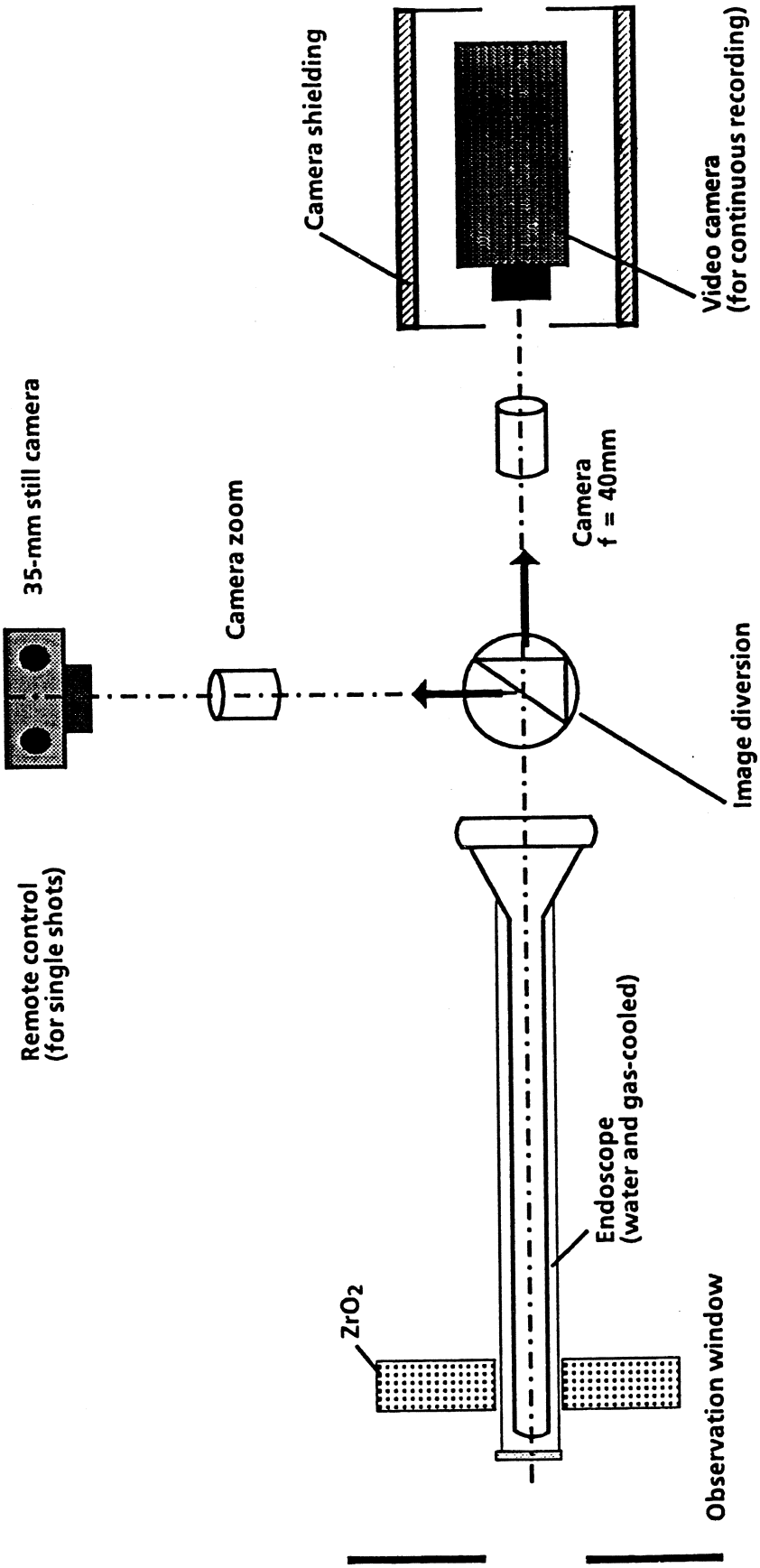

Fig.9: Videoscope system for the CORA test bundle, schematic

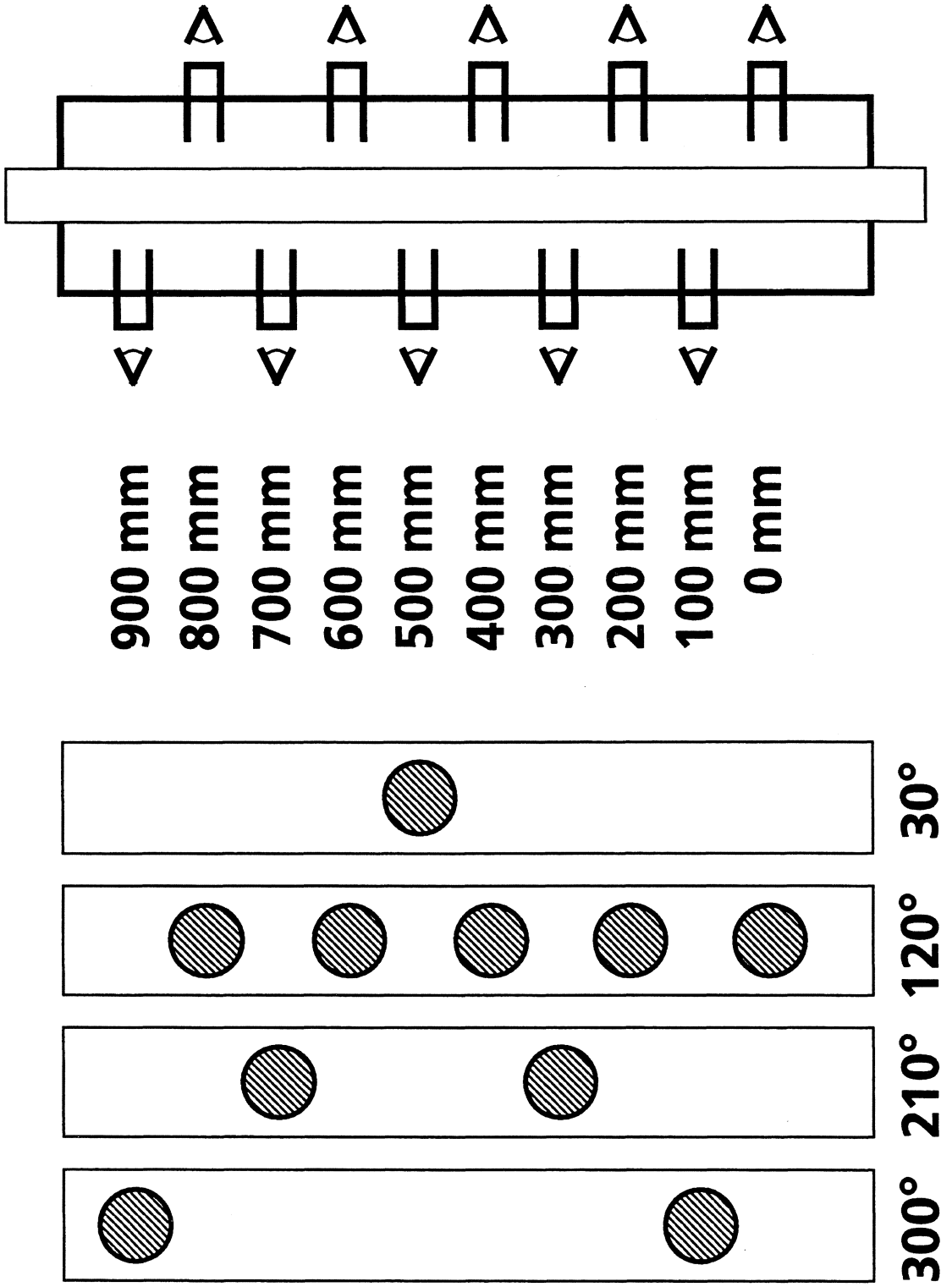

Fig. 9a: Videoscope positions of bundles CORA-5 and CORA-12

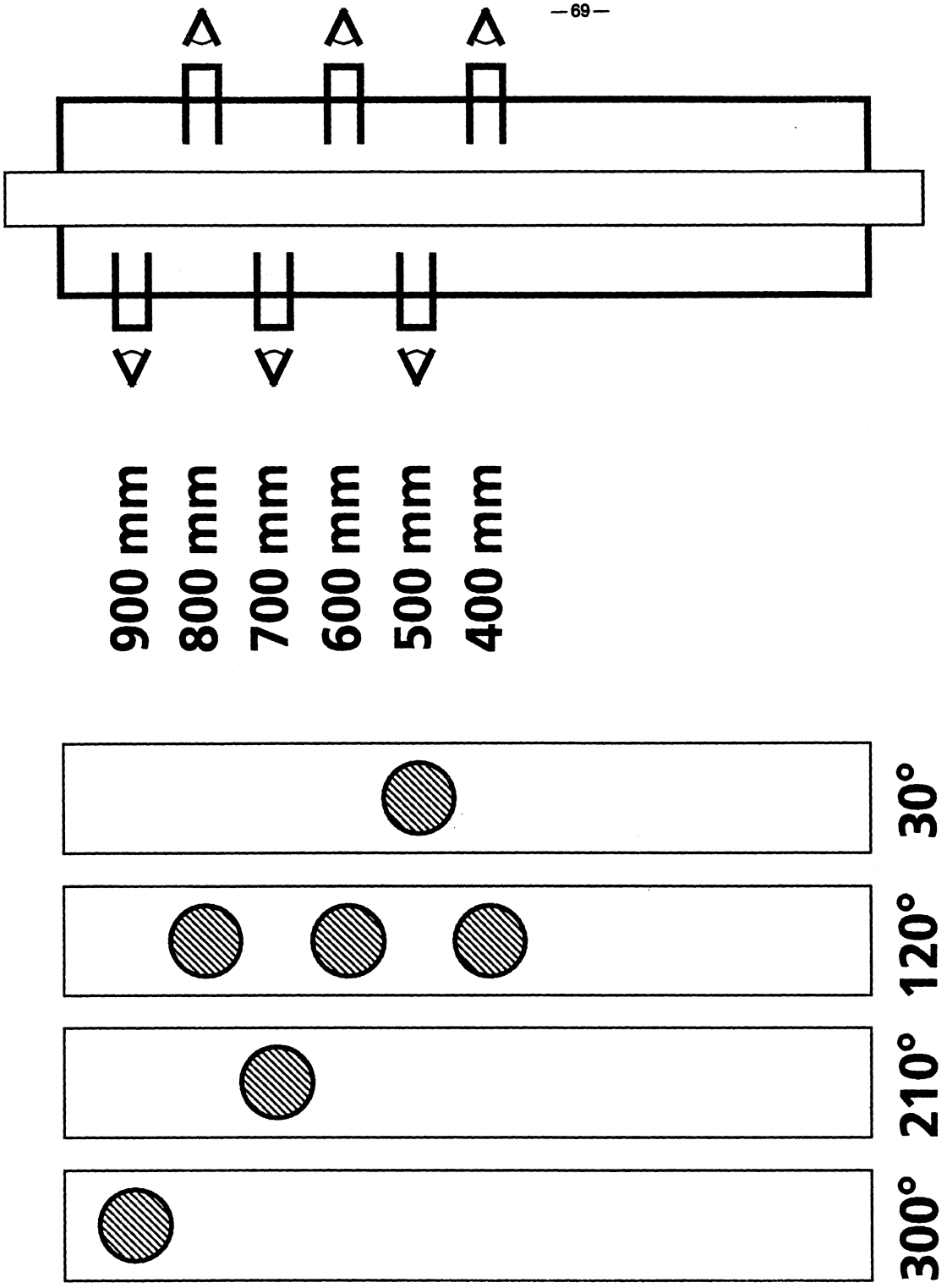

Fig. 9b: Videoscope positions of bundles CORA-9, CORA-15, and CORA 7

(a)

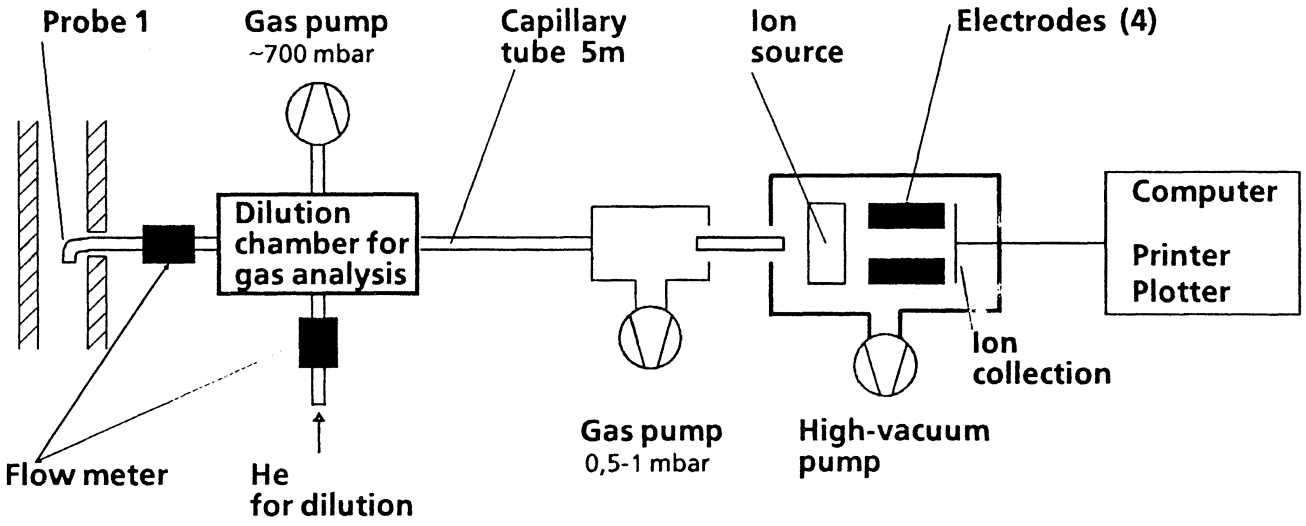

(b)

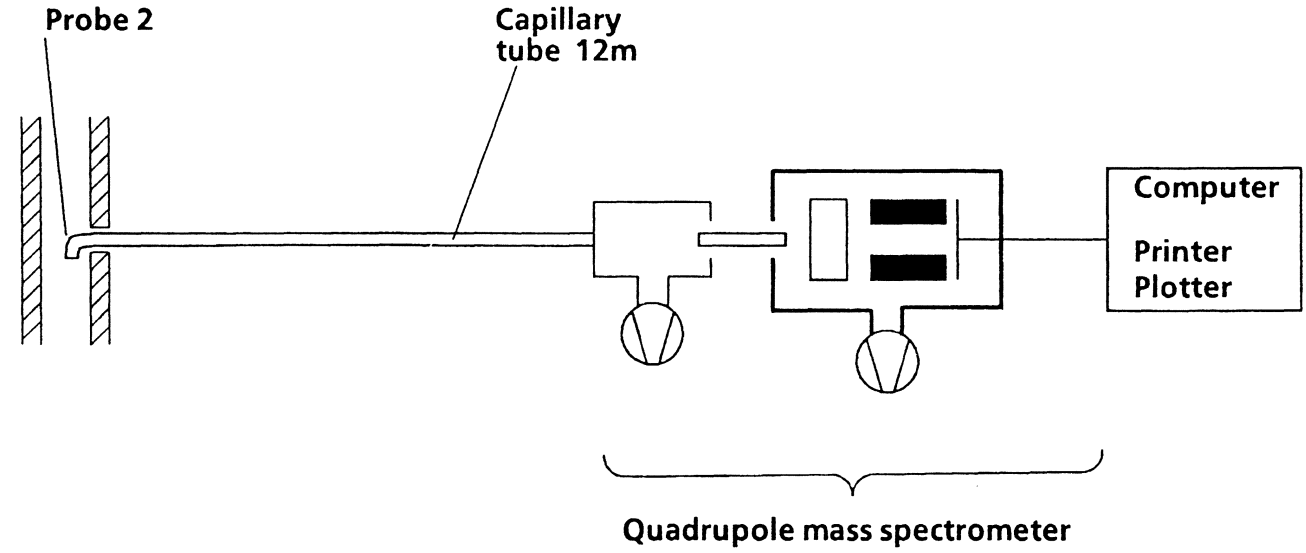

Location (a) : Outlet of test section

Location (b) : Mixing chamber

Fig. 10: Hydrogen probing at two locations of the CORA facility (see also Fig. 3). Gas analyses are performed by quadrupole mass spectrometer

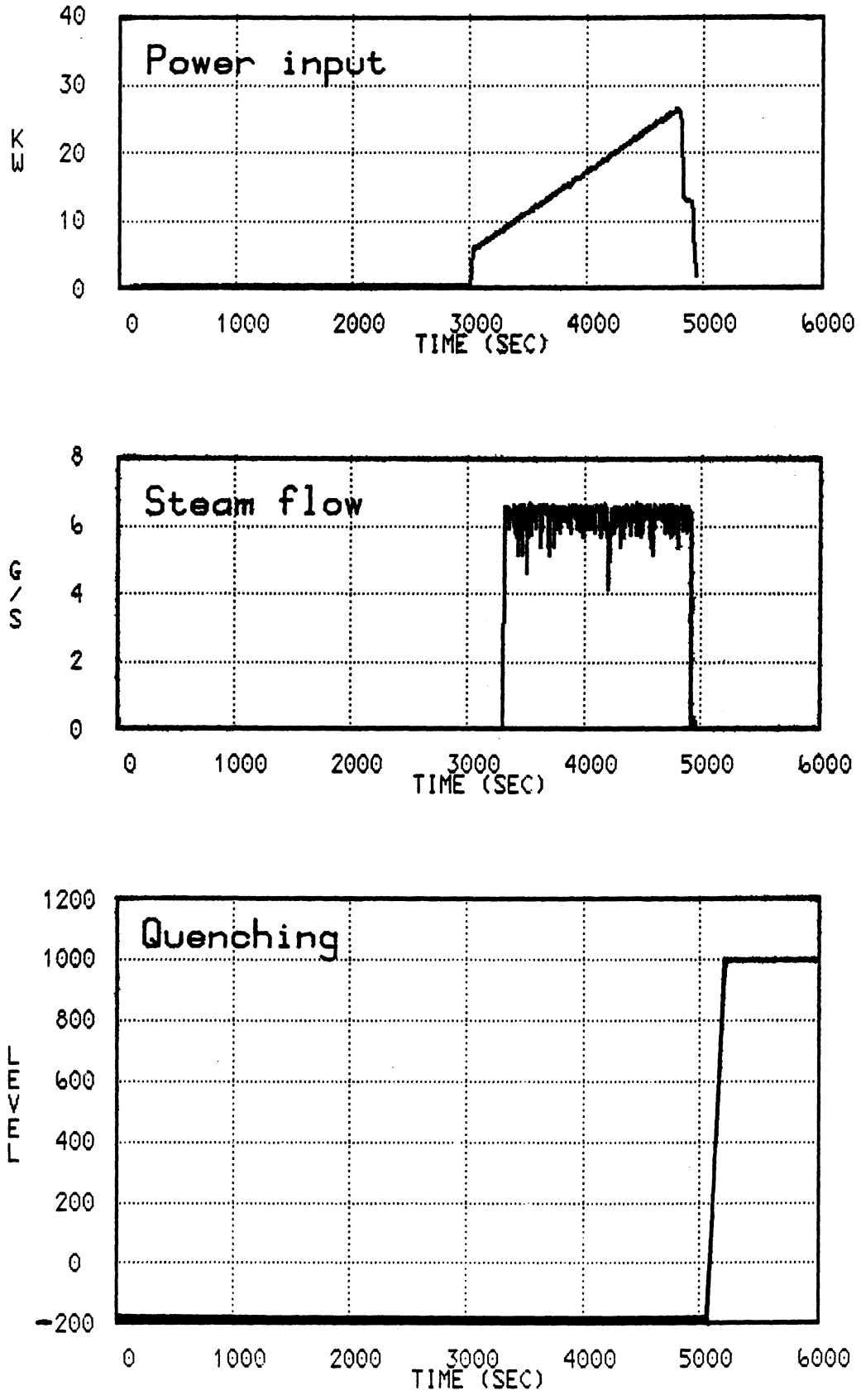

Fig.11: Test conduct of CORA-12

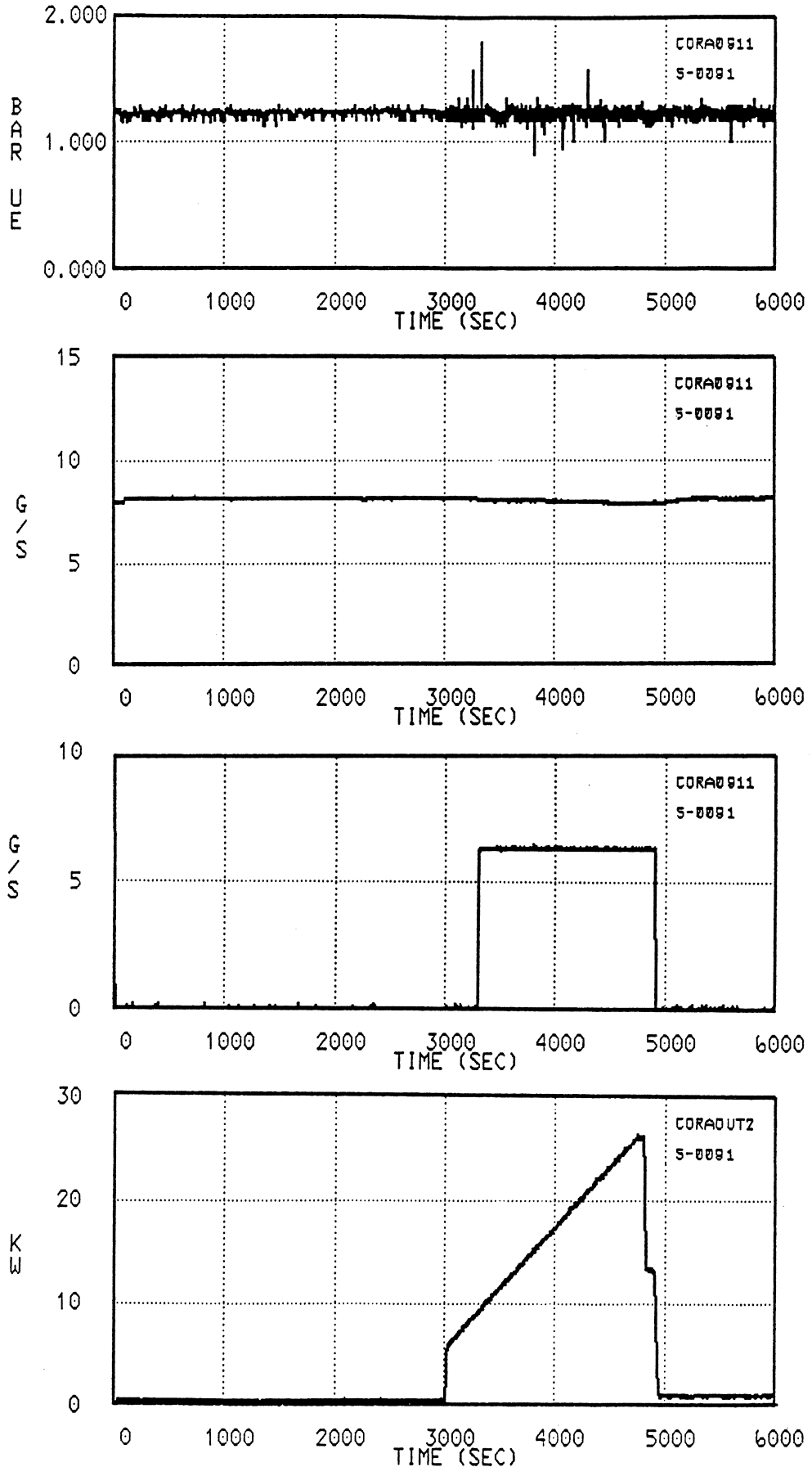

System pressure

Argon flow

Steam flow

Power

Fig.12: System pressure, argon flow, steam flow and power of CORA-15

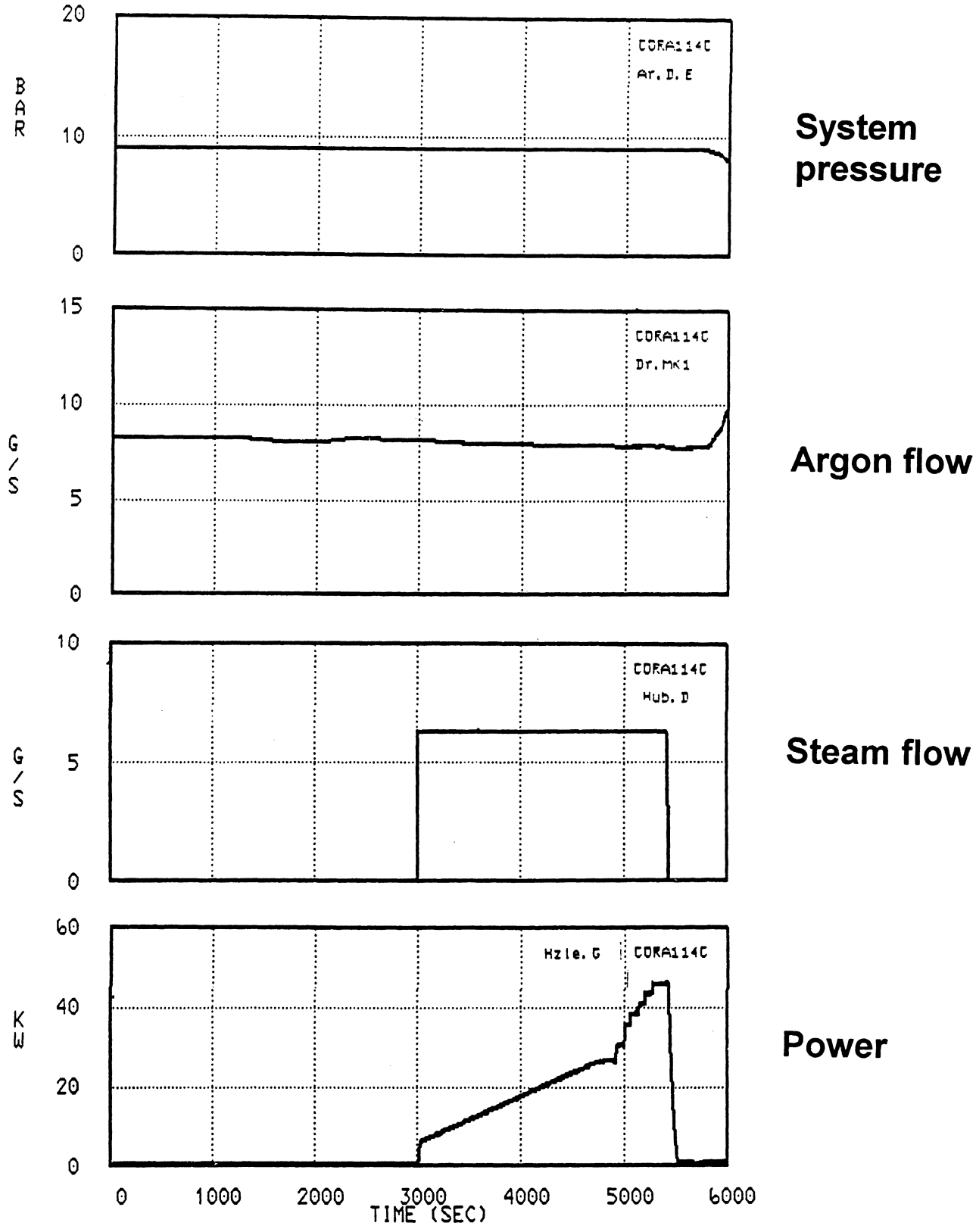

Fig.13: System pressure, argon flow, steam flow and power of CORA-9

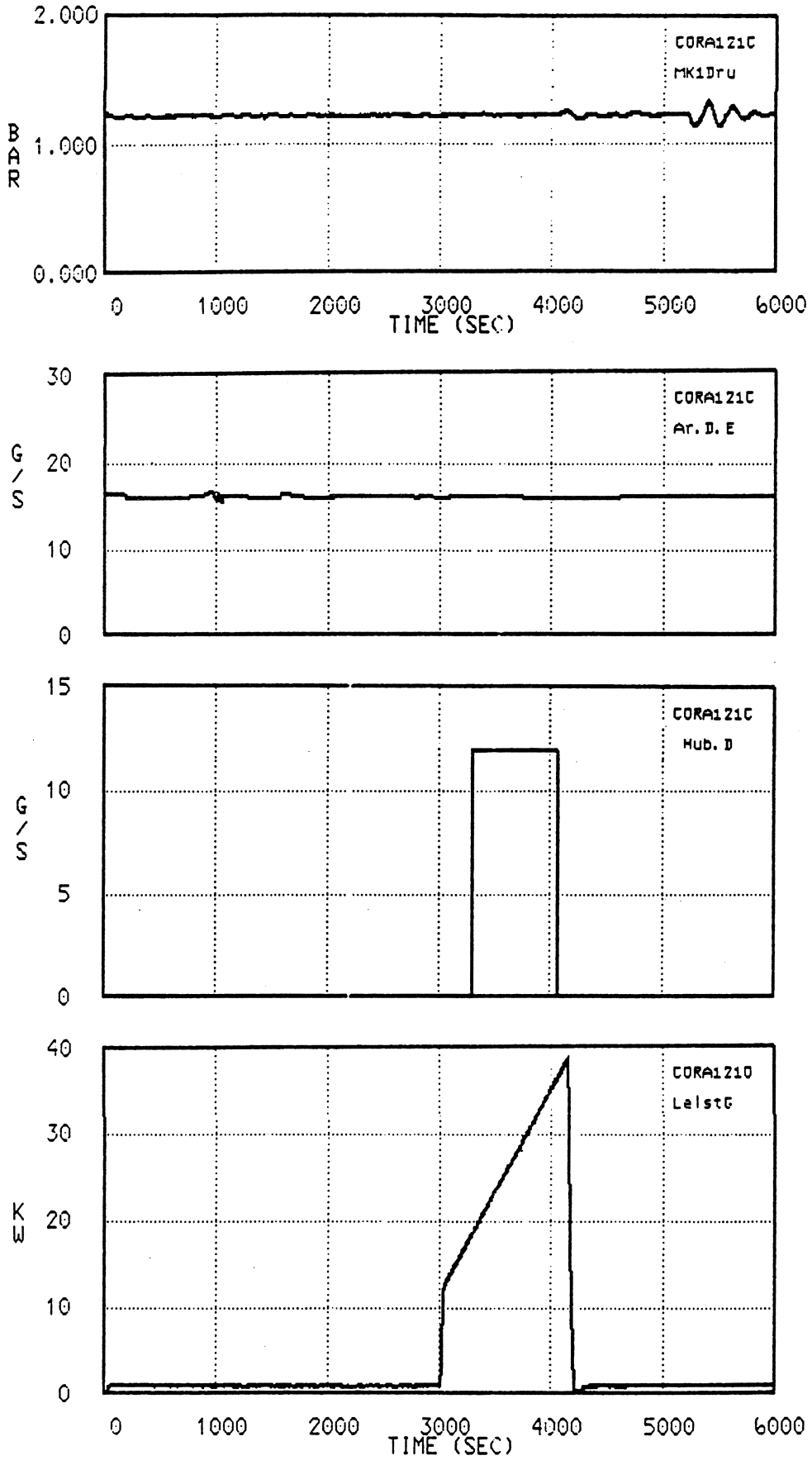

System pressure

Argon flow

Steam flow

Power

Fig.14: System pressure, argon flow, steam flow and power of CORA-7

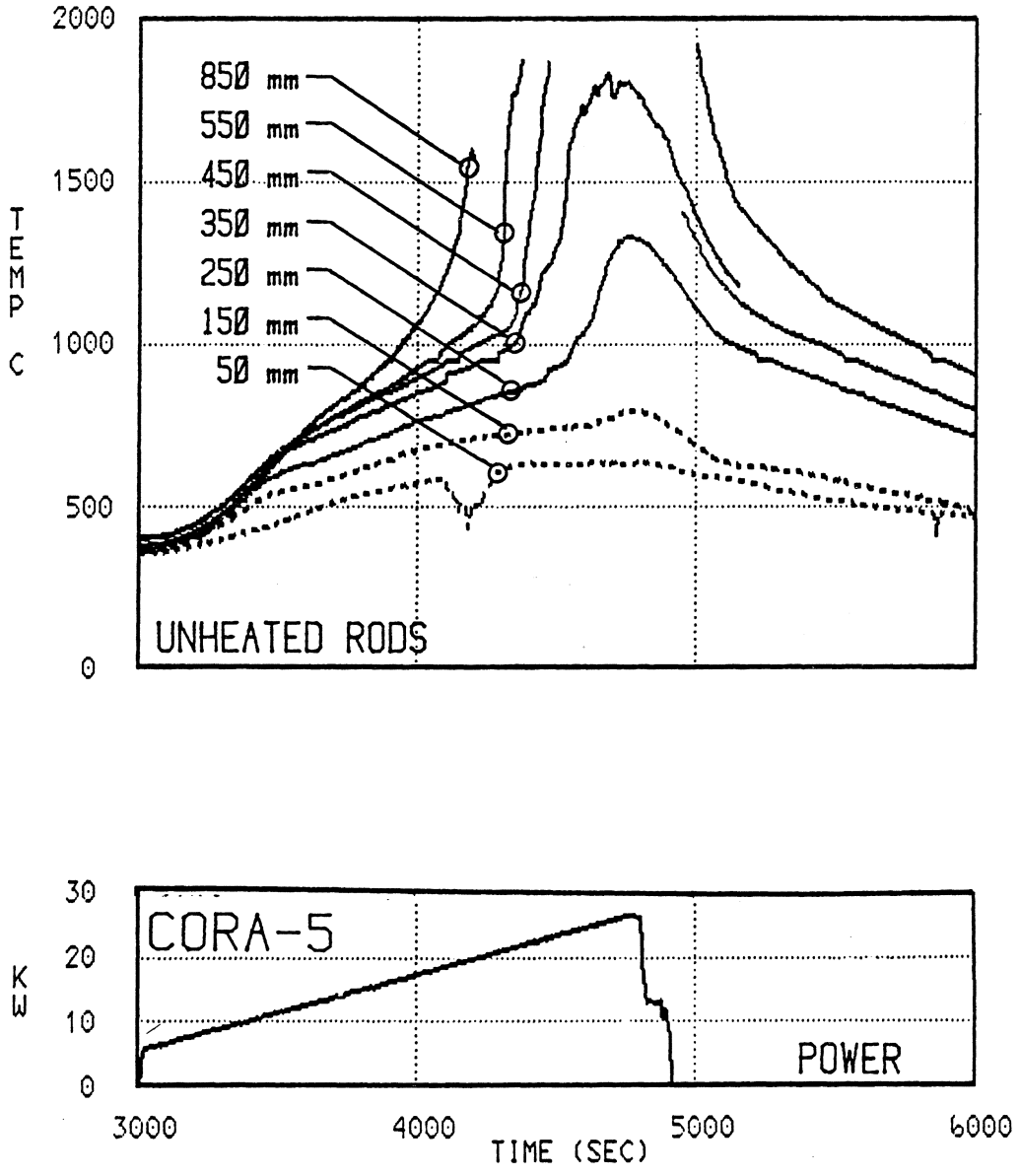

Fig.15: Temperatures of unheated rods and power history of CORA-5

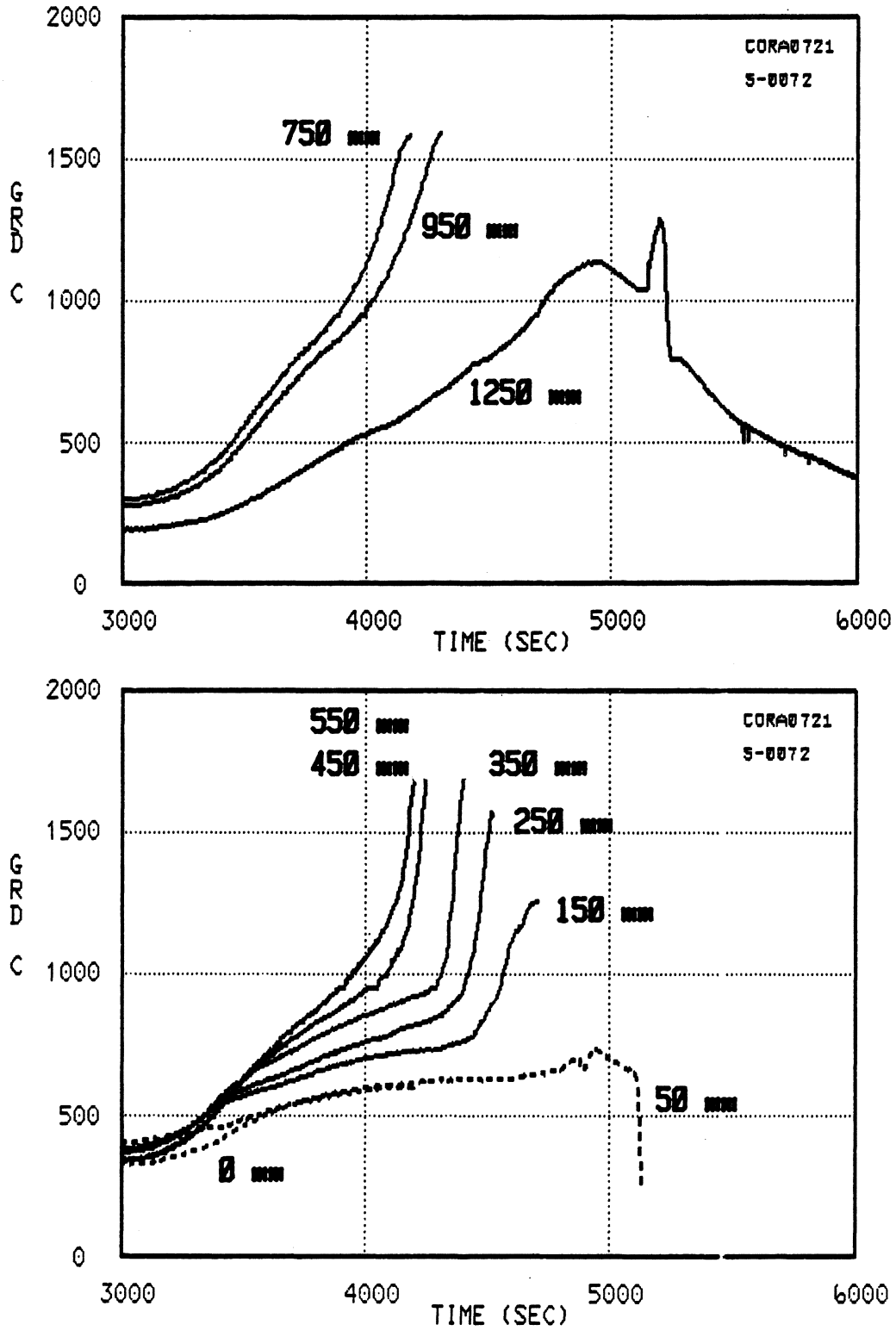

Fig.16: Temperatures of unheated rods during CORA-12

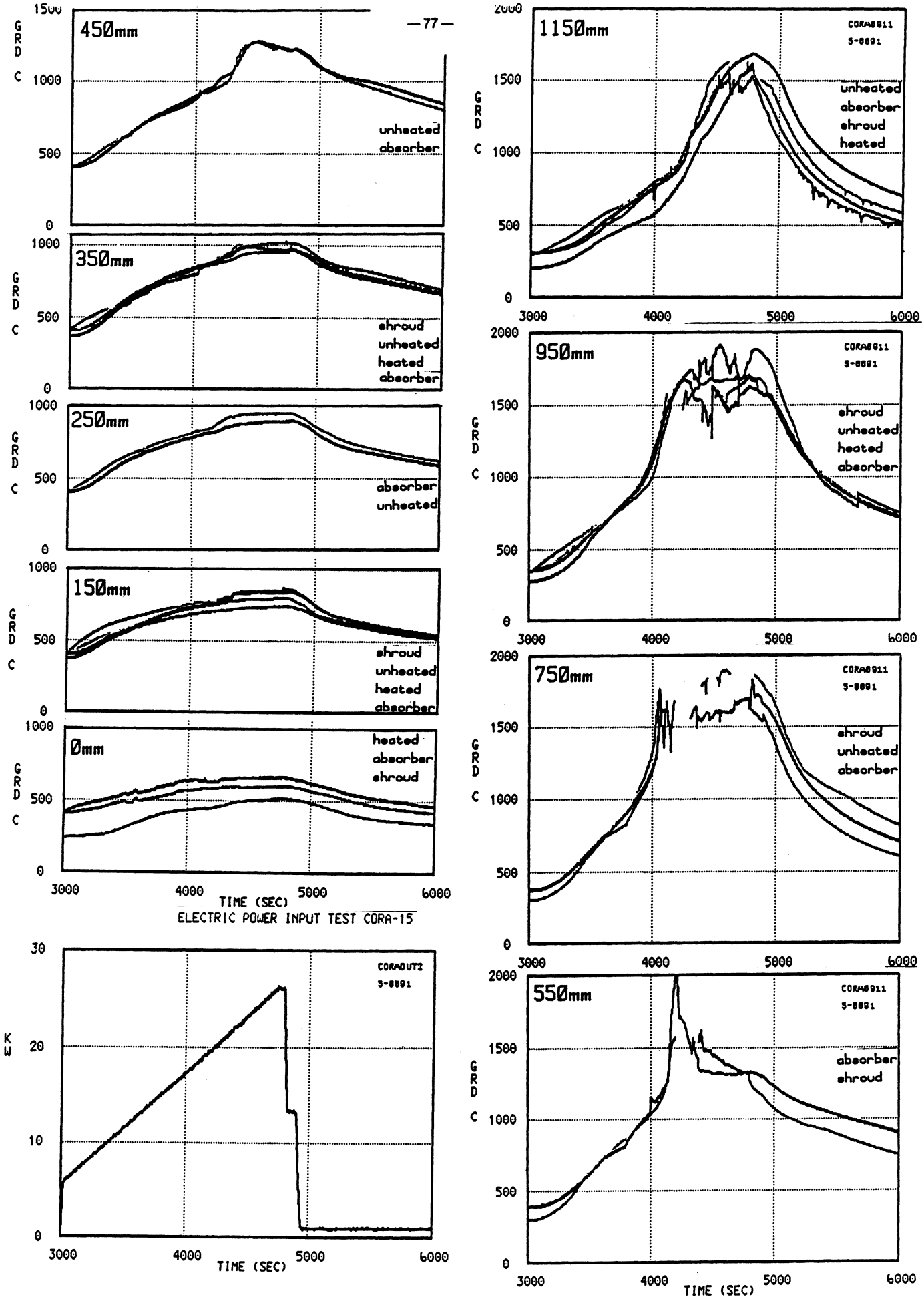

Fig.17: Temperatures at different elevations during CORA-15

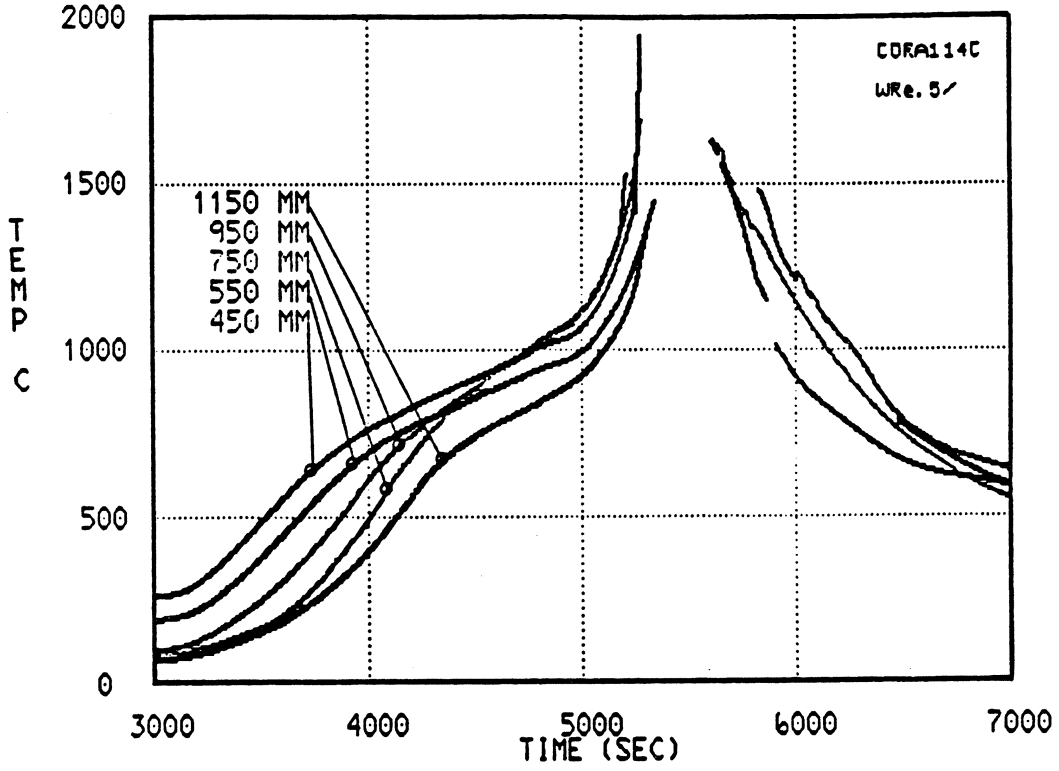

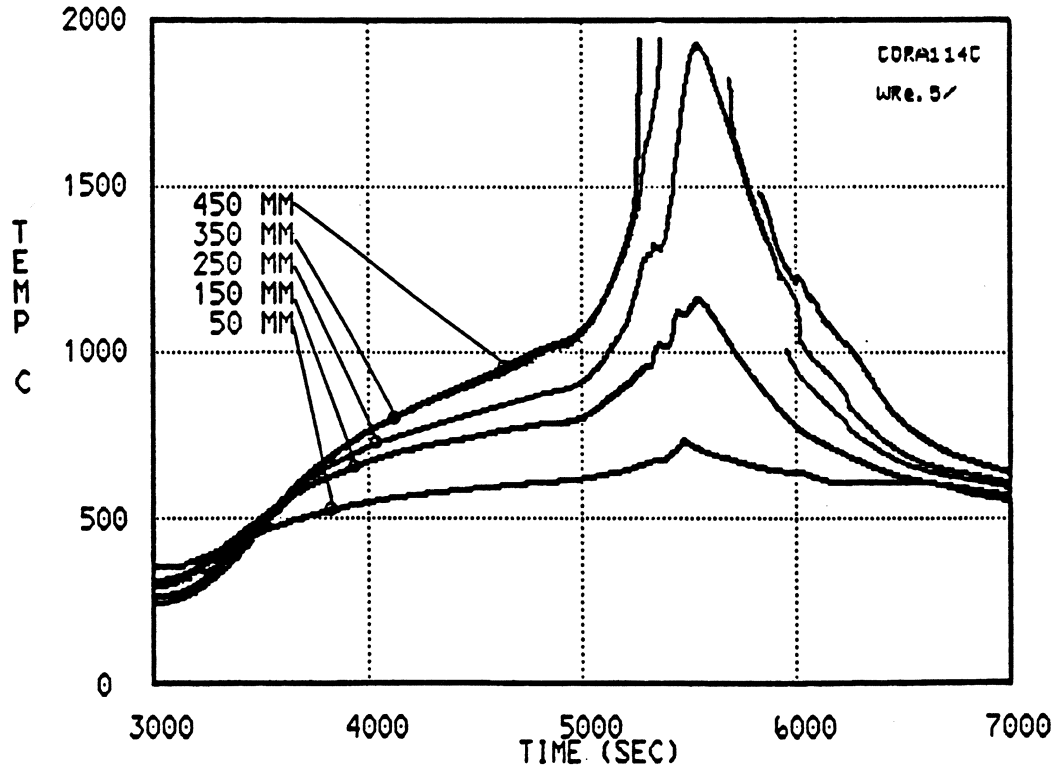

Fig.18: Temperatures of unheated rods during CORA-9

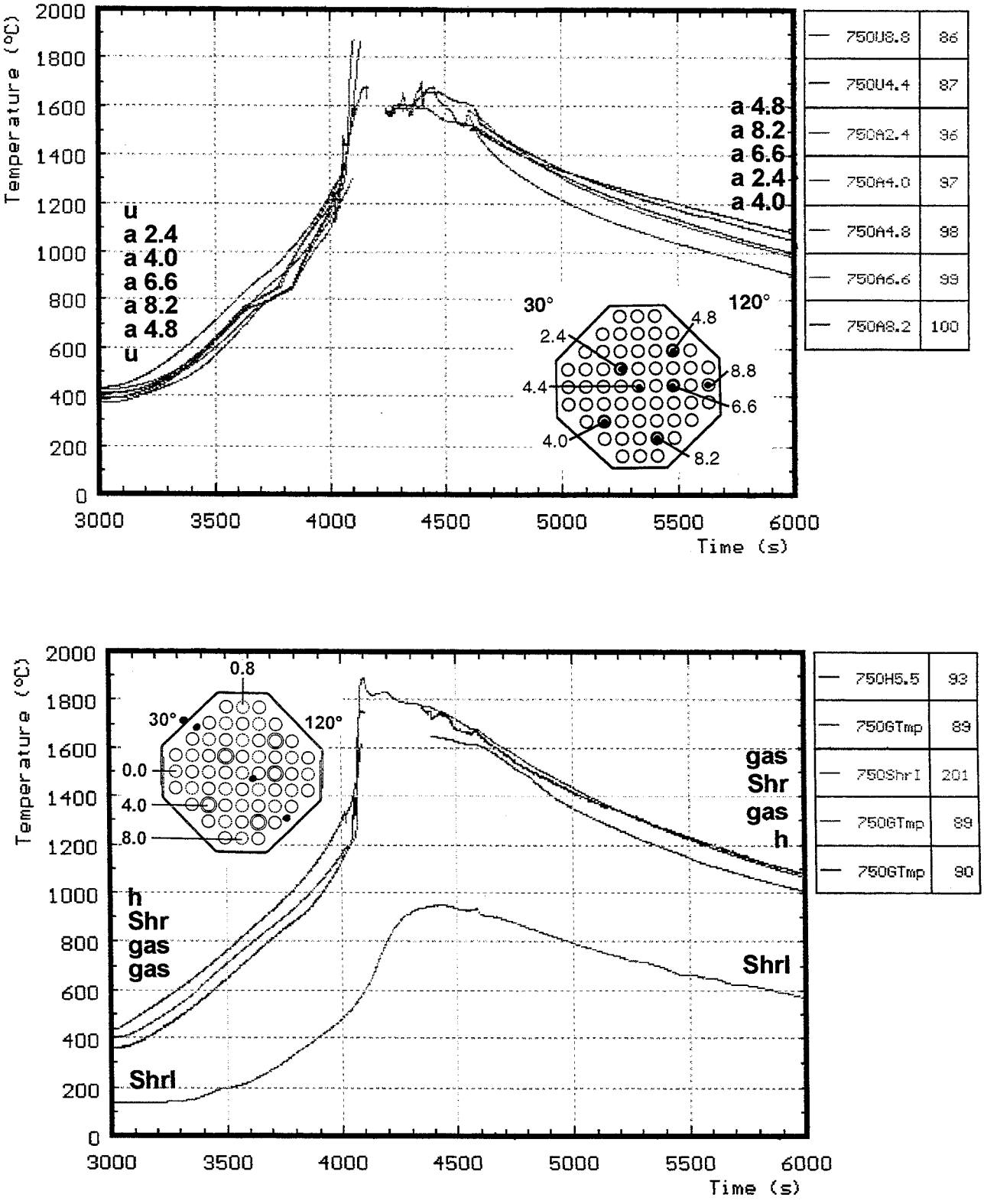

h : heated rods
u : unheated rods
a : in absorber

shr : outer side of shroud
shrl : on shroud insulation
gas : gas temperature

Fig. 19: CORA-7; Temperatures at elevations given (750 mm)

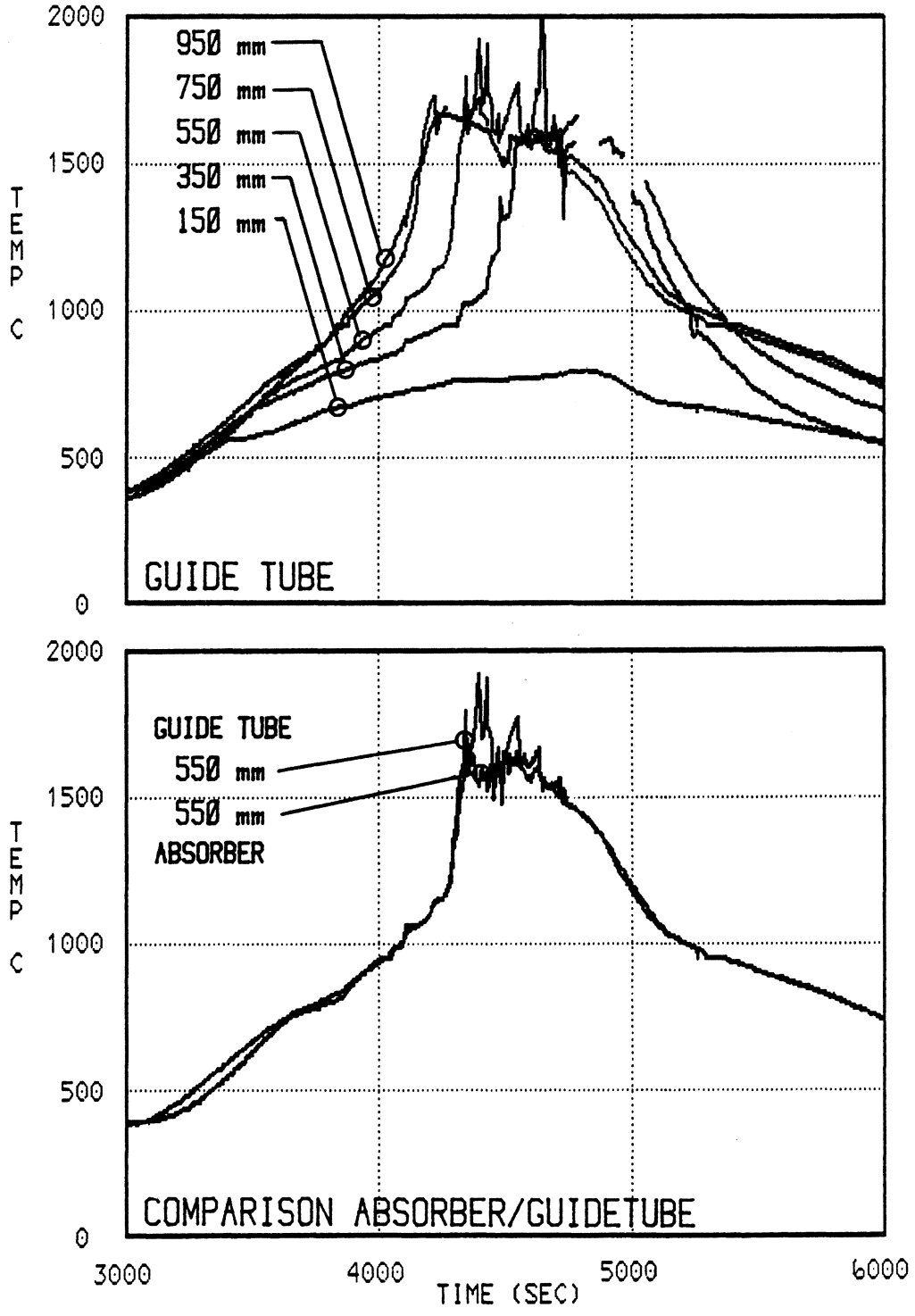

Fig. 20: Temperatures of guide tube and absorber rod during test CORA-5

Rod Nr.	Bursting time/sec
5.1	3493.8
3.3	3547.8
3.5	3561.5
1.3	3562.1
5.5	3562.7
5.3	3564.2
2.4	3565.1
3.1	3570.2
1.1	3579.4
7.5	3579.5
7.3	3585.1
1.5	3588.7
5.7	3588.9
7.7	3593.9
7.1	3600.8
4.4	3600.9
3.7	3602.0
6.4	3602.2
4.2	3604.0
2.2	3616.3
1.7	3617.8
2.6	3624.8
6.6	3644.5

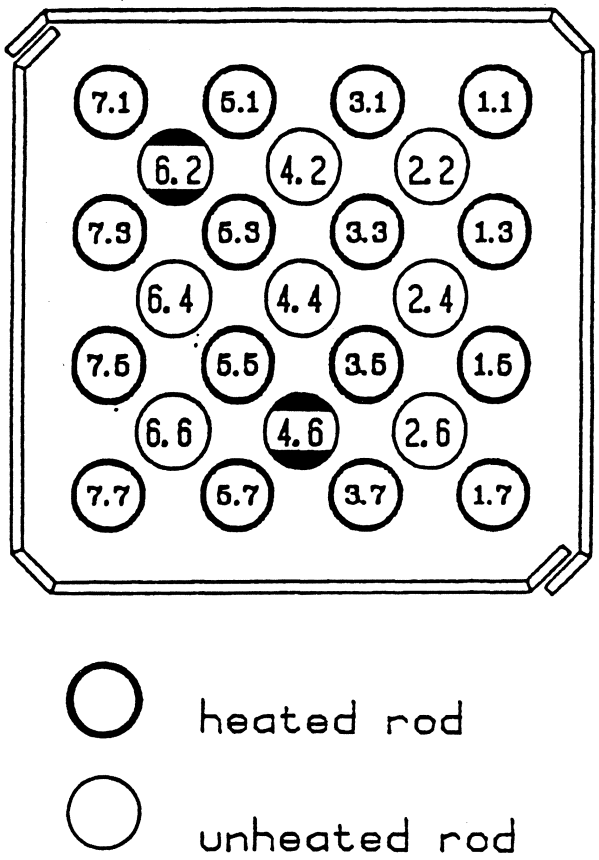

Fig. 21: Sequence of rupture for the fuel rod simulators during test CORA-15

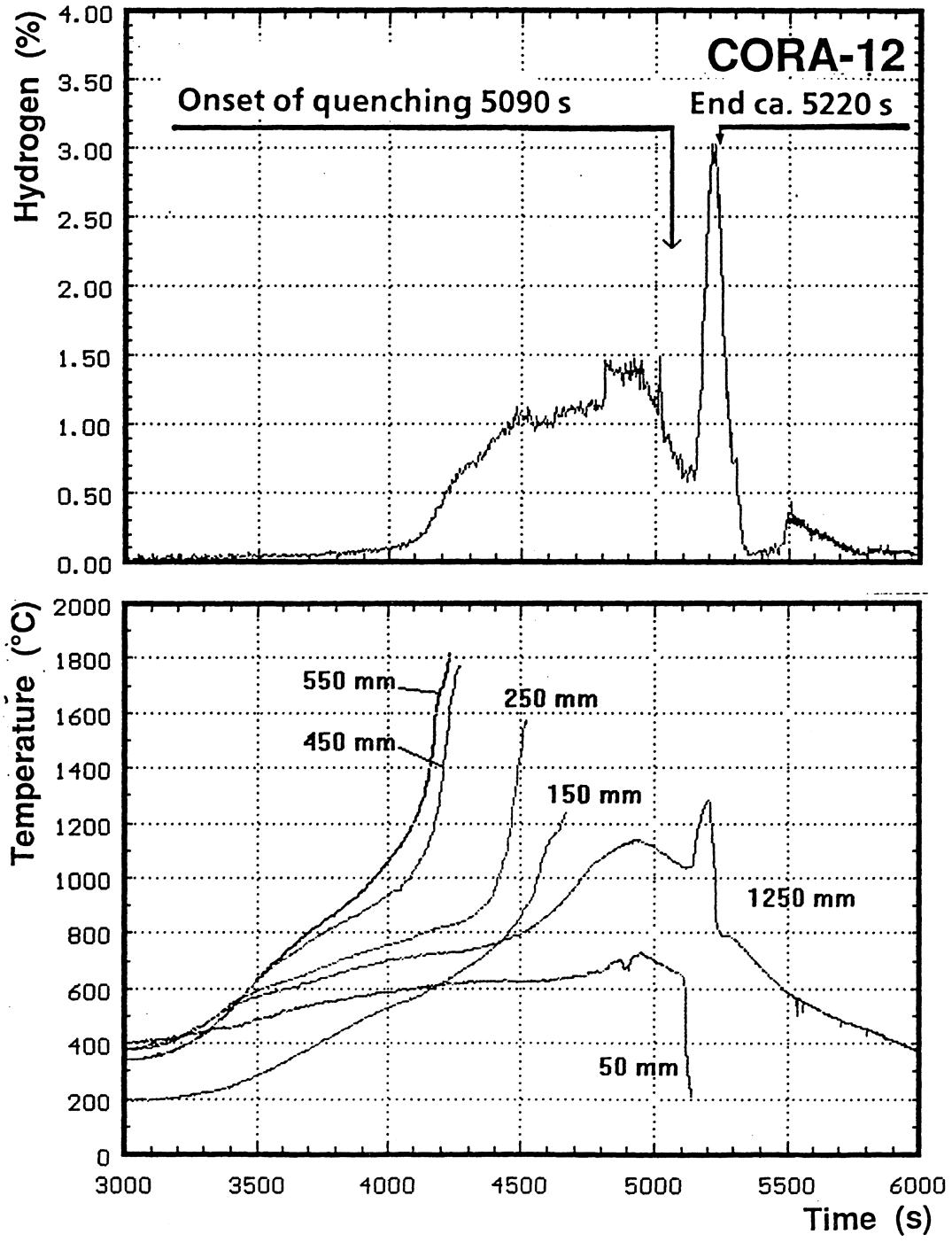

Fig. 22: Temperature and hydrogen response, during quench test CORA-12

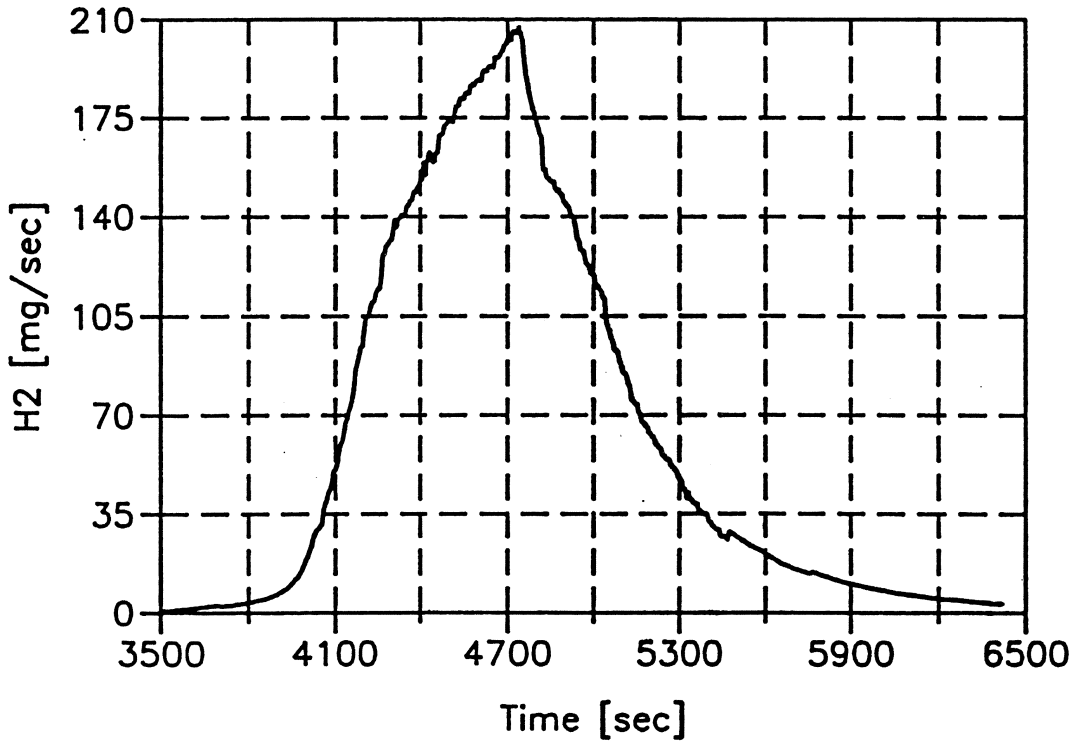

Fig.23: Hydrogen production during test CORA-15

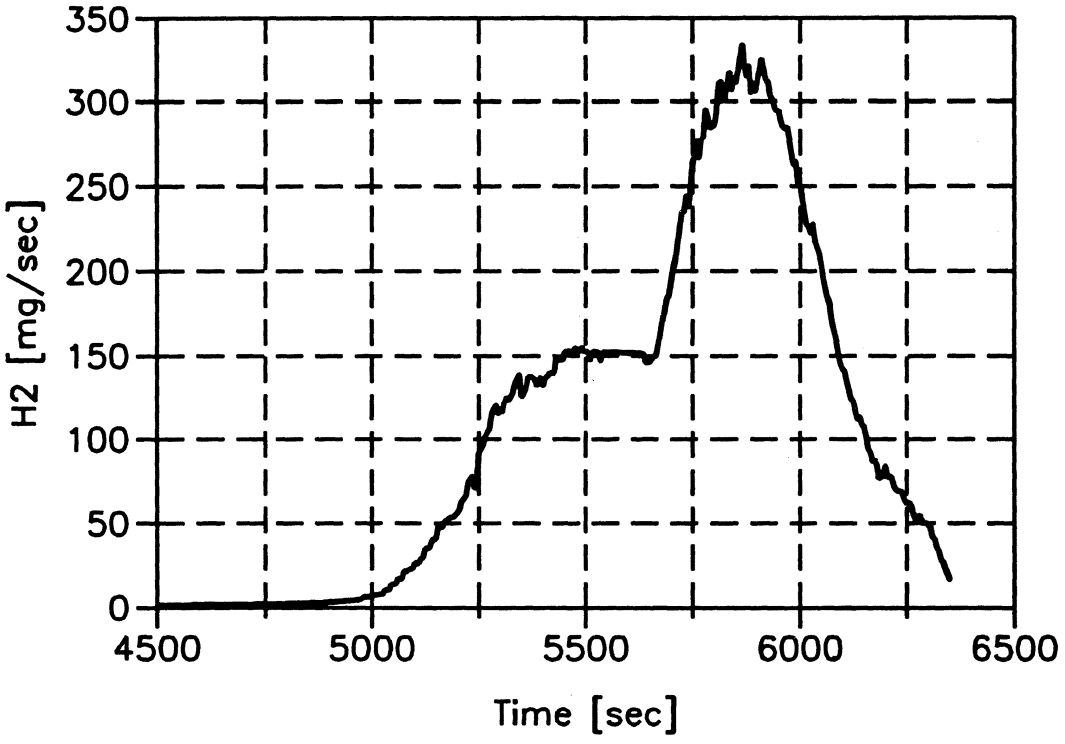

Fig. 24: Hydrogen production during test CORA-9

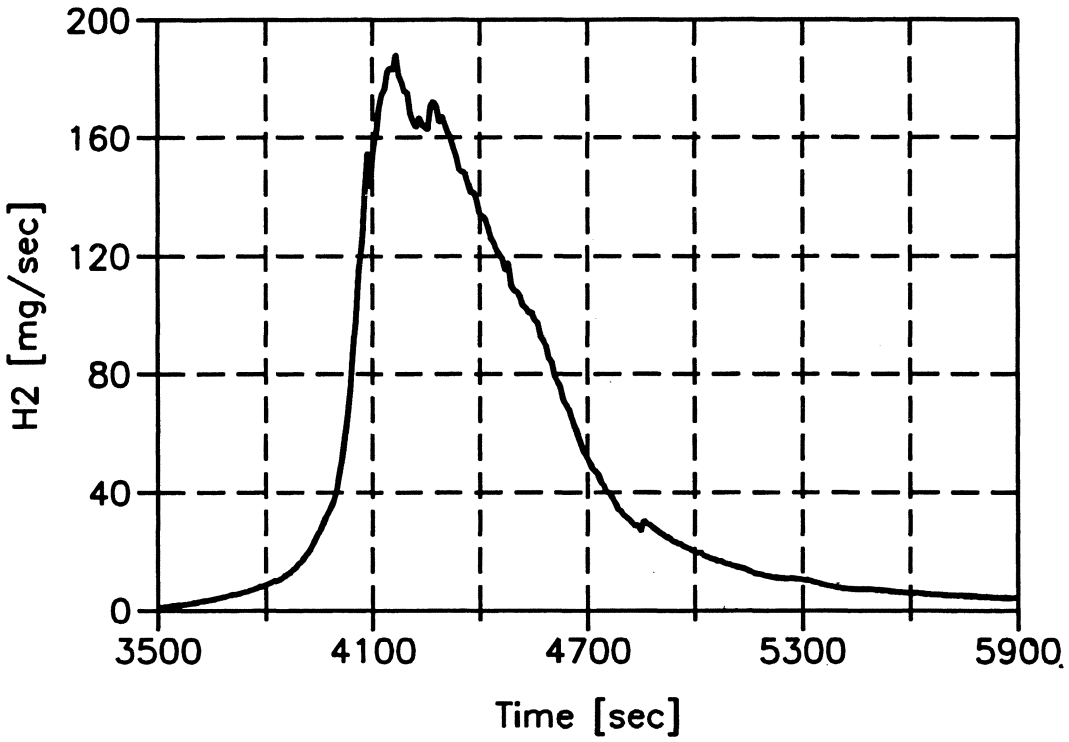

Fig. 25: Hydrogen production during test CORA-7

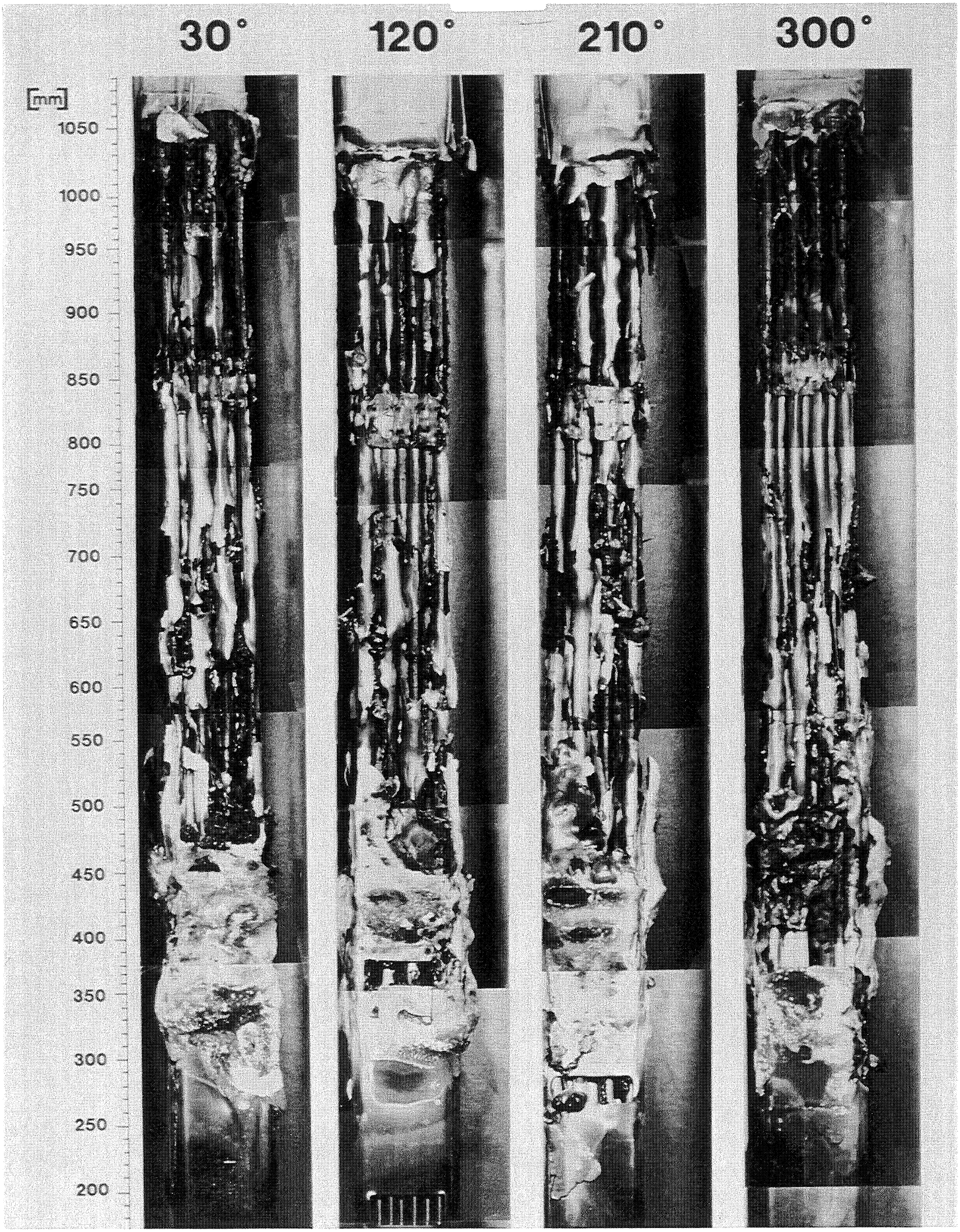

Fig. 26: Posttest appearance of CORA-5

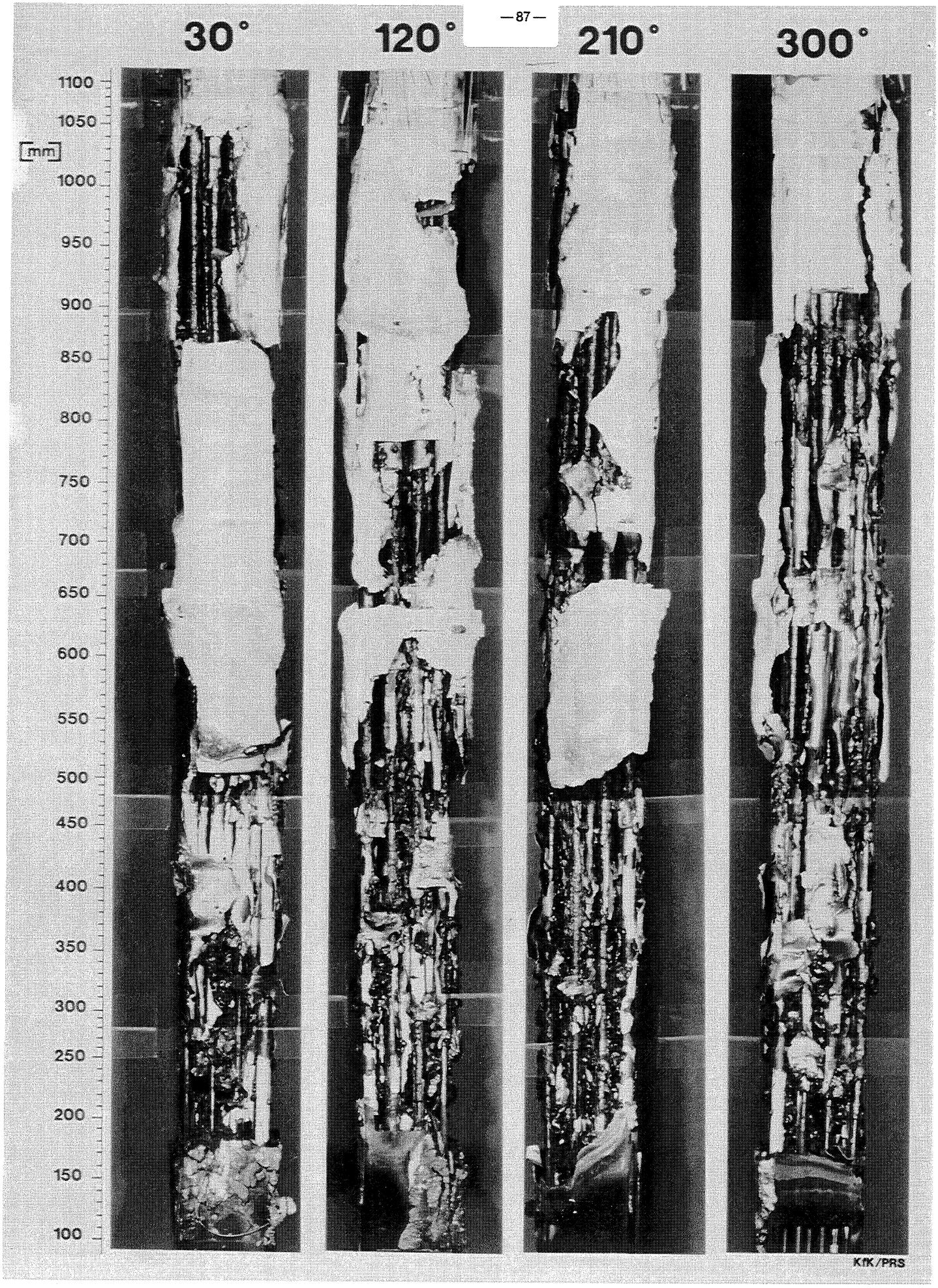

Fig. 27: Posttest appearance of CORA-12

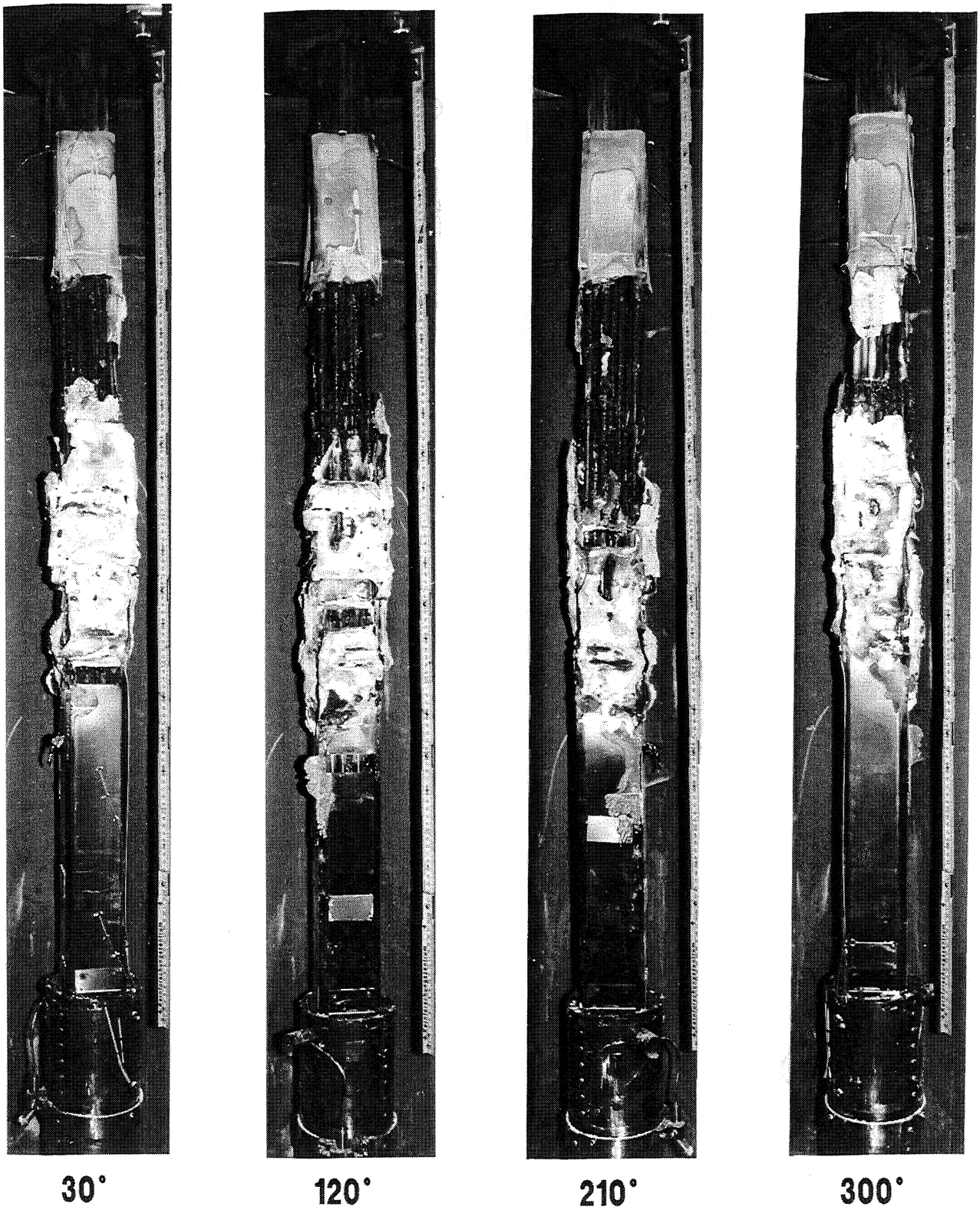

Fig. 28: CORA-15; Posttest appearance of the bundle after removal of the insulation

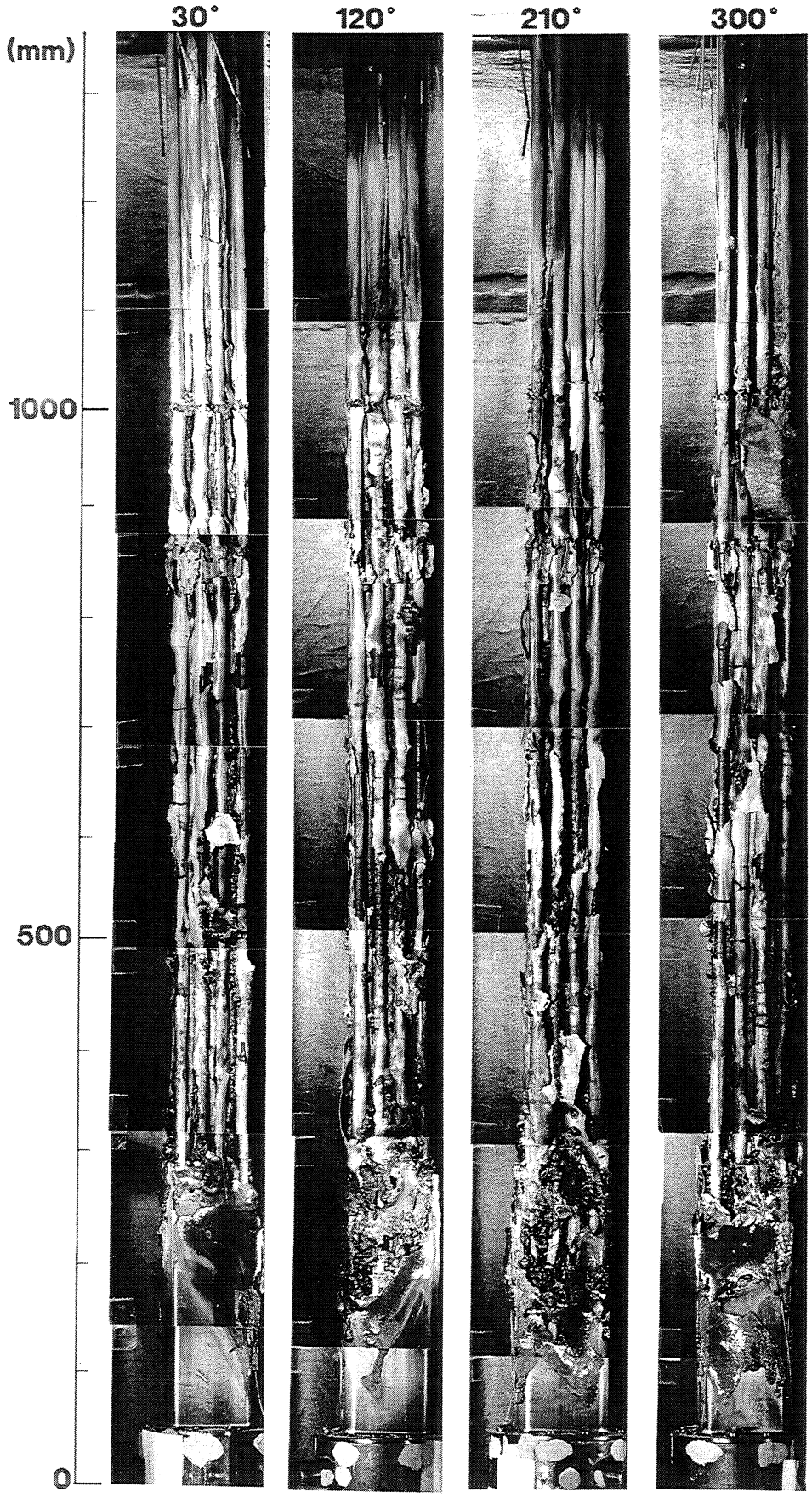

Fig.29: CORA-9; Posttest appearance of the bundle

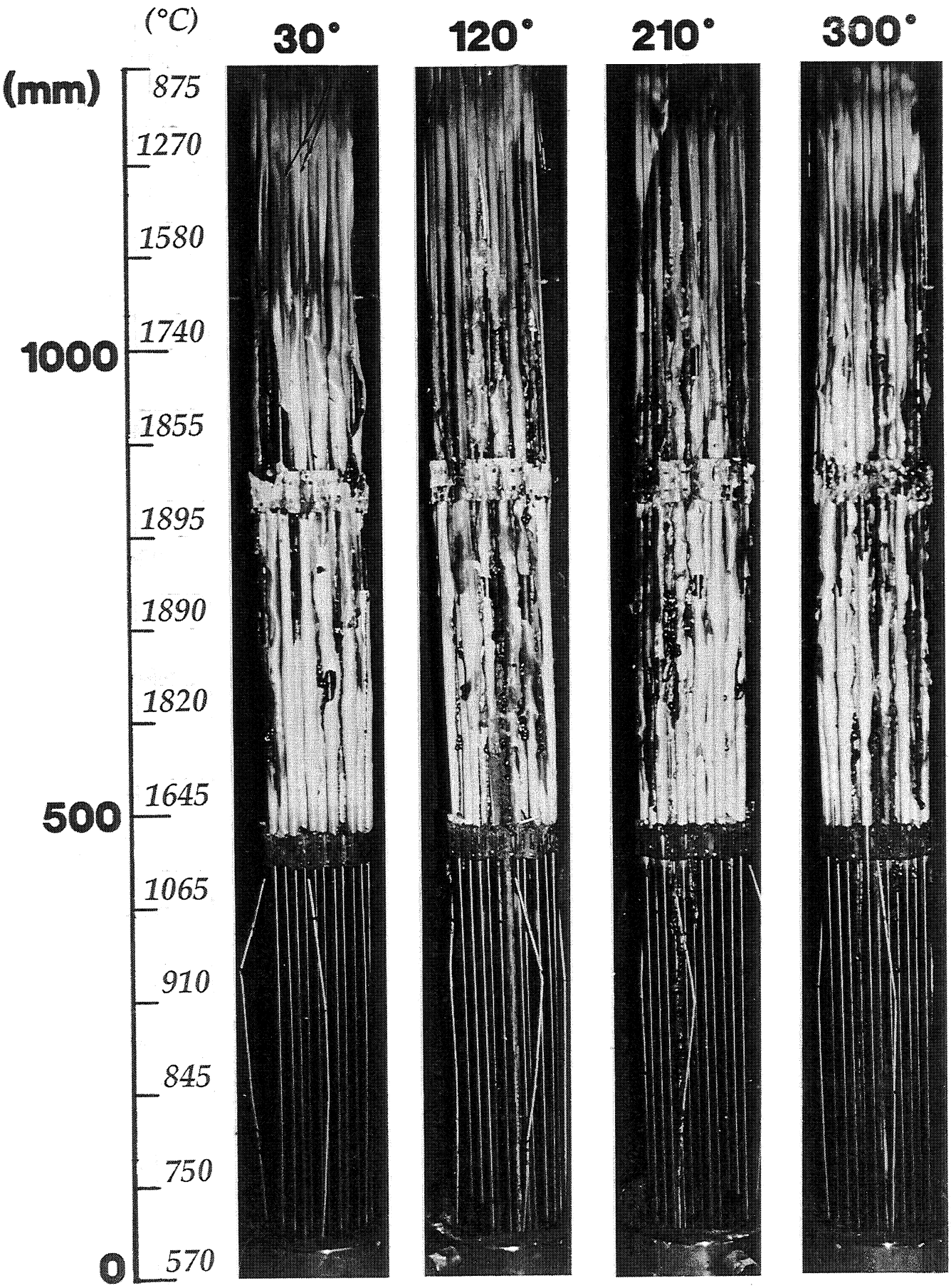

Fig.30: CORA-7; Posttest appearance

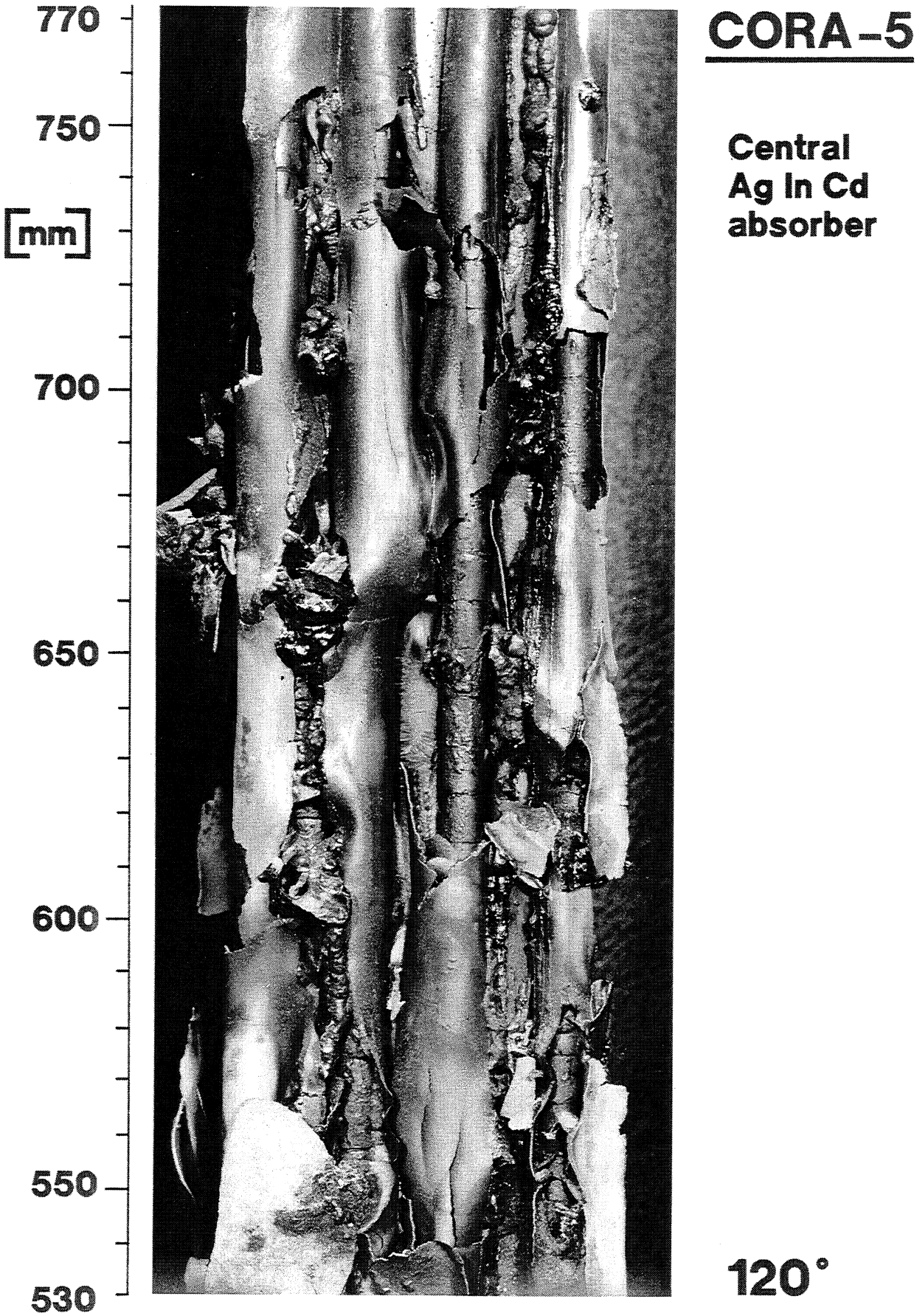

Fig. 31: CORA-5; Posttest view of the upper section

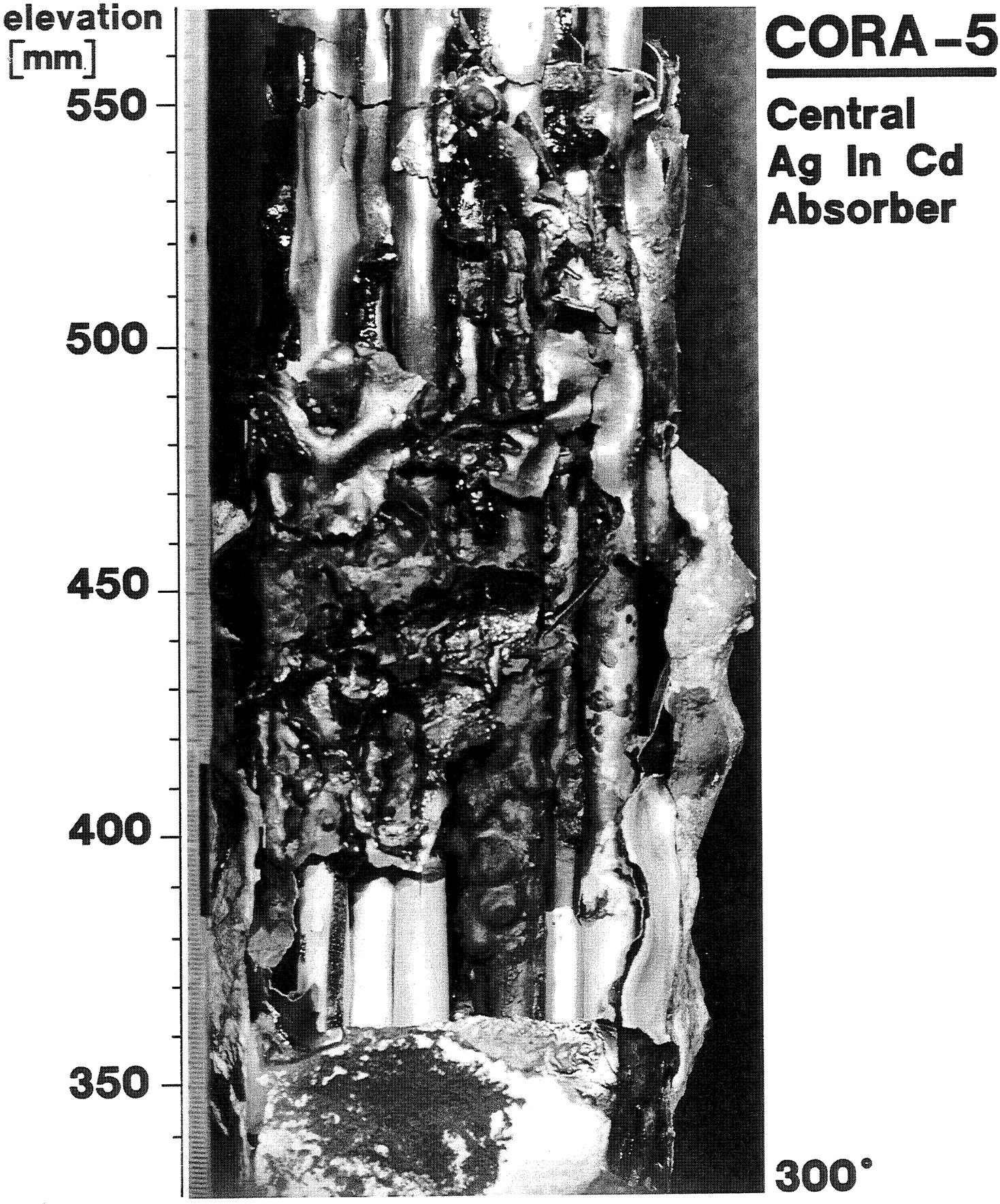

Fig. 32: CORA-5; Posttest view of the central bundle region

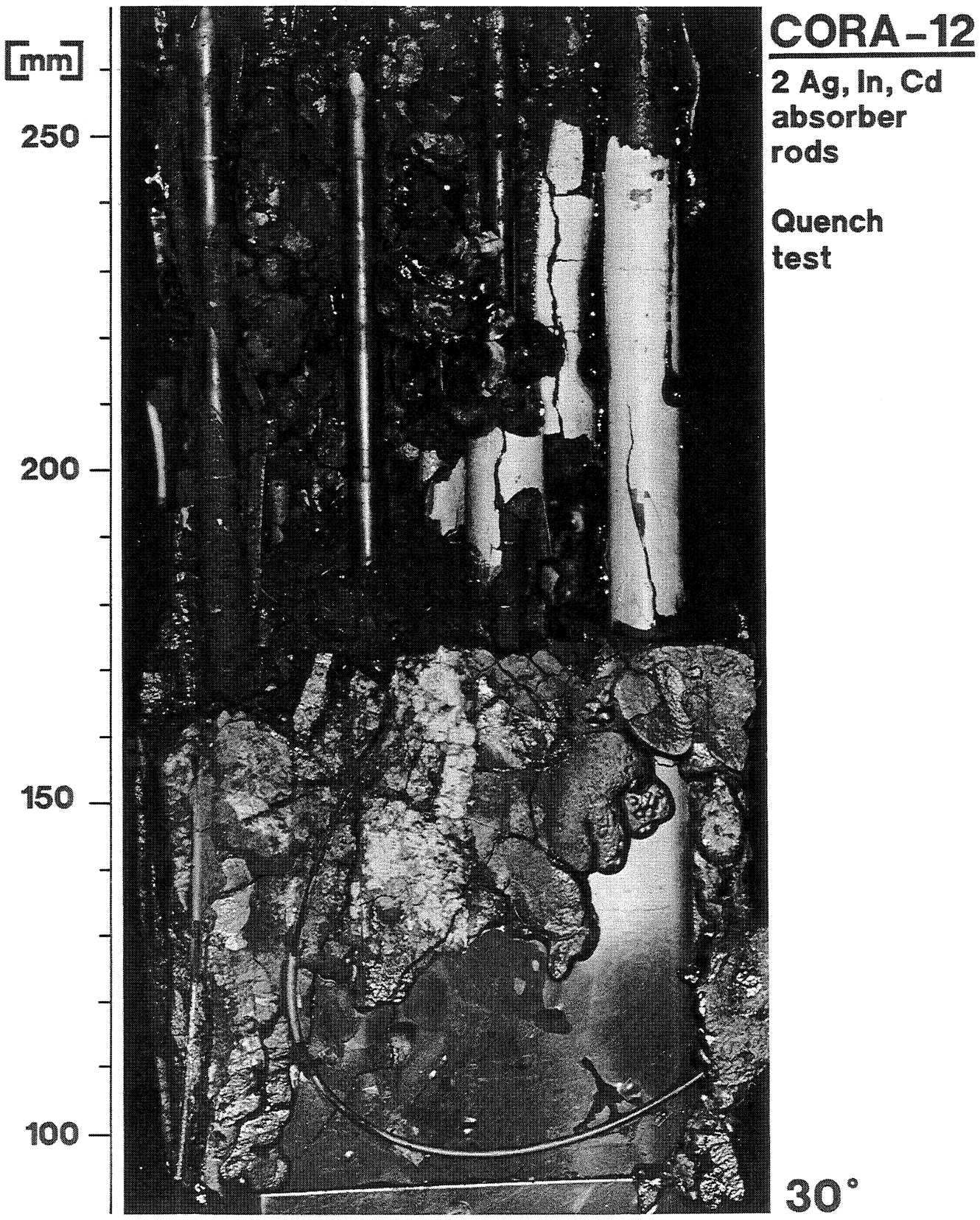

Fig. 33: CORA-12; Posttest view of the lower bundle region

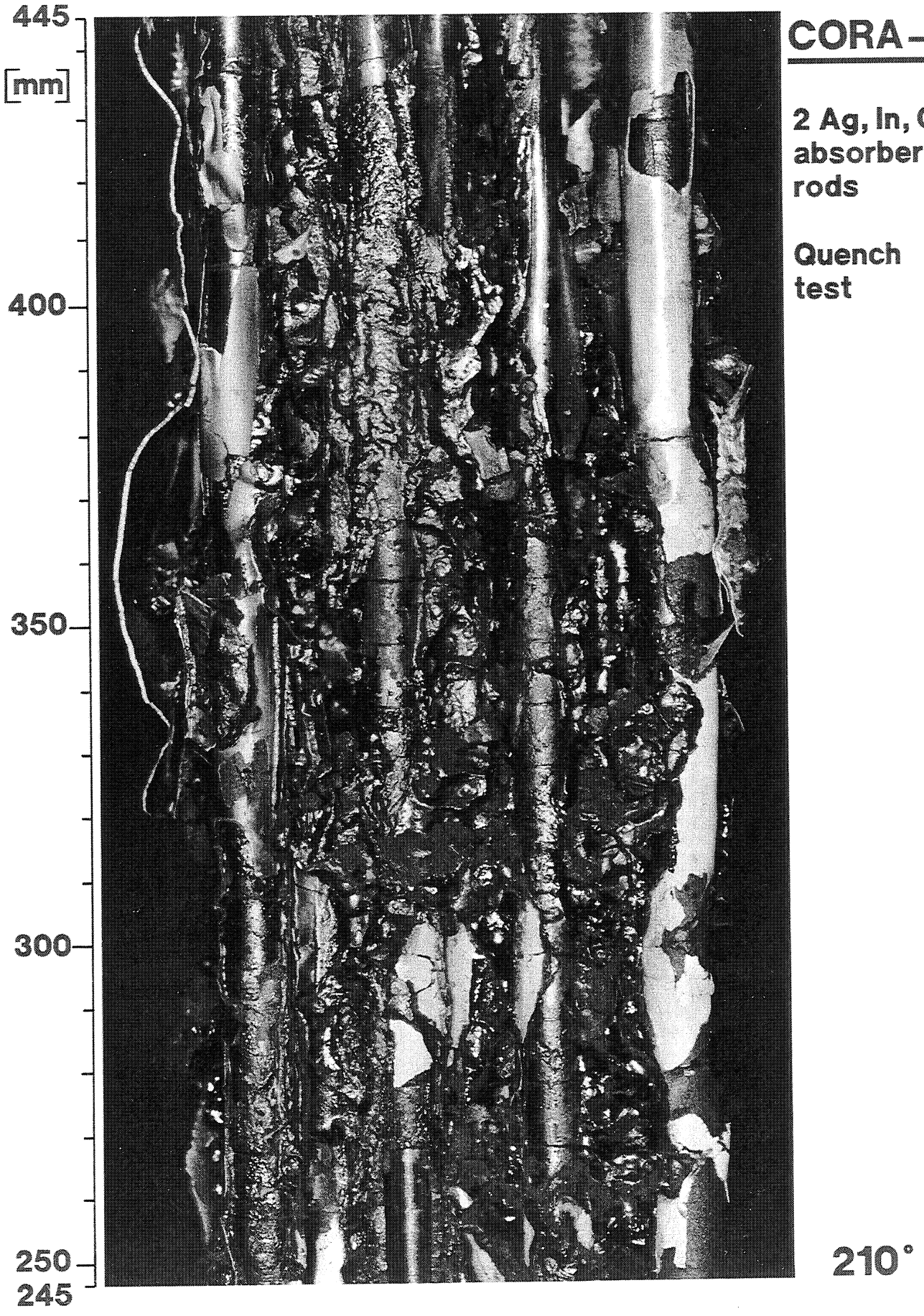

Fig. 34: CORA-12; Posttest view of the bottom part of the bundle

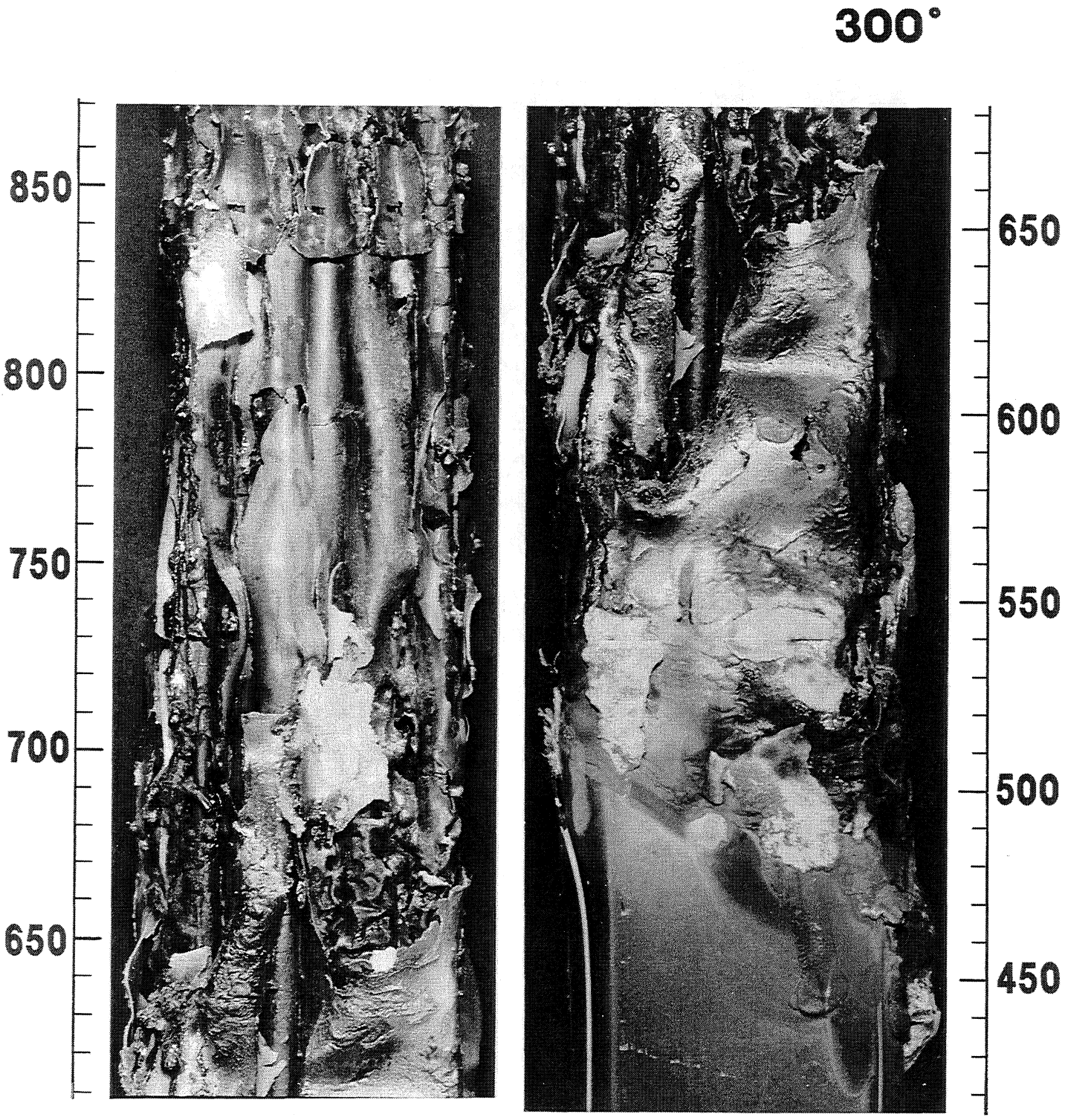

Fig. 35: CORA-15; Posttest appearance of the bundle

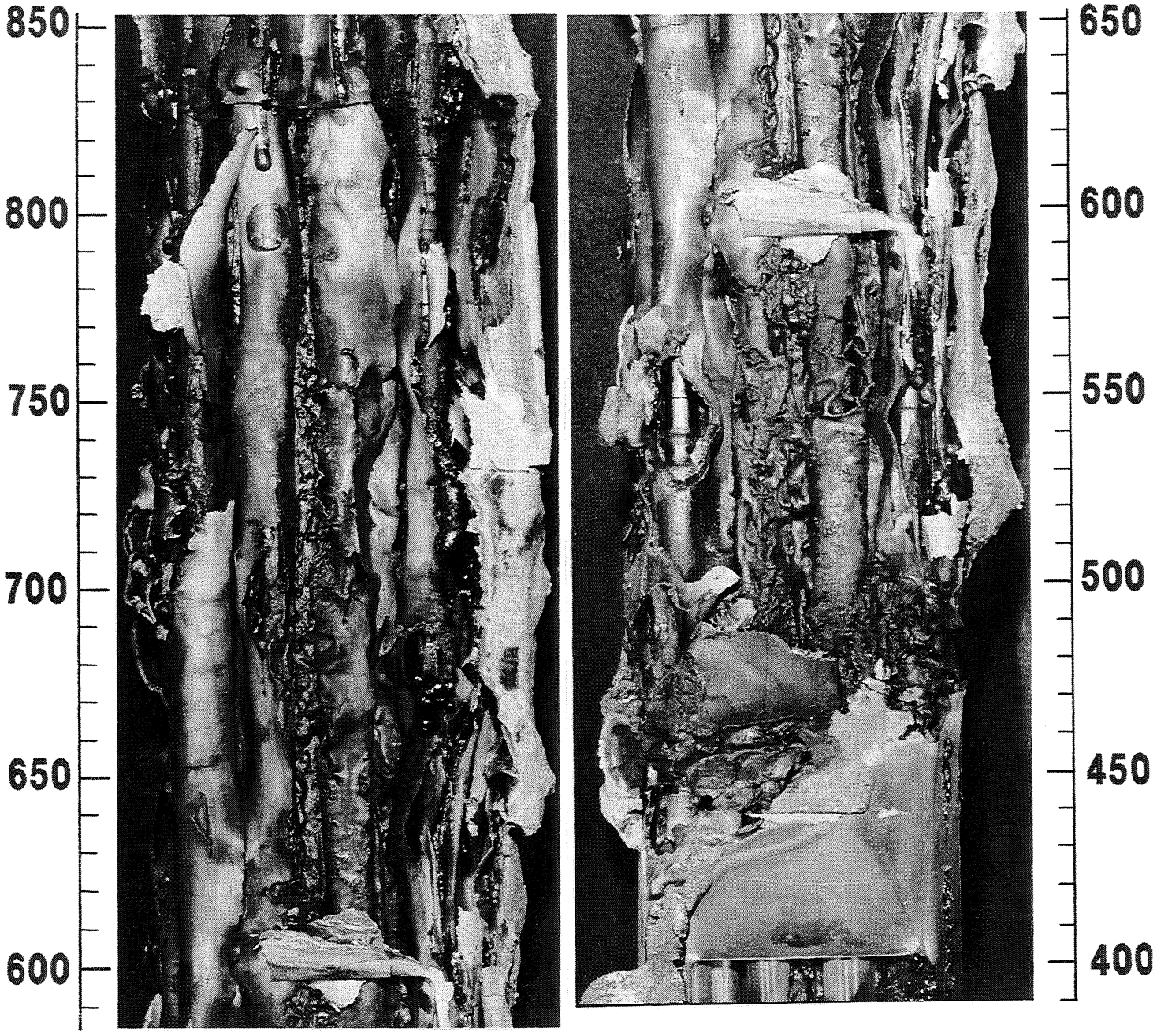

Fig.36: CORA-15; Posttest appearance of the bundle

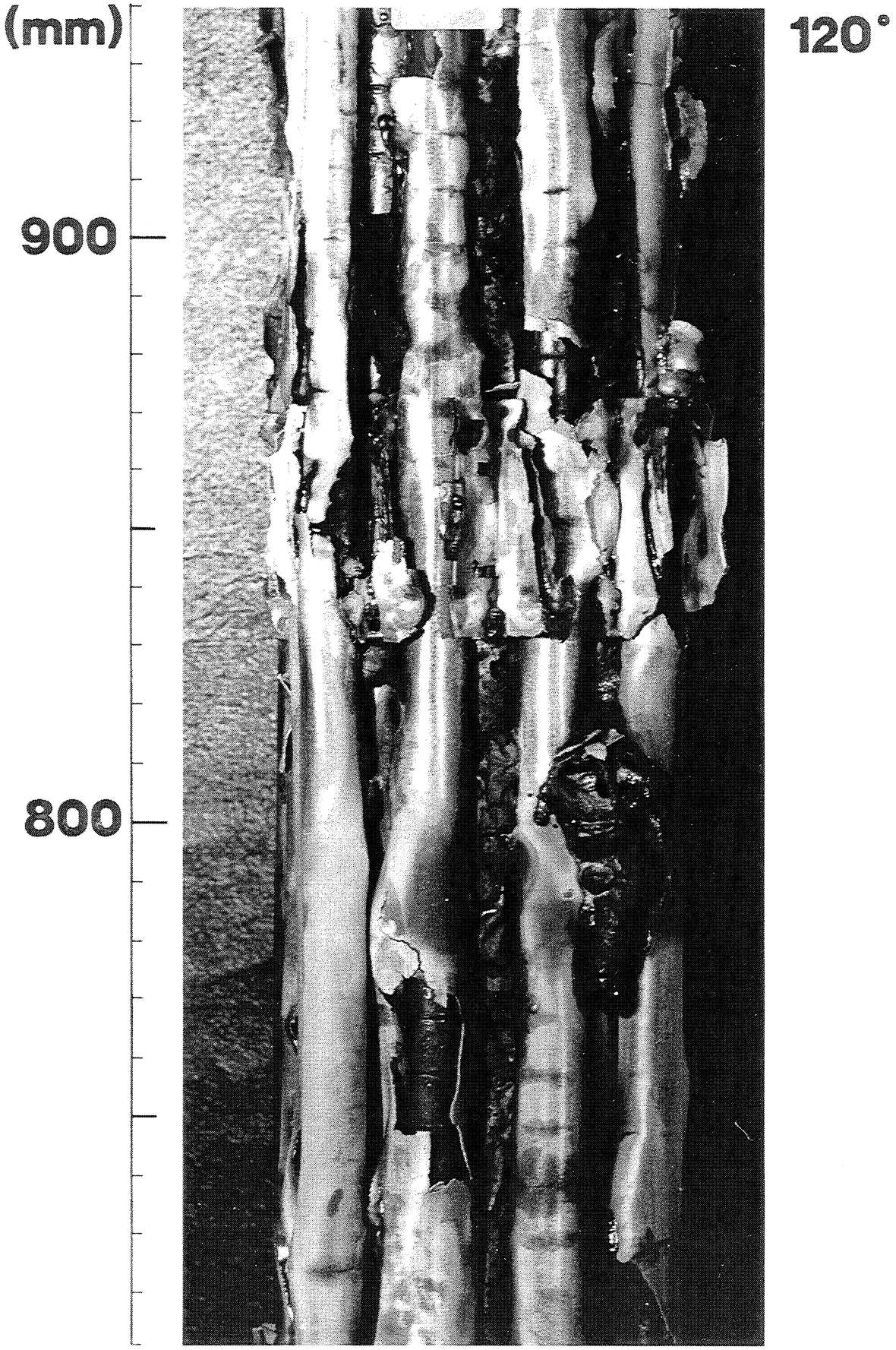

Fig. 37: CORA-9; Posttest view of the top grid spacer location

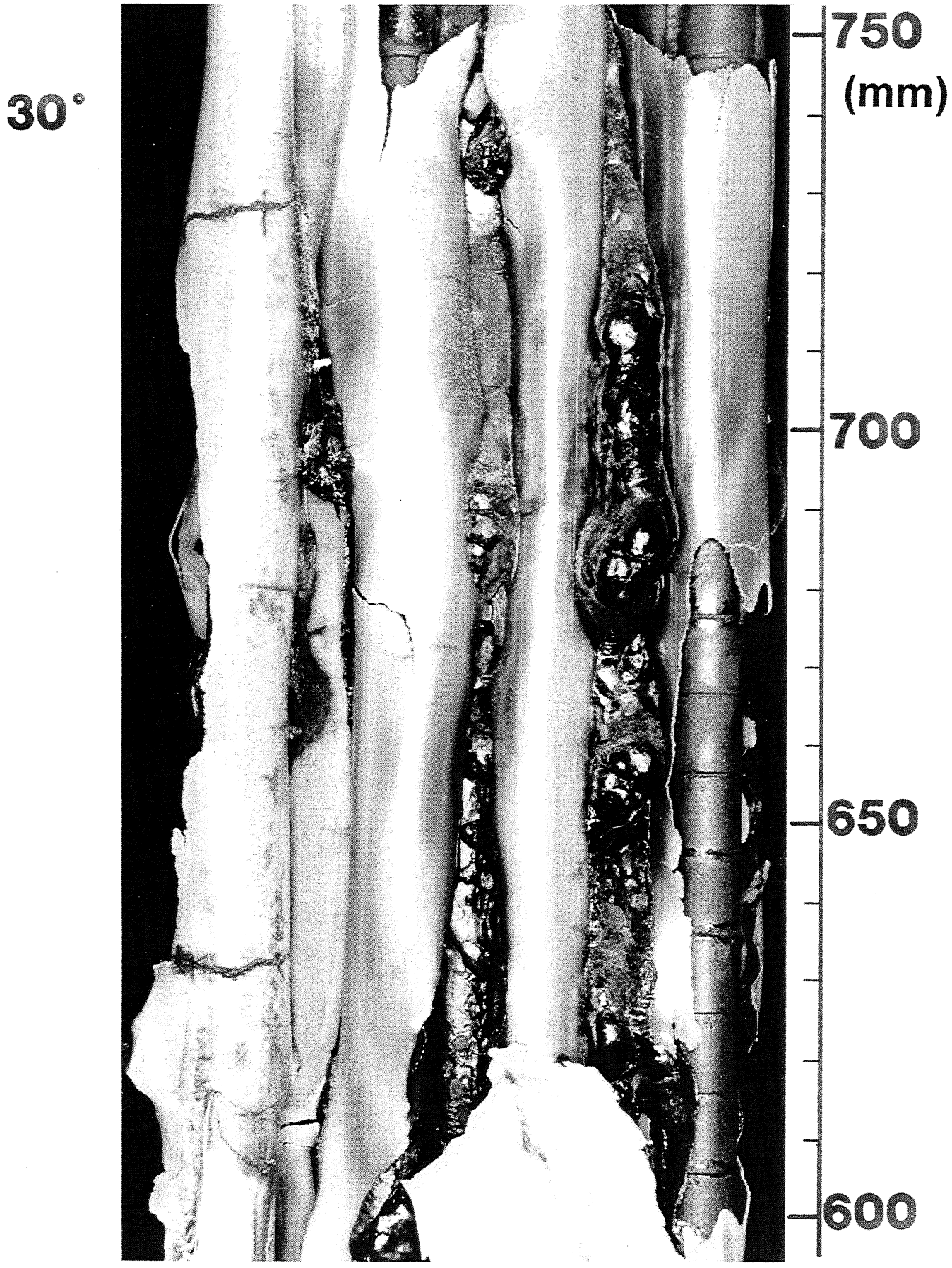

Fig. 38: CORA-9; Posttest view of the upper bundle part

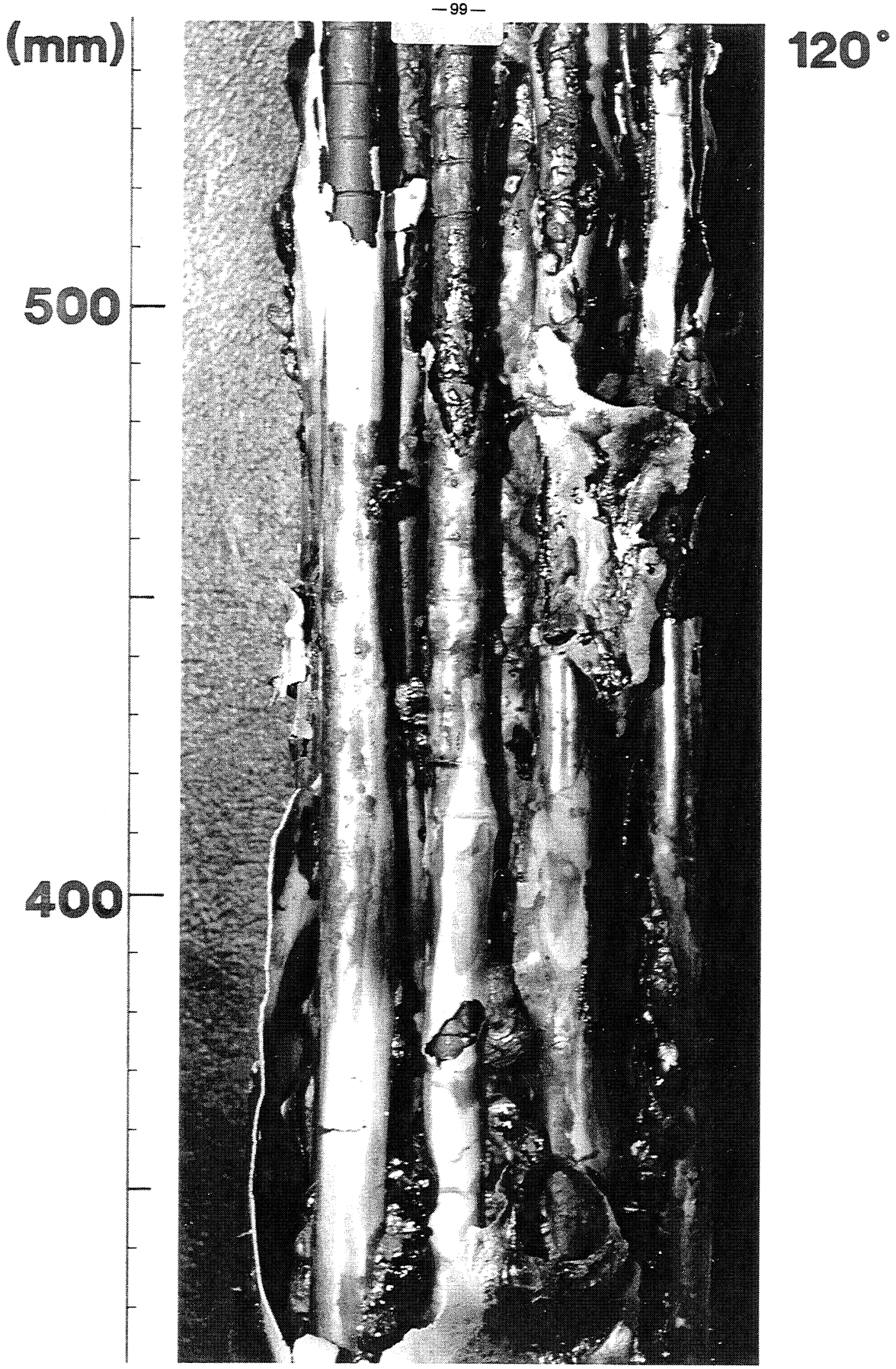

Fig. 39: CORA-9; Posttest view of the central region

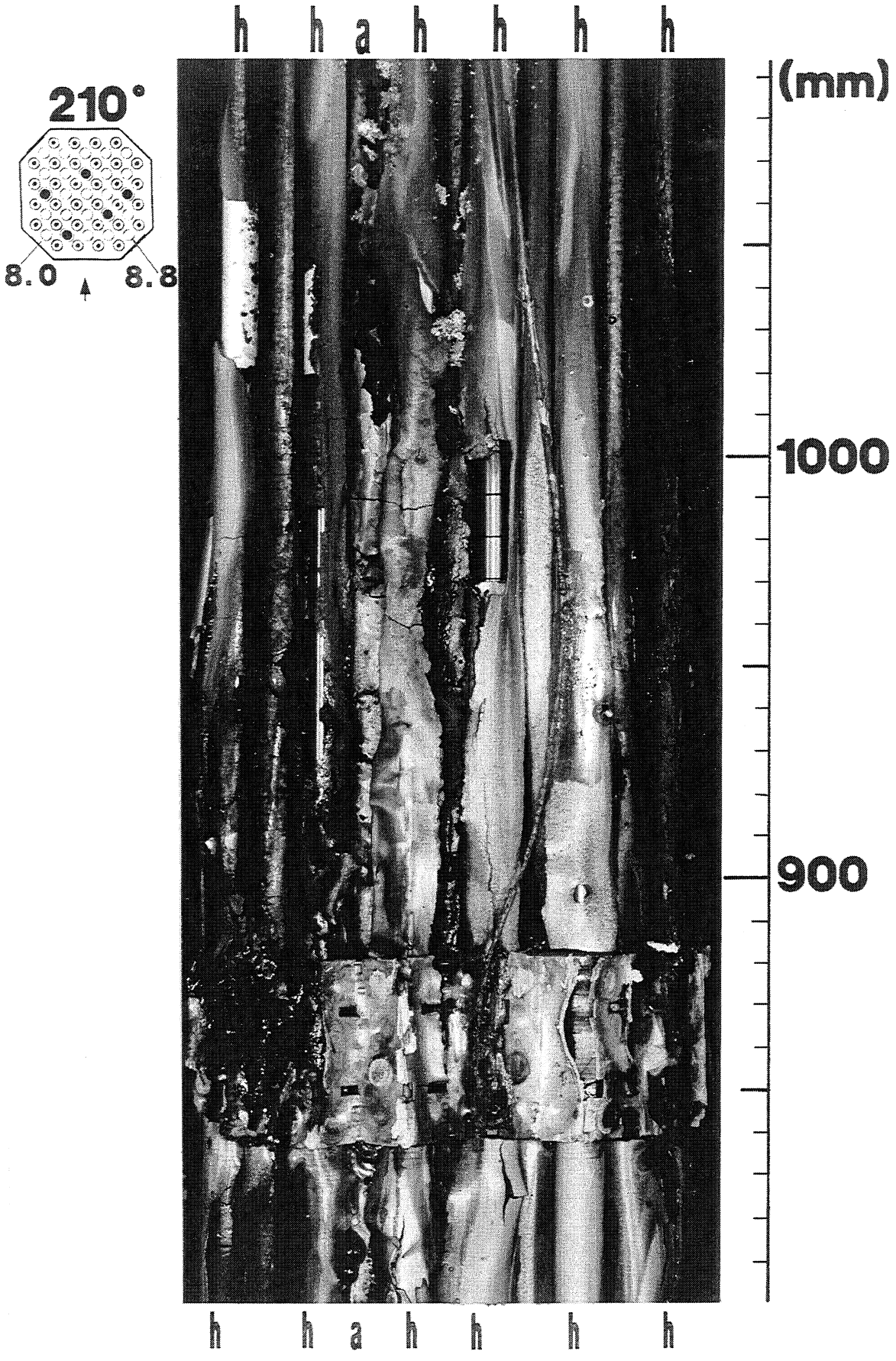

Fig. 40: CORA-7; Posttest view of the upper bundle location

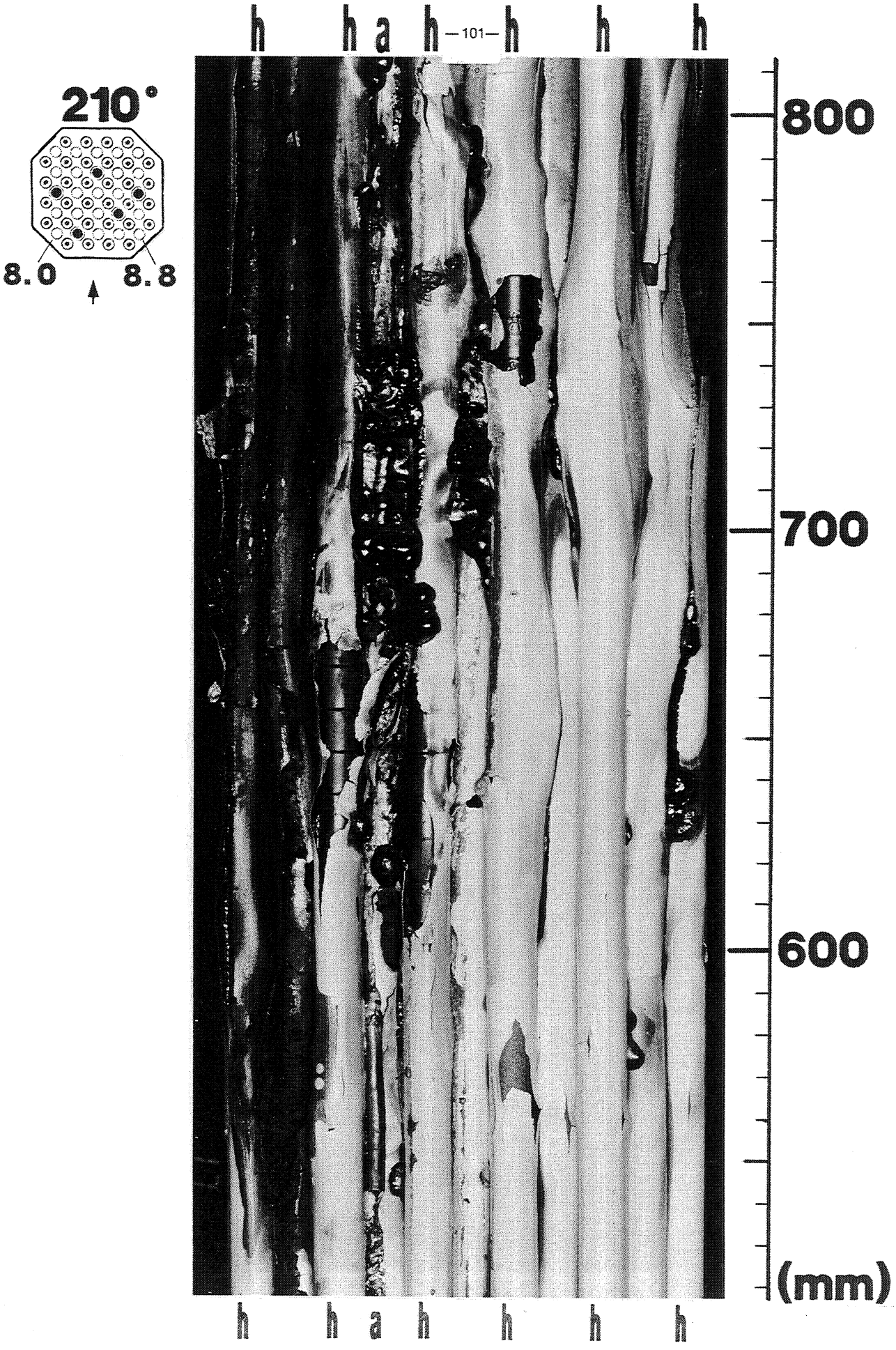

Fig.41: CORA-7; Posttest view of the upper part of the bundle

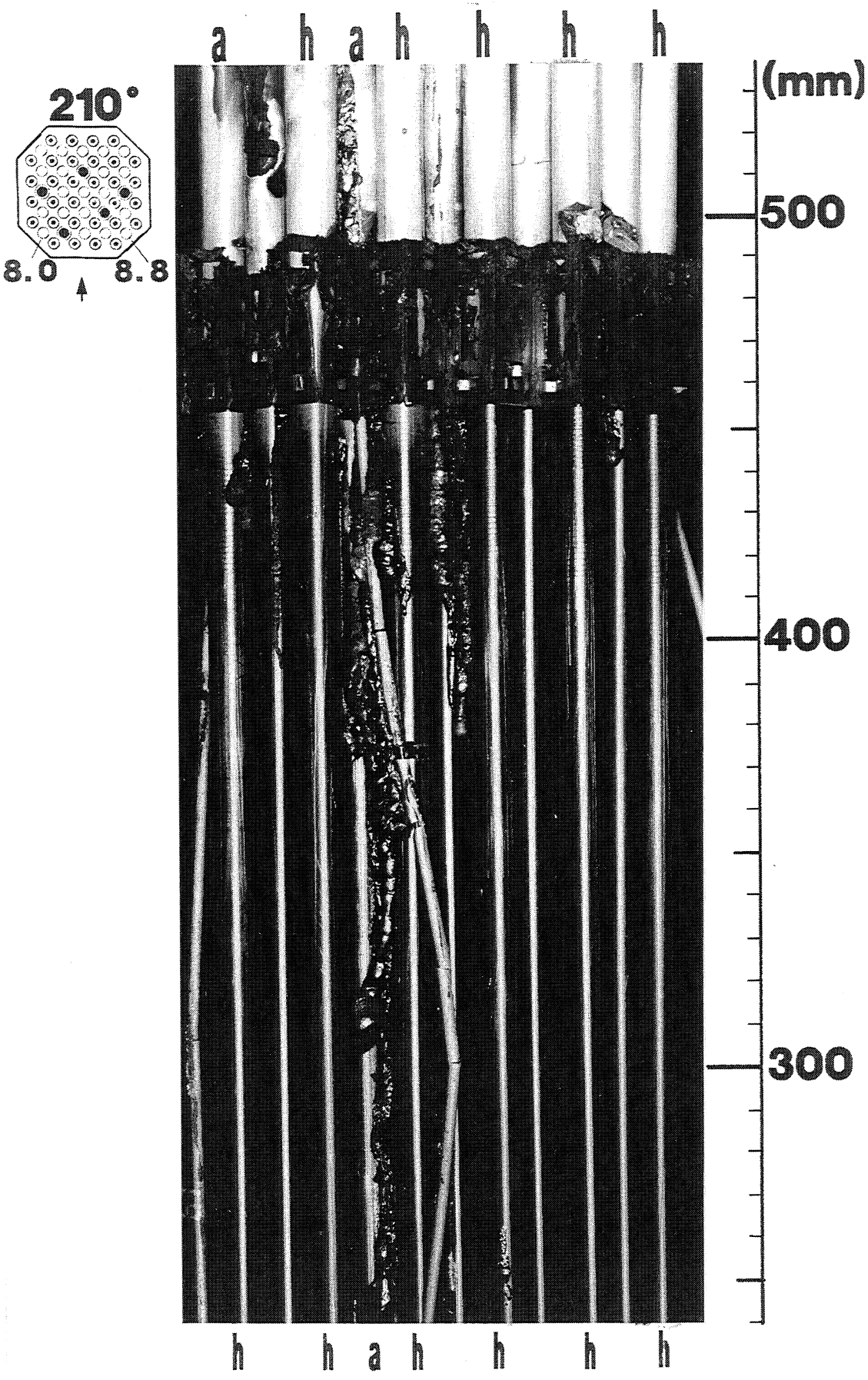

Fig. 42: CORA-7; Posttest view of the central region

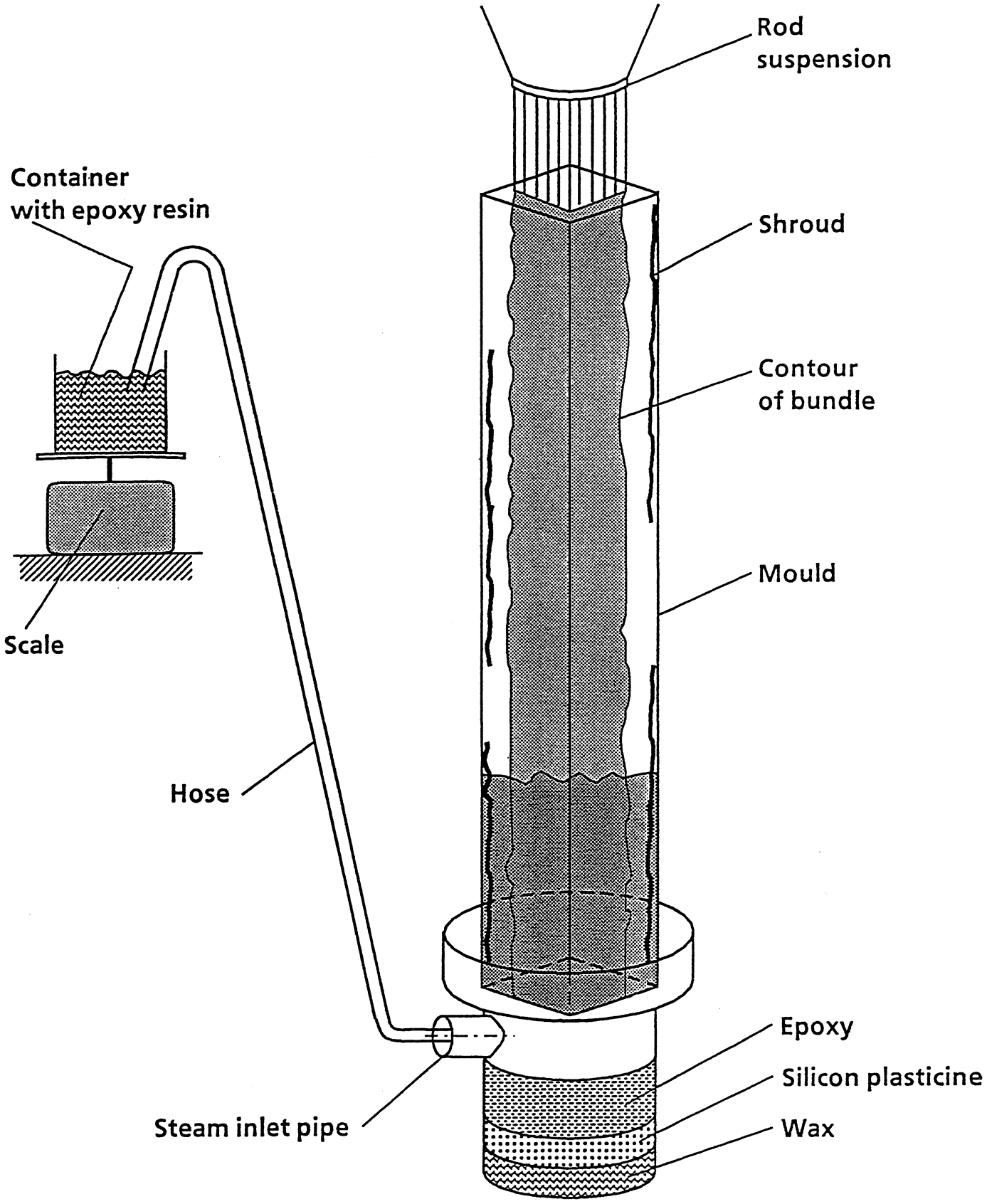

Fig.43: Epoxying process of the tested bundle

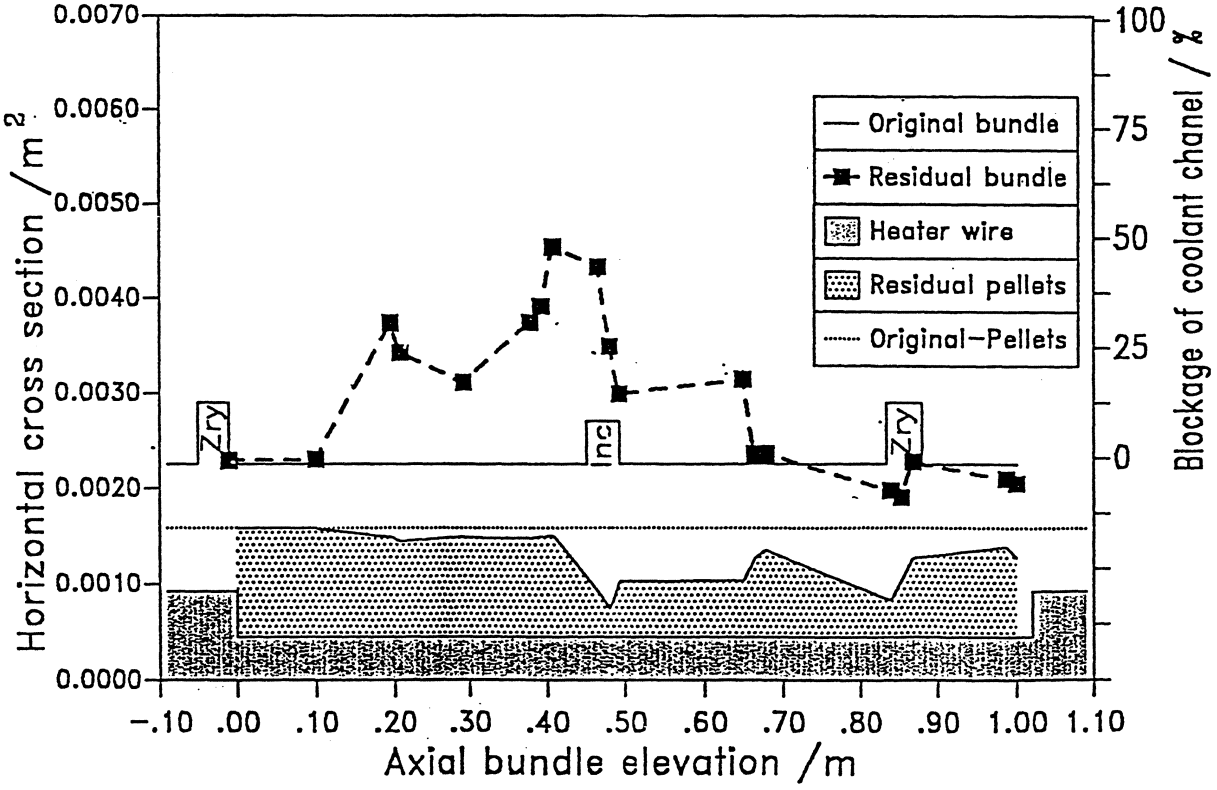

Fig. 44a: CORA-5; Blockage profile

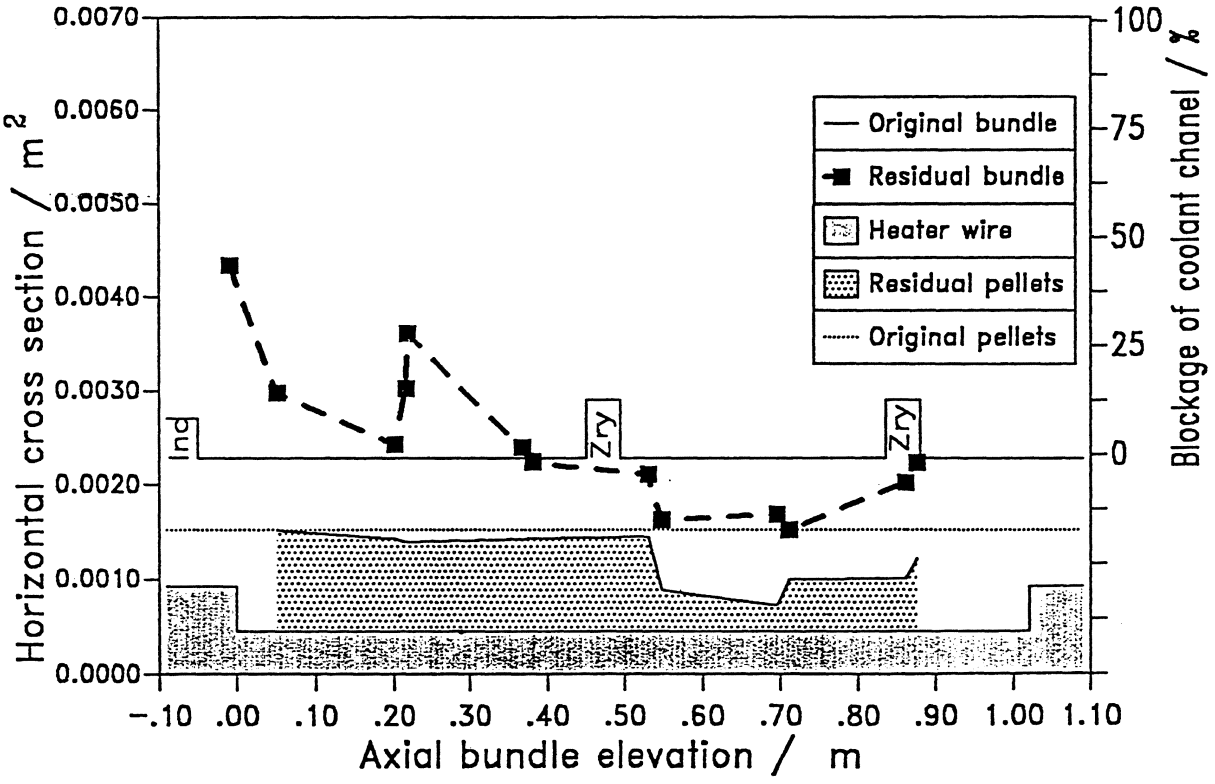

Fig. 44b: CORA-12; Blockage profile

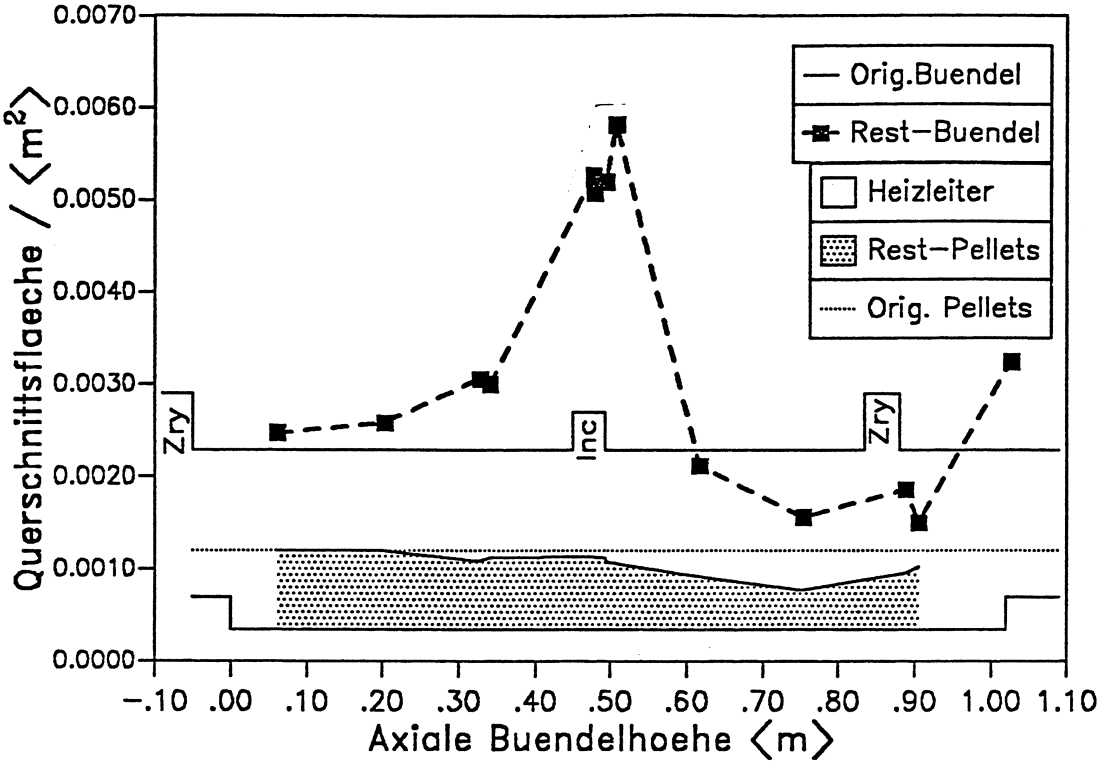

Fig. 44c: CORA-15; Blockage profile

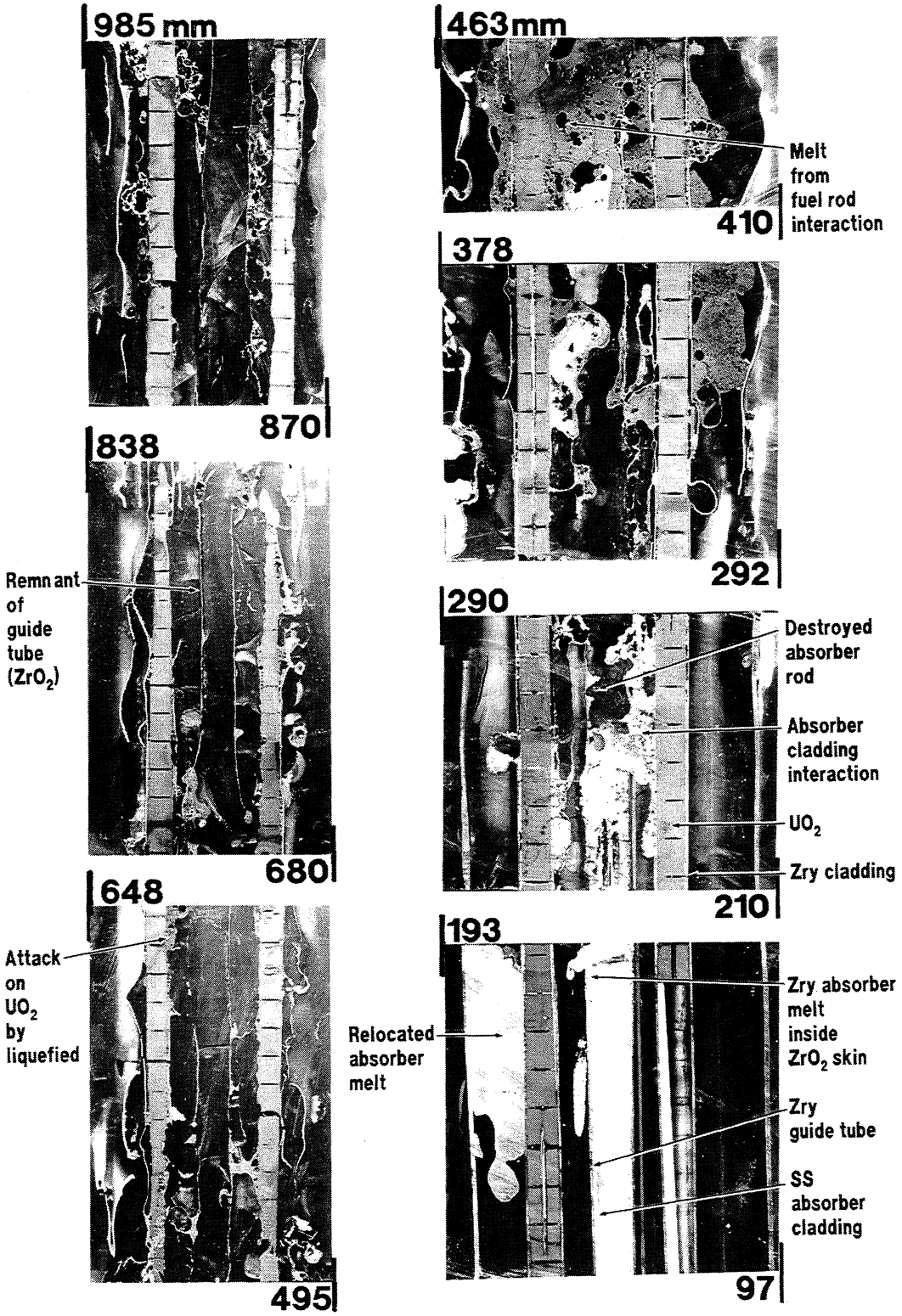

Fig. 45: Vertical cross sections of test CORA-5

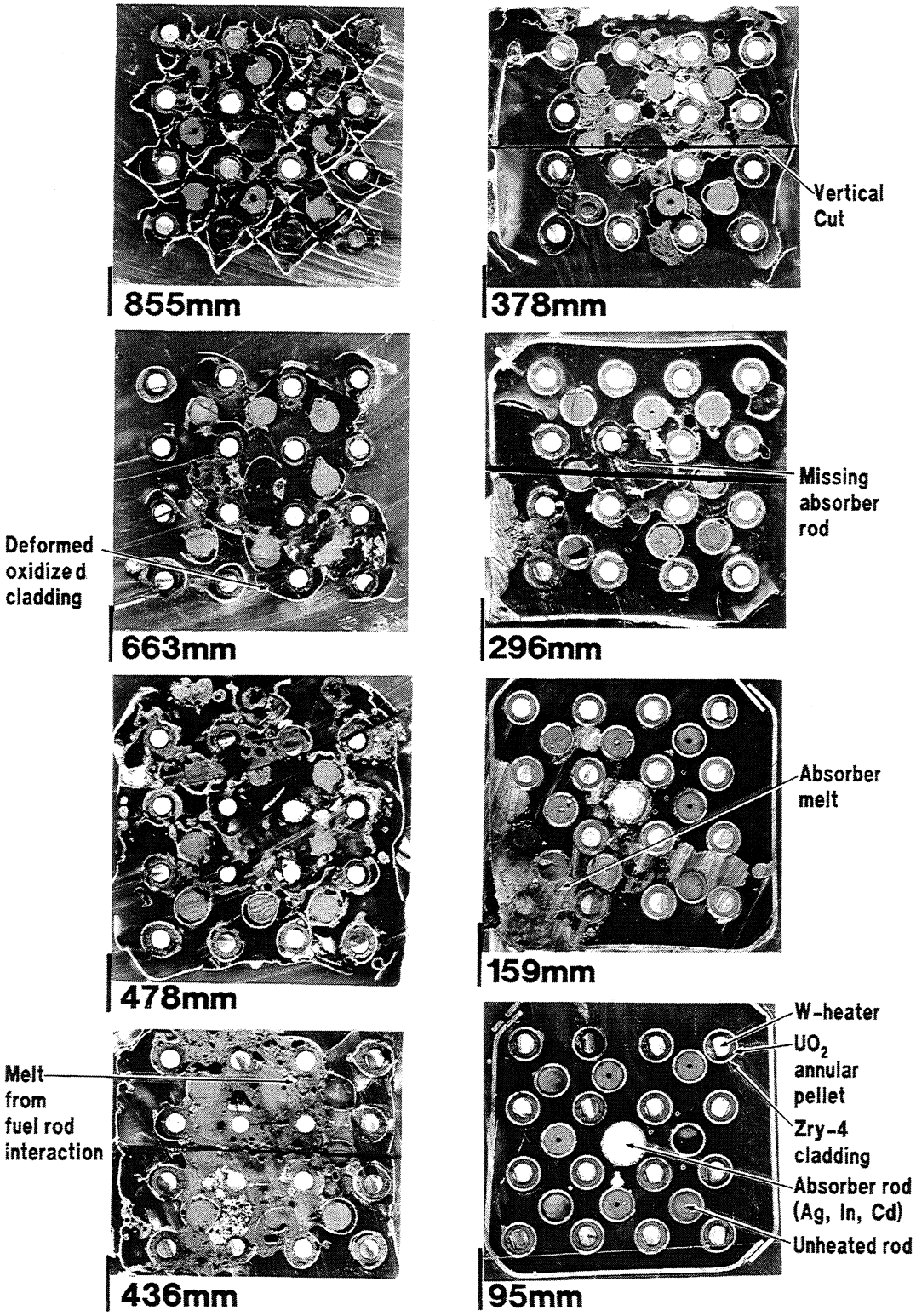

Fig. 46: Horizontal cross sections of test CORA-5

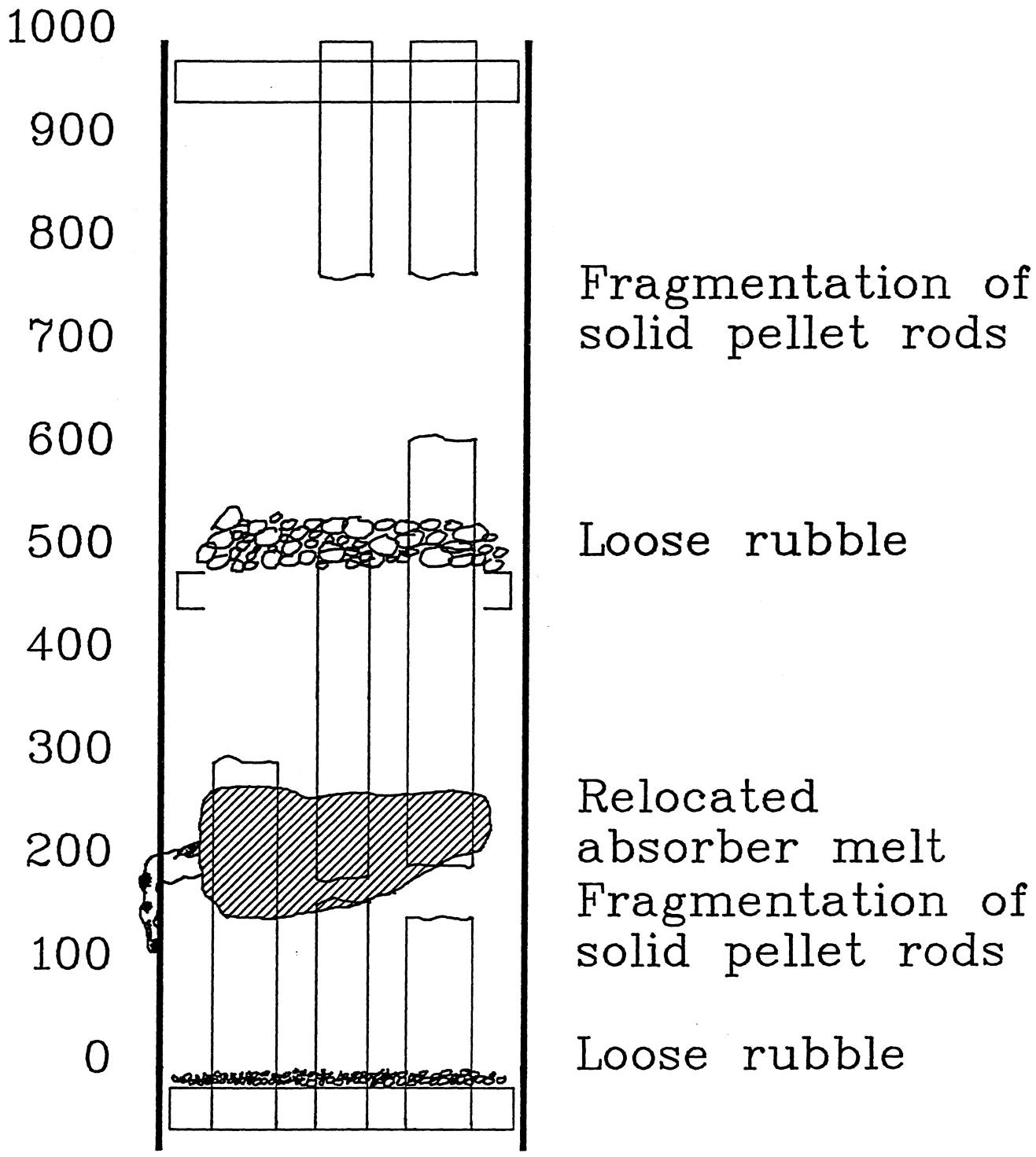

Fig.47: CORA-12; Posttest status of the bundle (schematic)

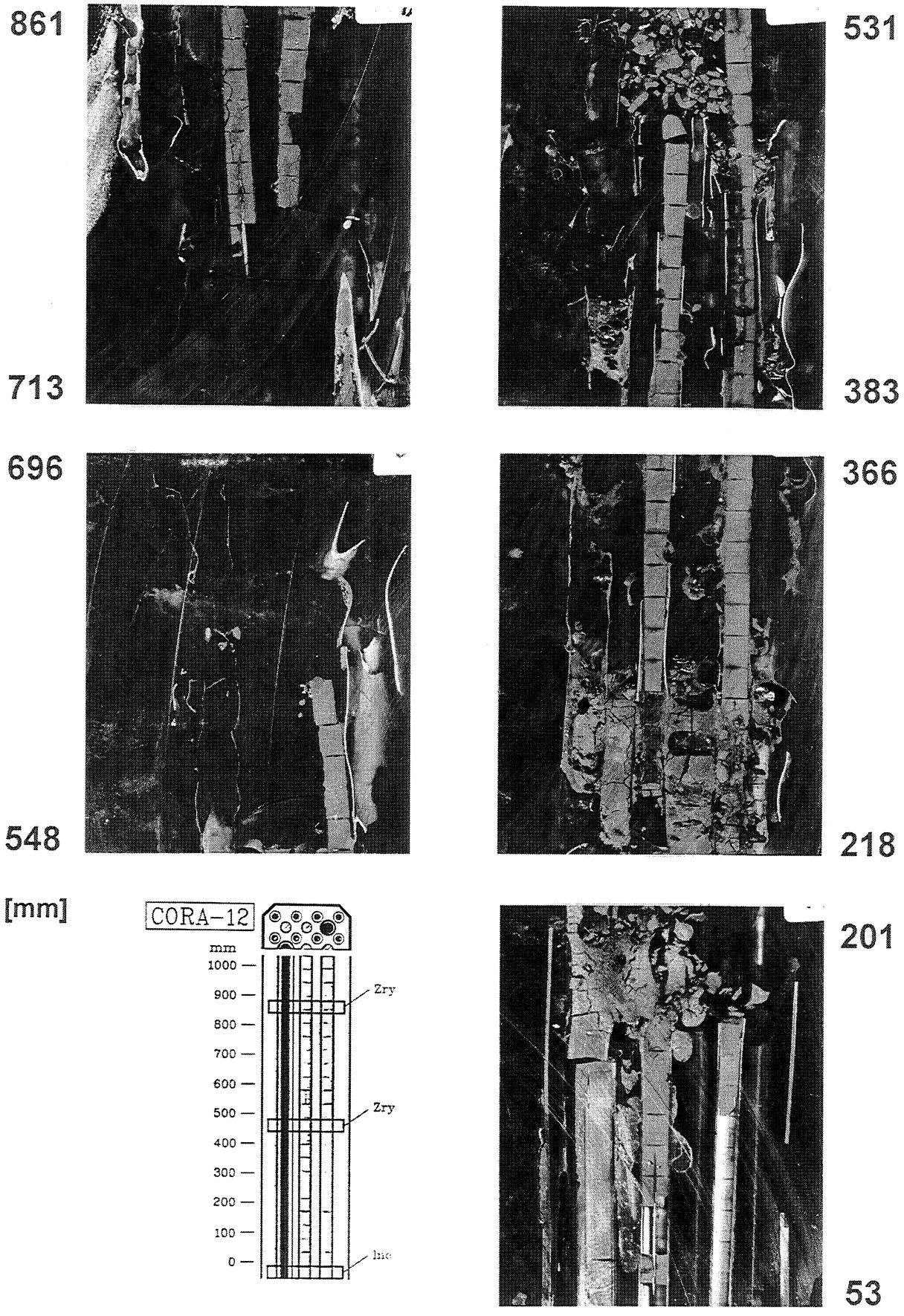

Fig.48: CORA-12; Vertical cross sections

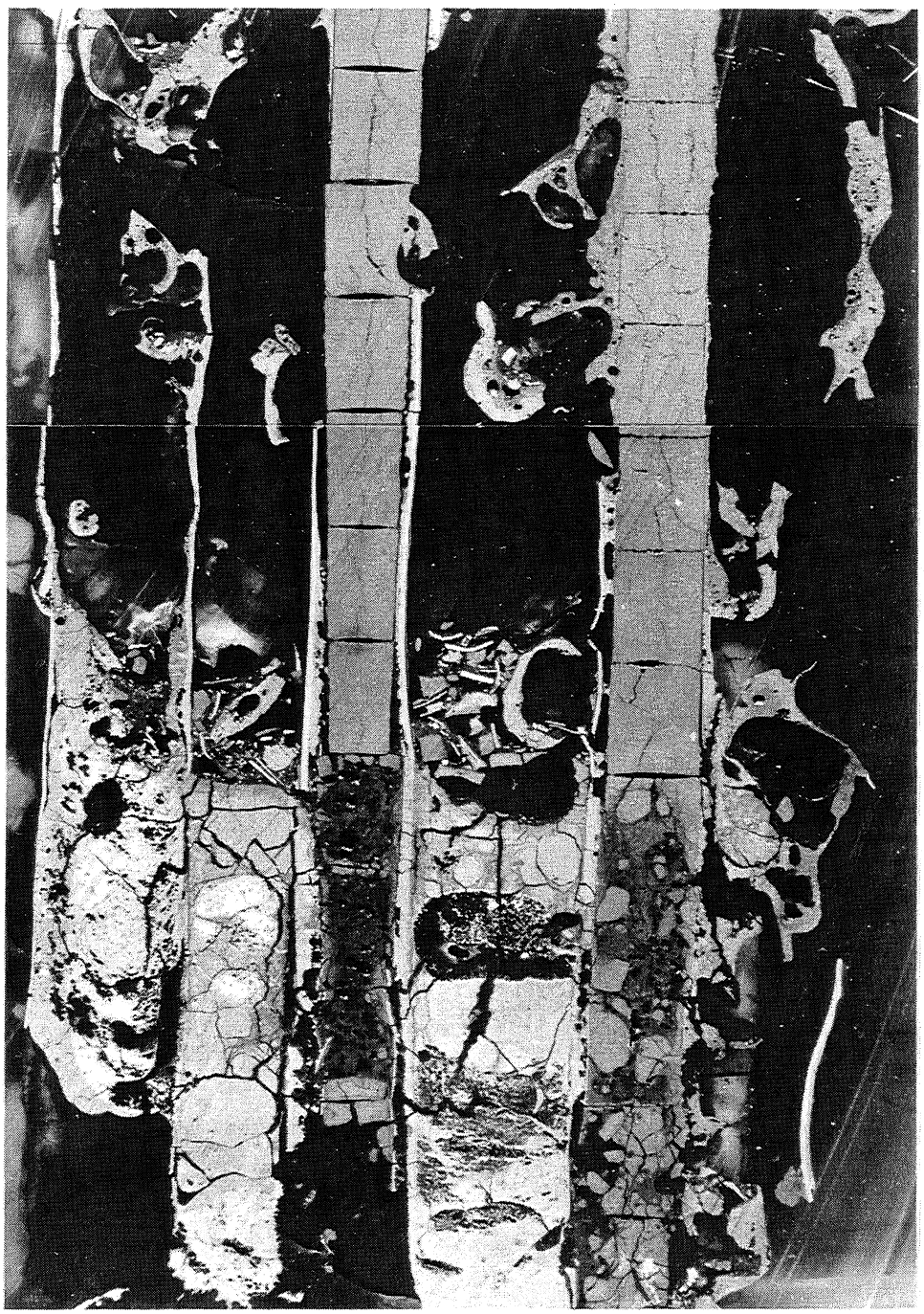

Fig.49: CORA-12; Vertical cross sections

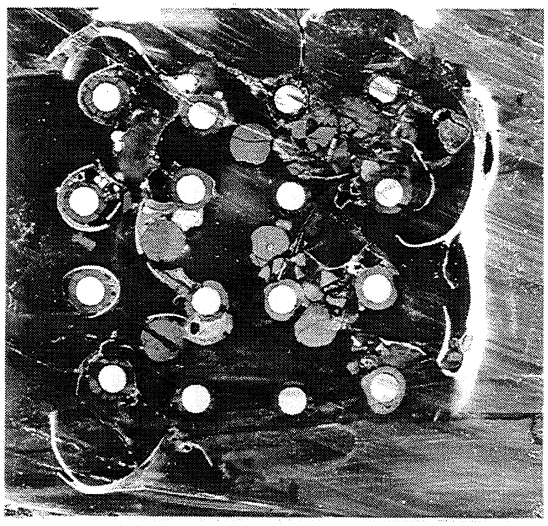

bottom 863mm

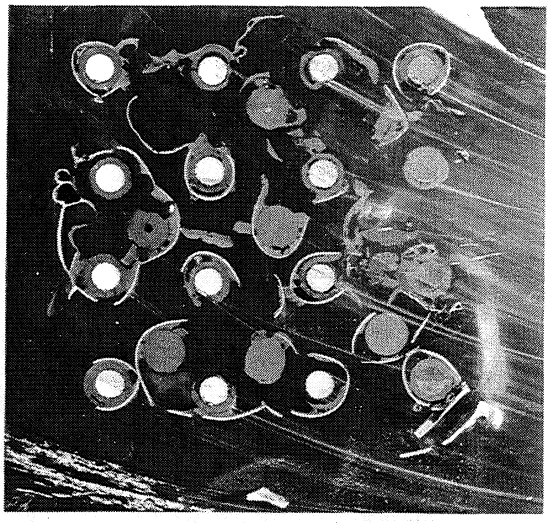

bottom 383mm

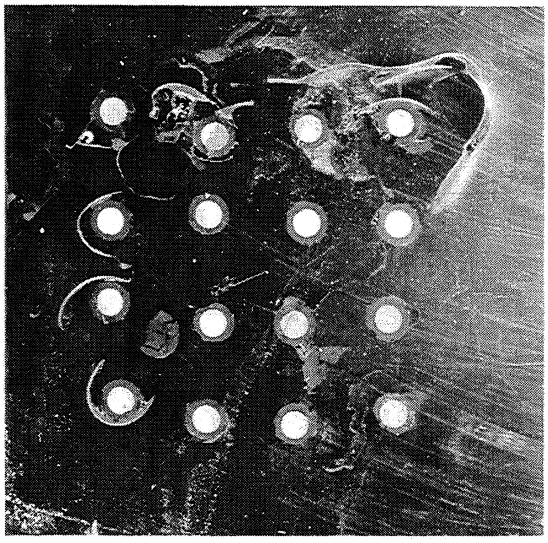

bottom 713mm

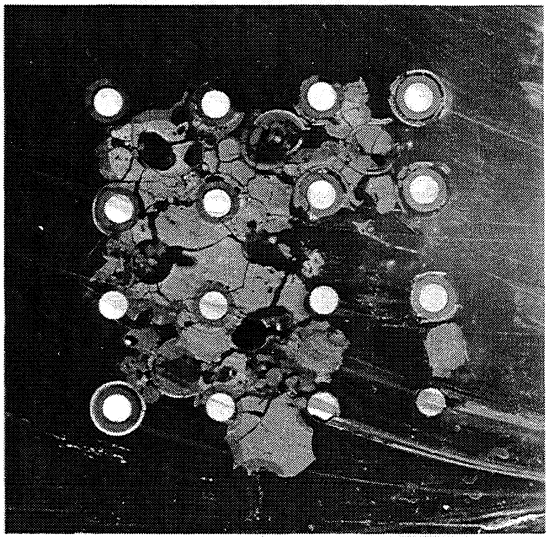

bottom 218mm

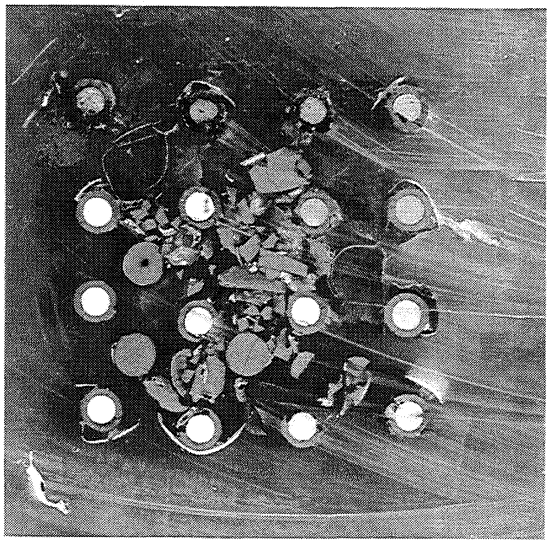

bottom 533mm

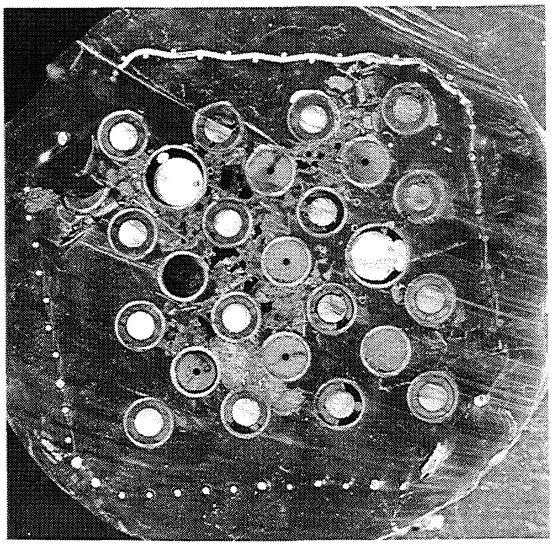

bottom -6mm

Fig.50: CORA-12; Horizontal cross sections

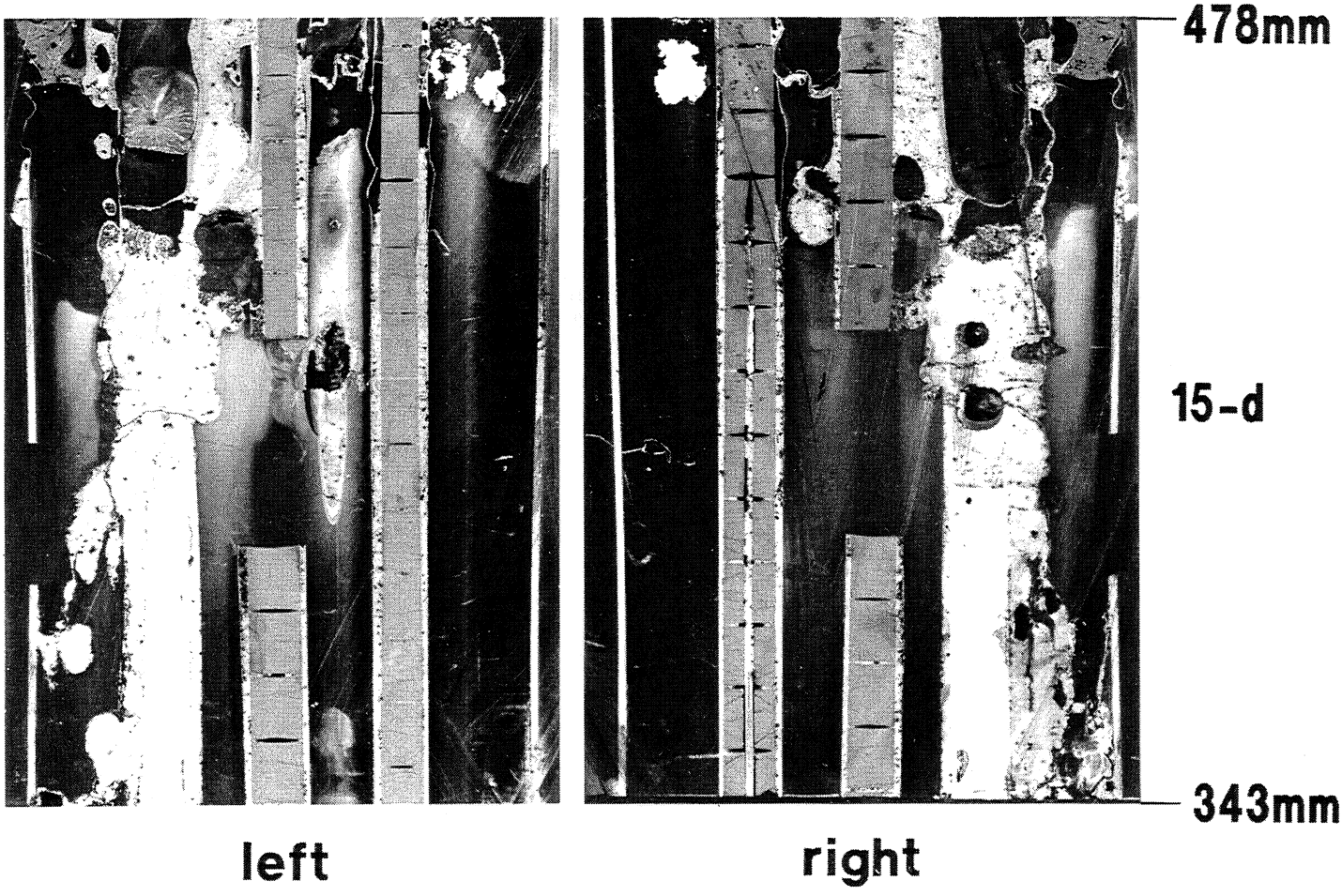

Fig. 51: Vertical cross sections of CORA-15

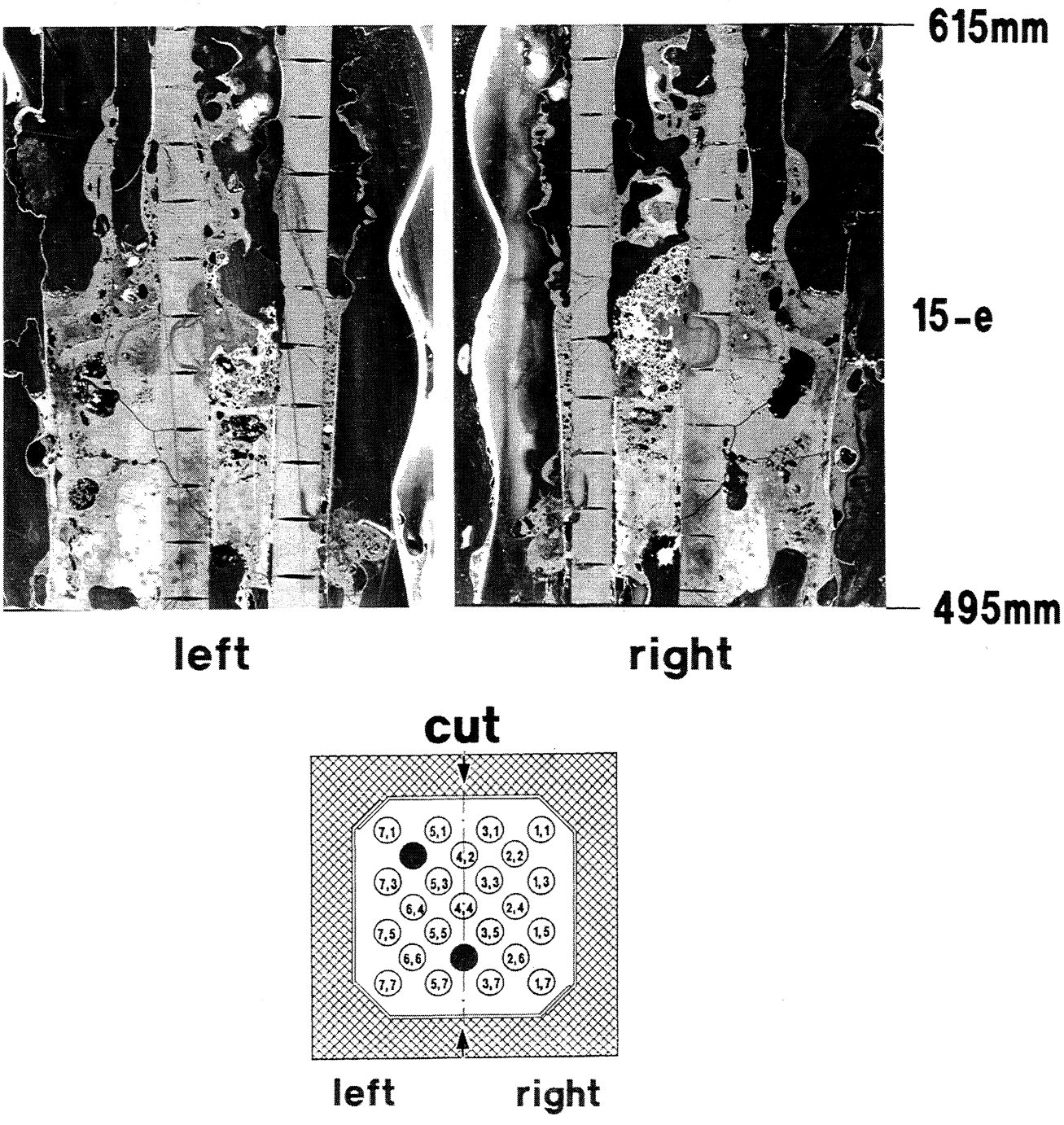

Fig. 52: Vertical cross sections of CORA-15

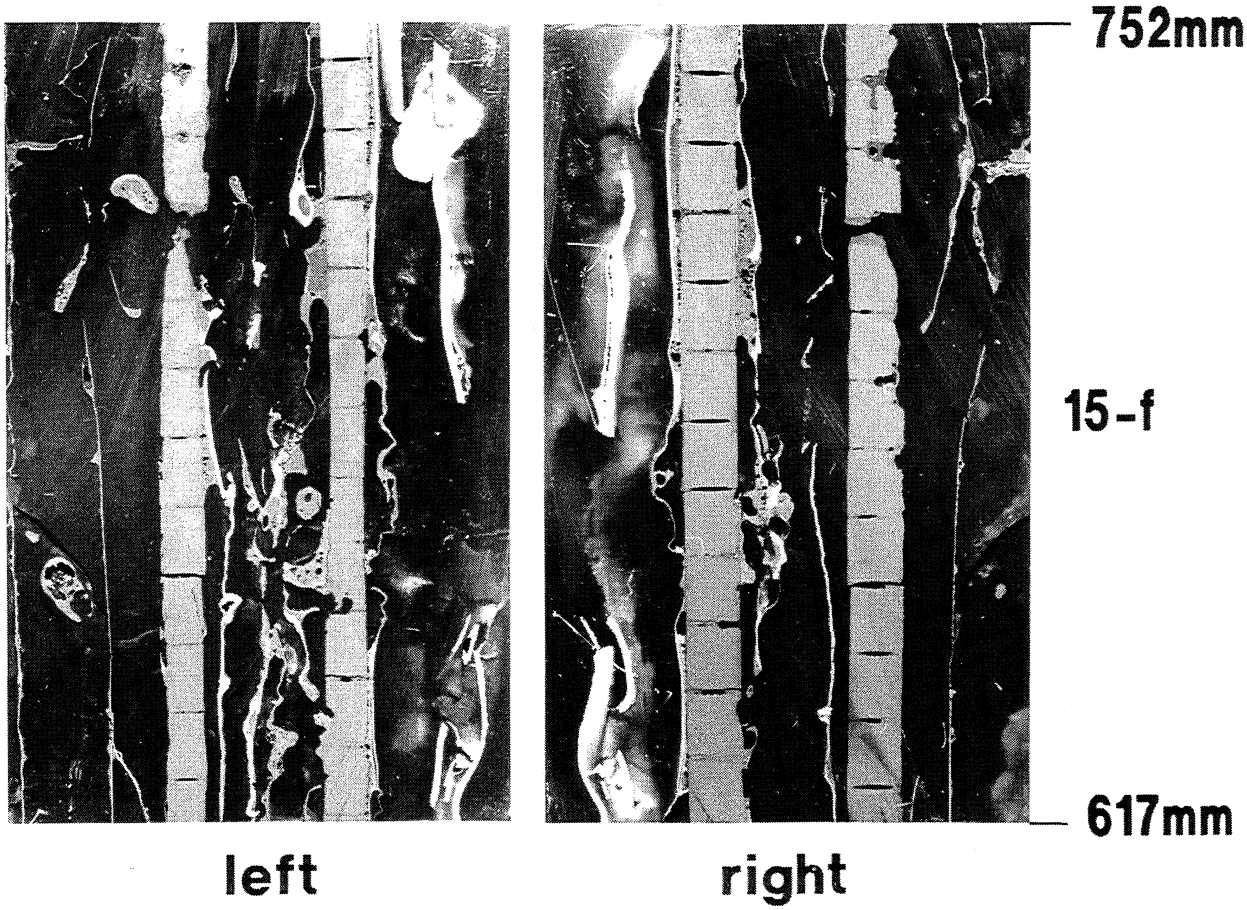

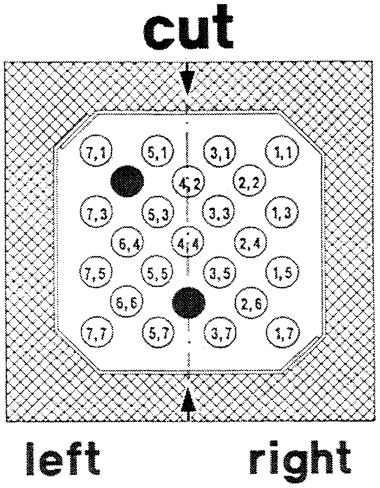

Fig. 53: Vertical cross sections of CORA-15

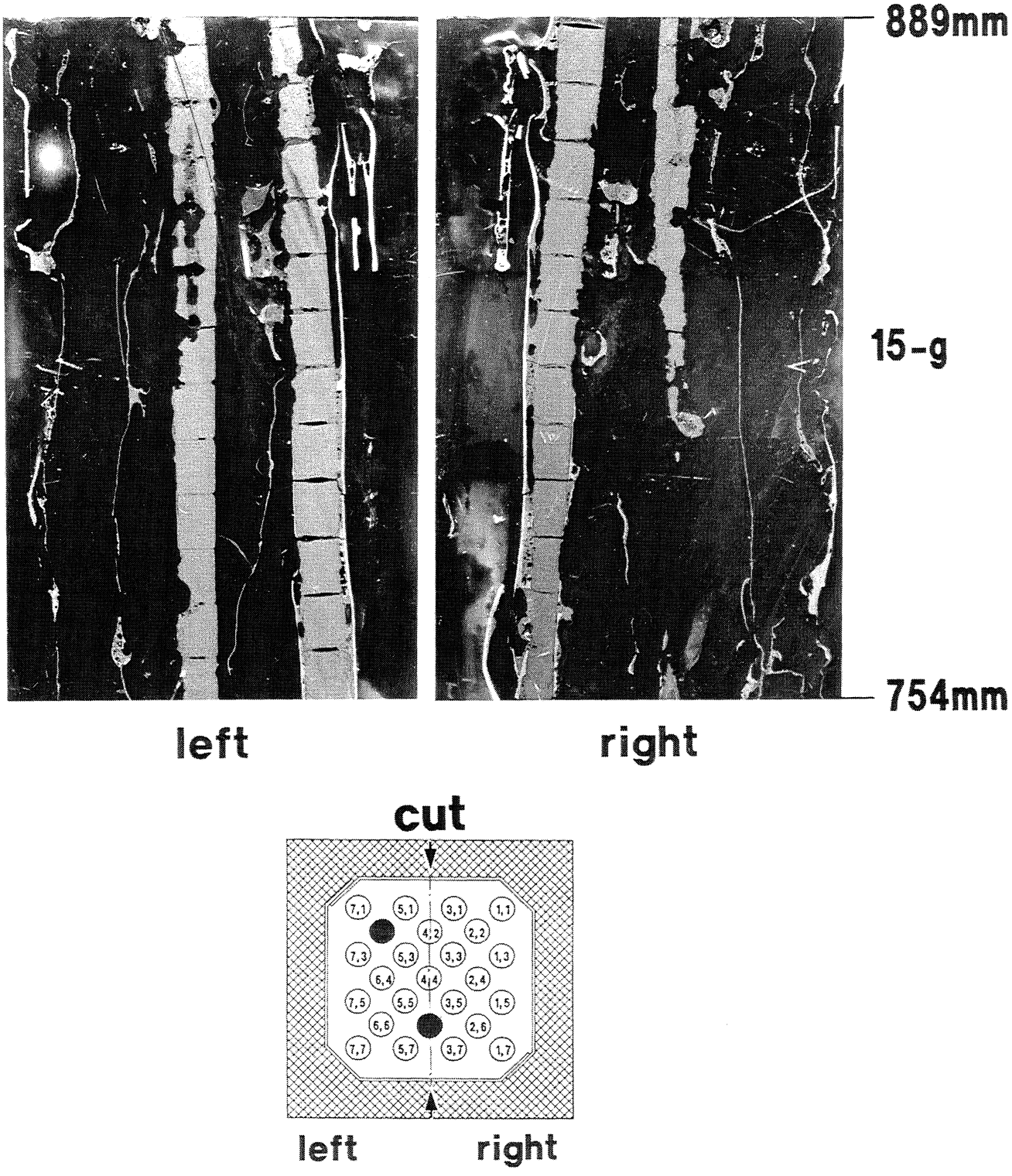

Fig. 54: Vertical cross sections of CORA-15

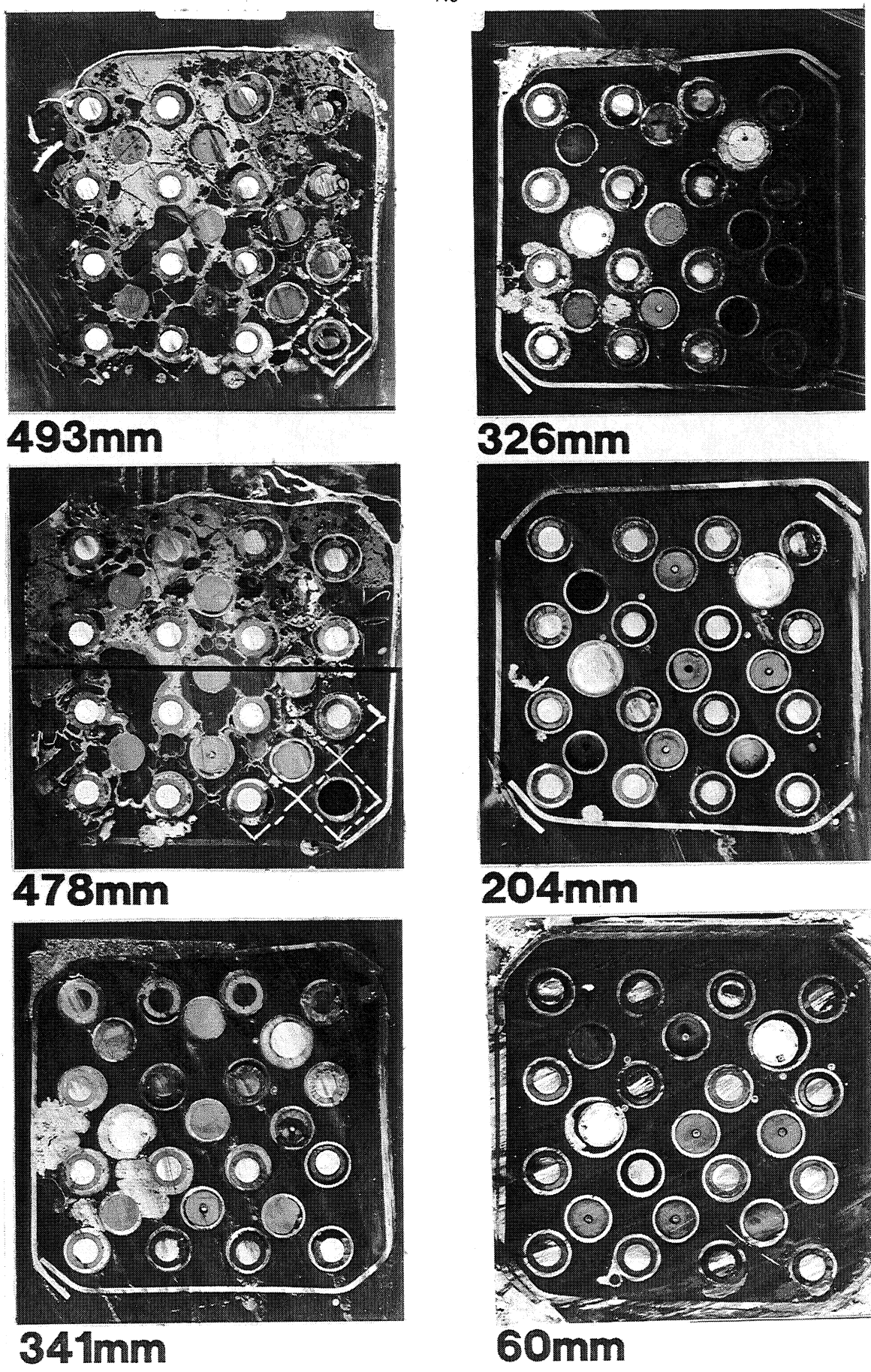

Fig. 55: CORA-15; Horizontal cross sections

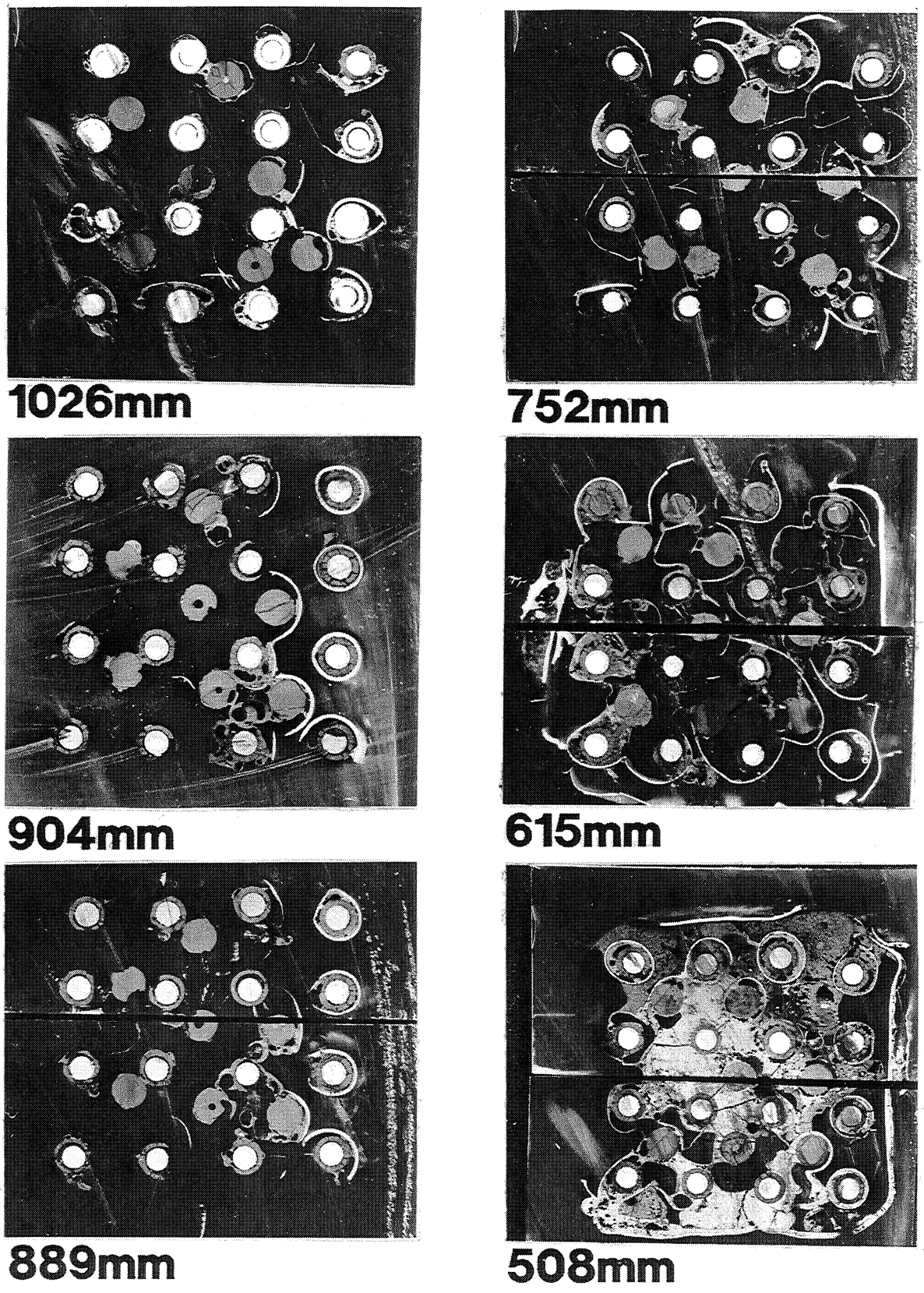

Fig.56: CORA-15; Horizontal cross sections

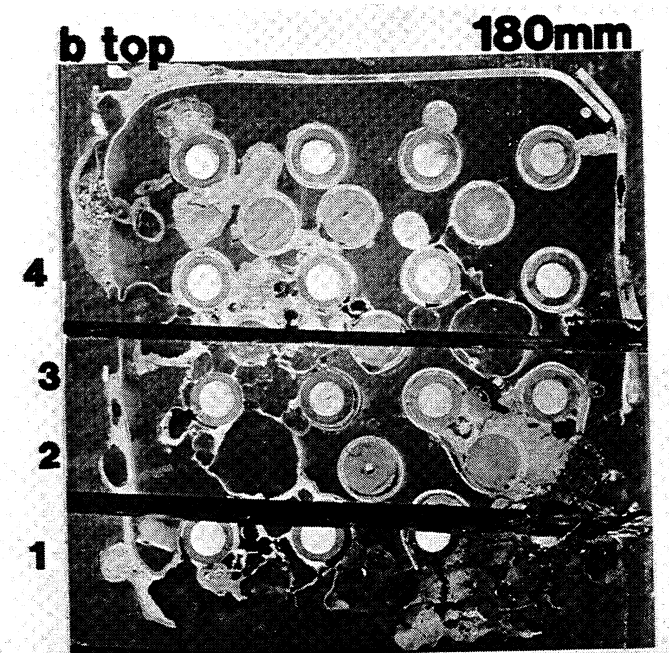

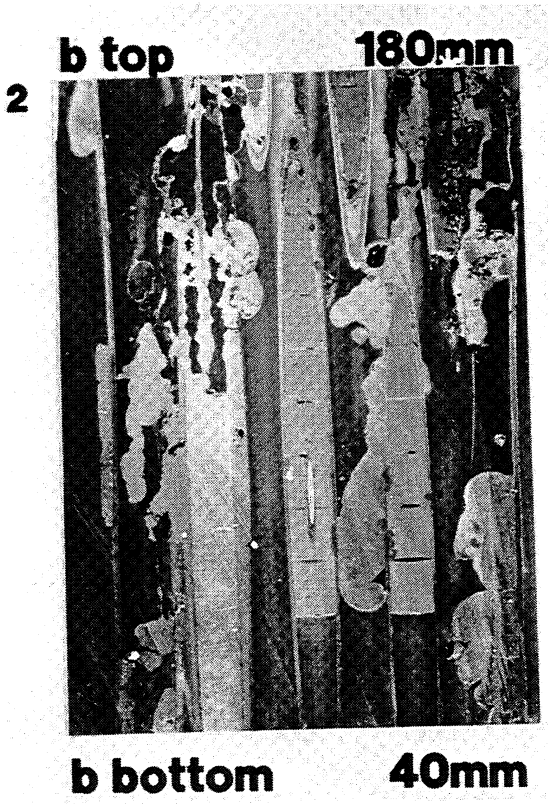

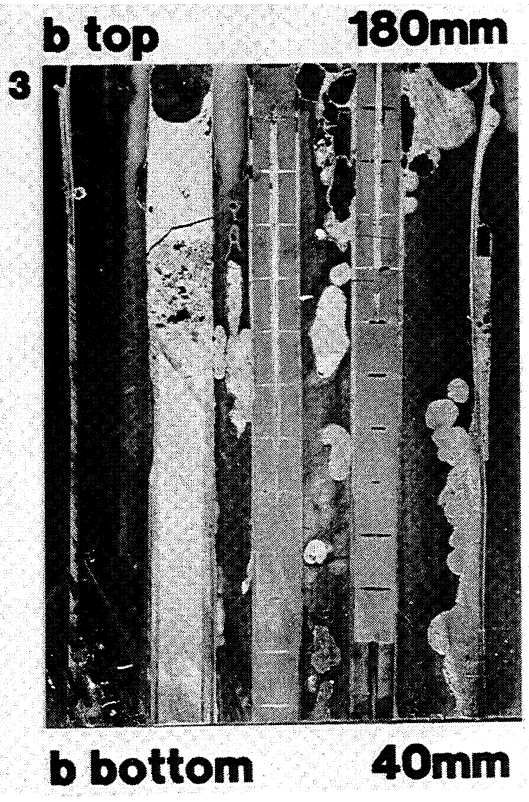

Fig.57: CORA-9; Vertical cross sections

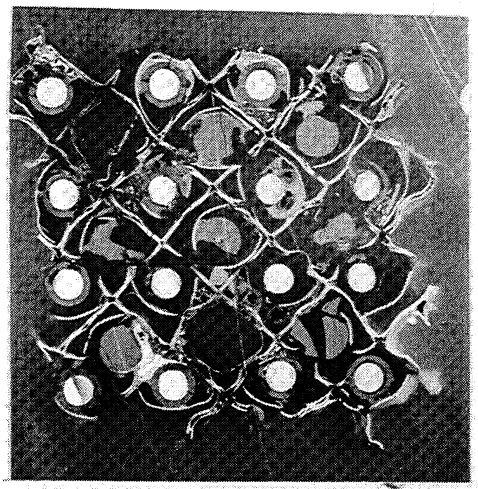

05 863mm

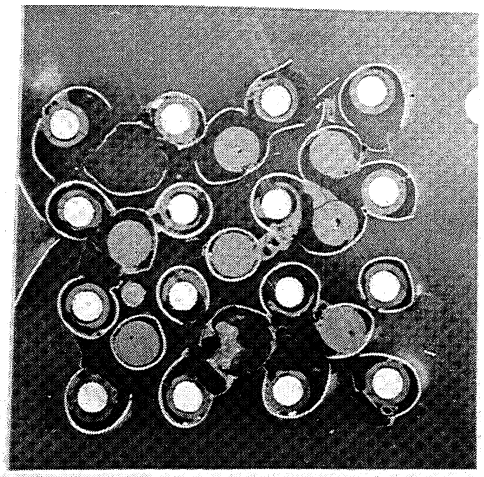

02 352mm

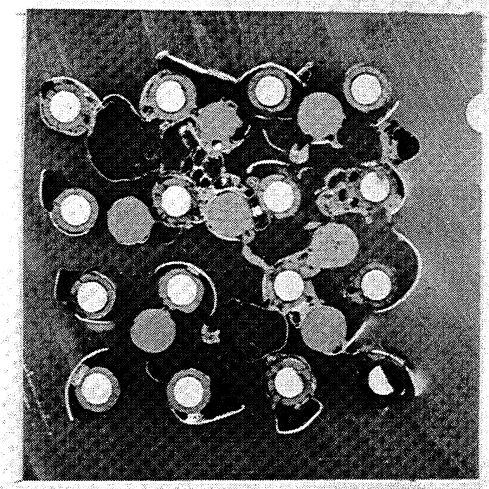

04 666mm

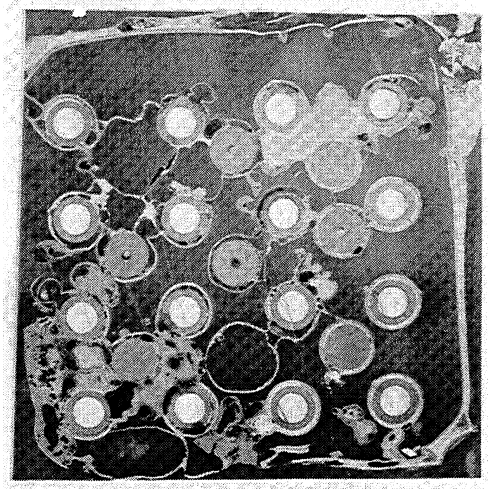

01 195mm

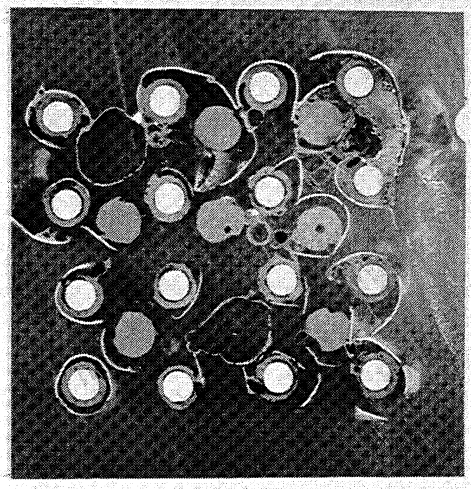

03 509mm

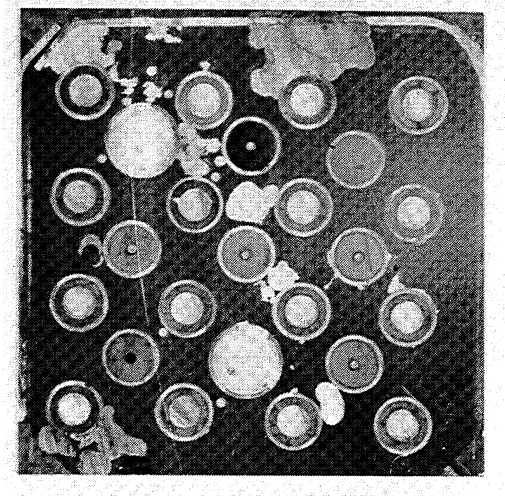

a2 38mm

Fig.58: CORA-9; Horizontal cross sections

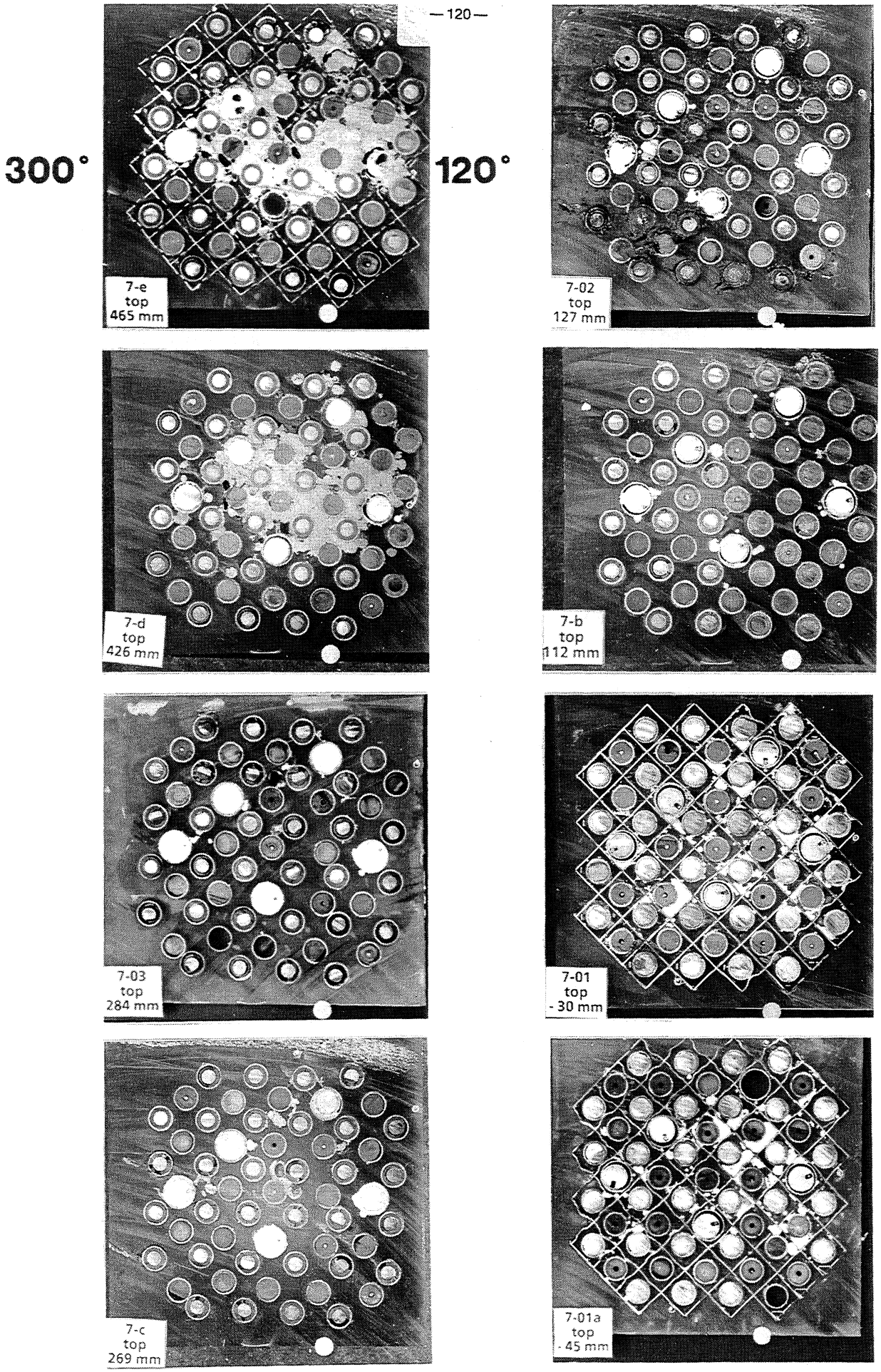

Fig. 59: CORA-7; Horizontal cross sections

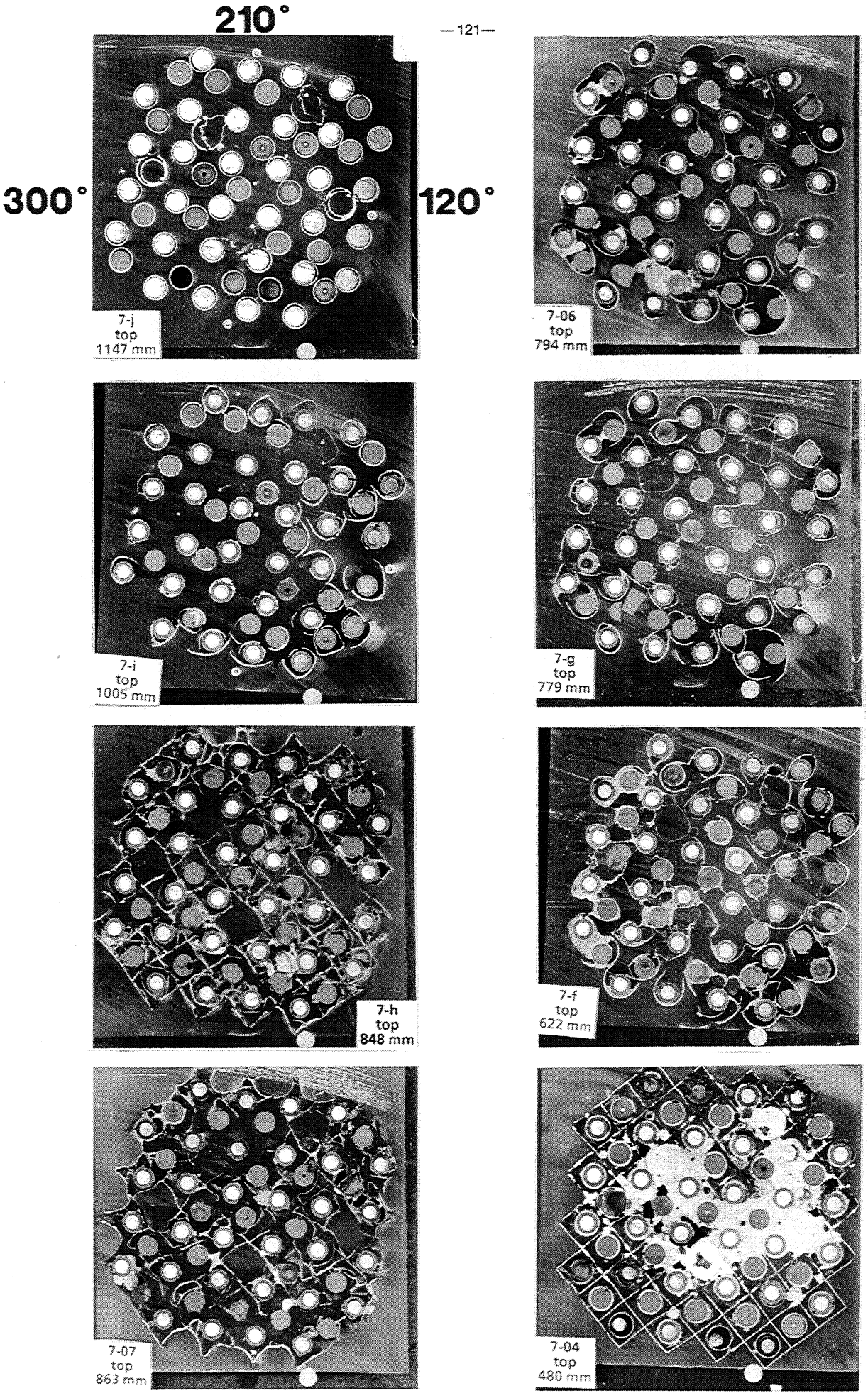

Fig.60: CORA-7; Horizontal cross sections

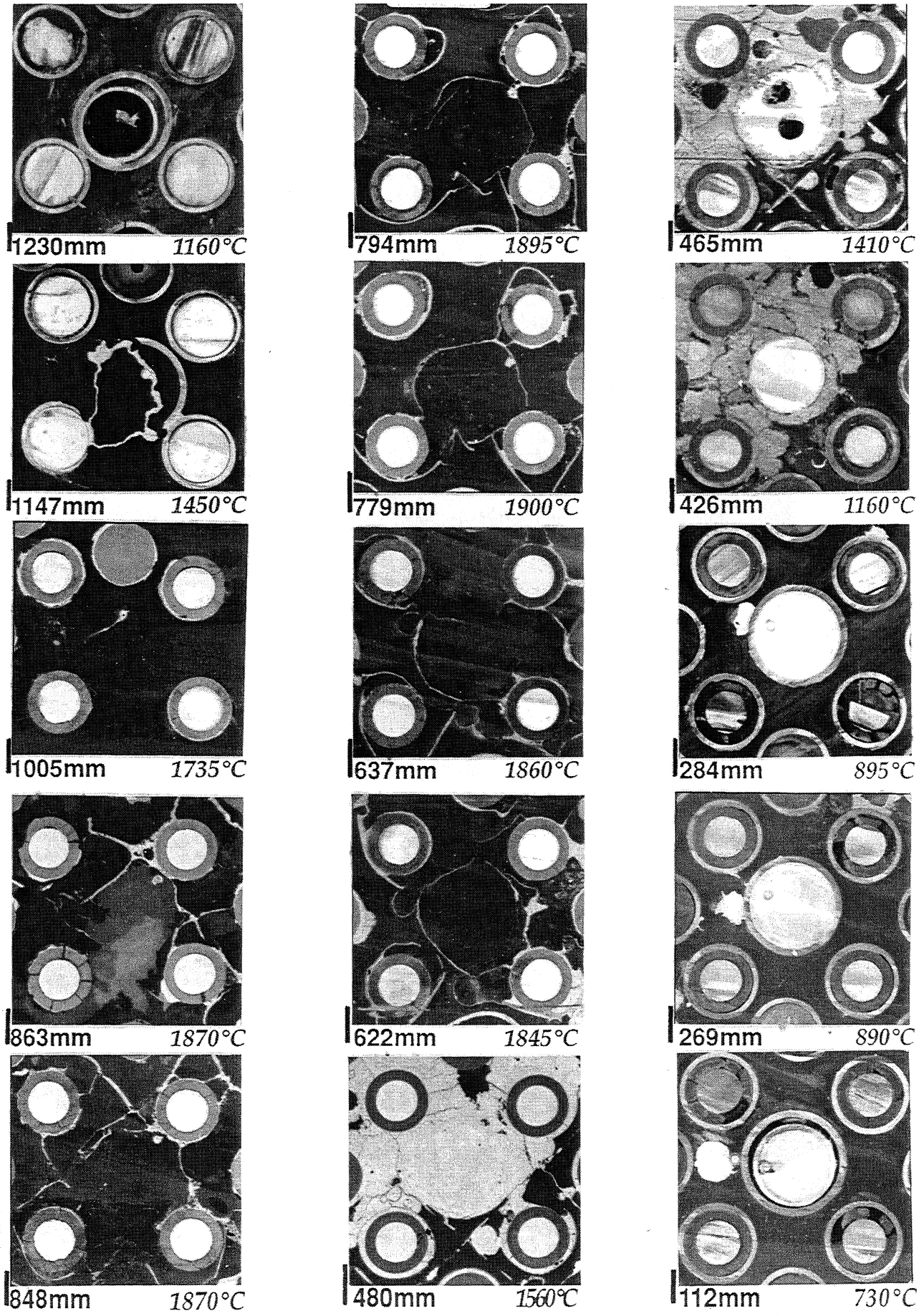

Fig.61: CORA-7, Cross sections of absorber rod 6.6

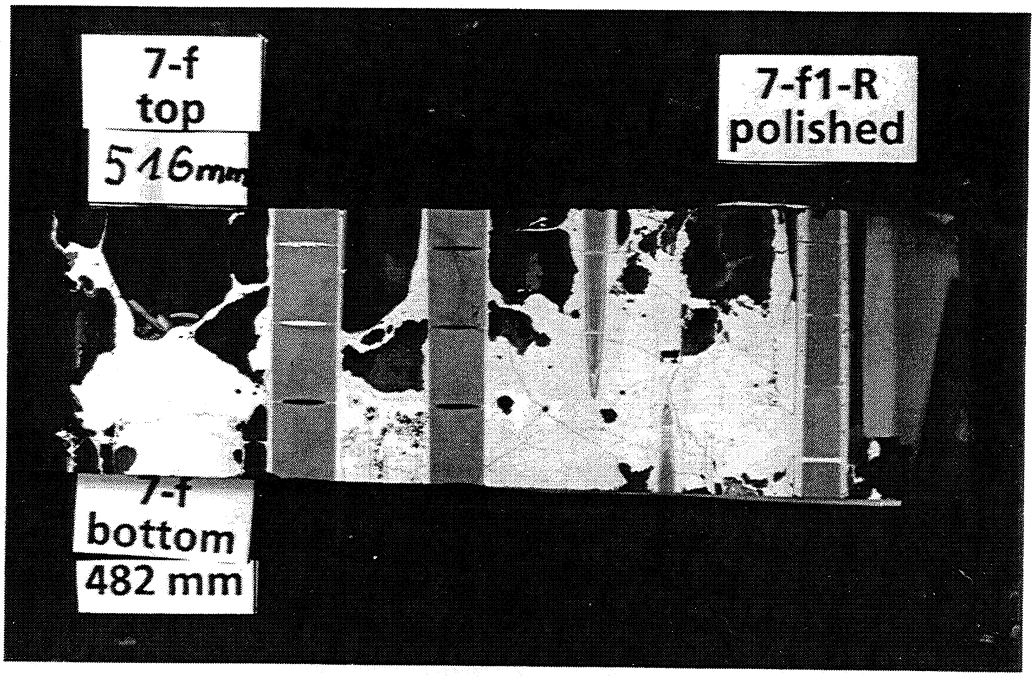

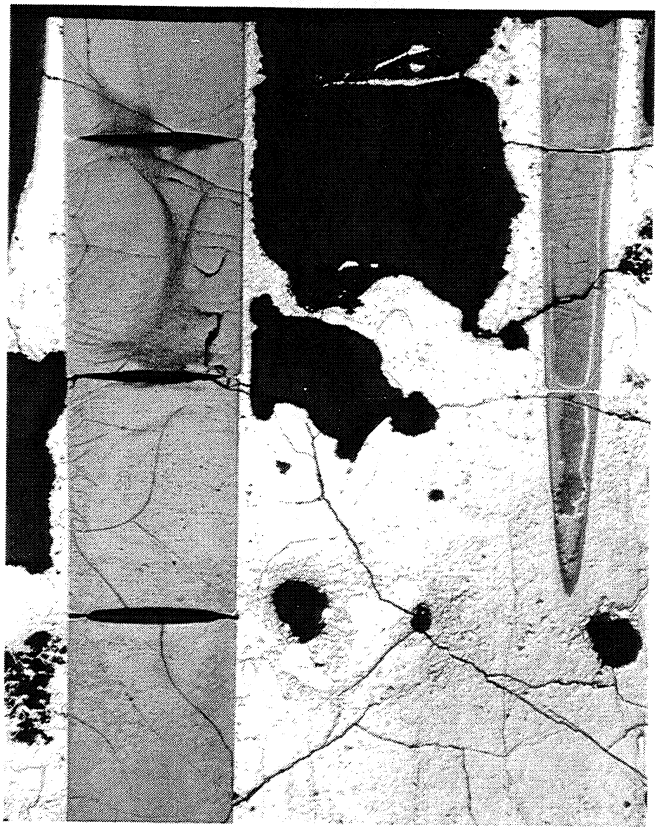

Fig. 62: CORA-7; Longitudinal sections between 482 and 516 mm elevation

vertical cross-section # 5-d (210-290mm)

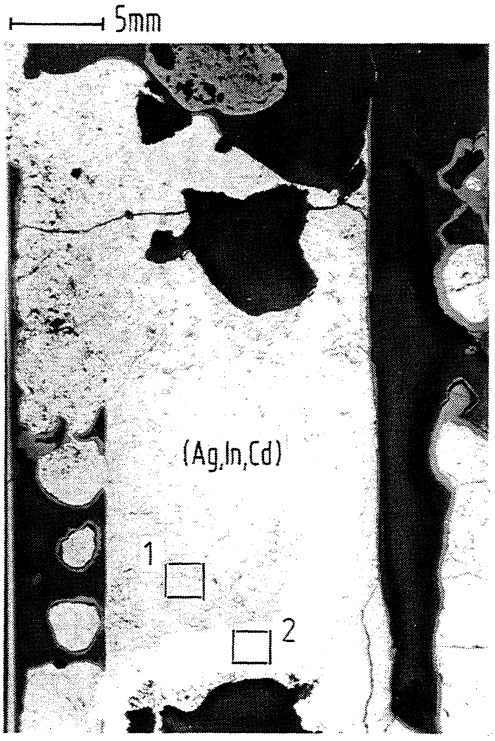

destroyed absorber rod

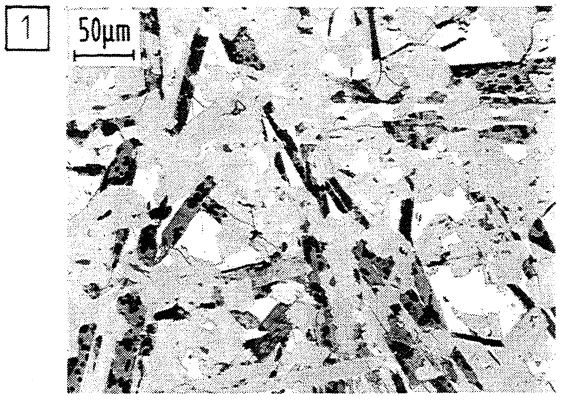

solidified absorber melts

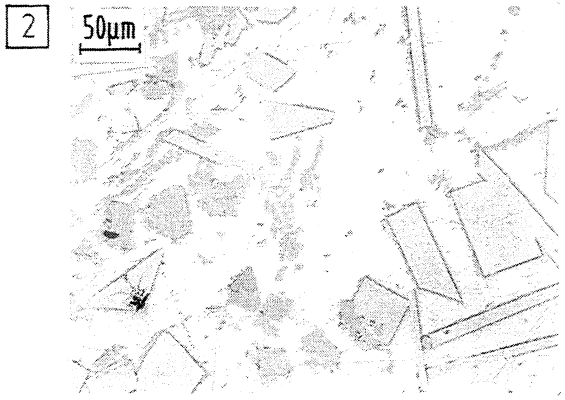

Fig. 63: Longitudinal section CORA-5-d;(210 - 290 mm)

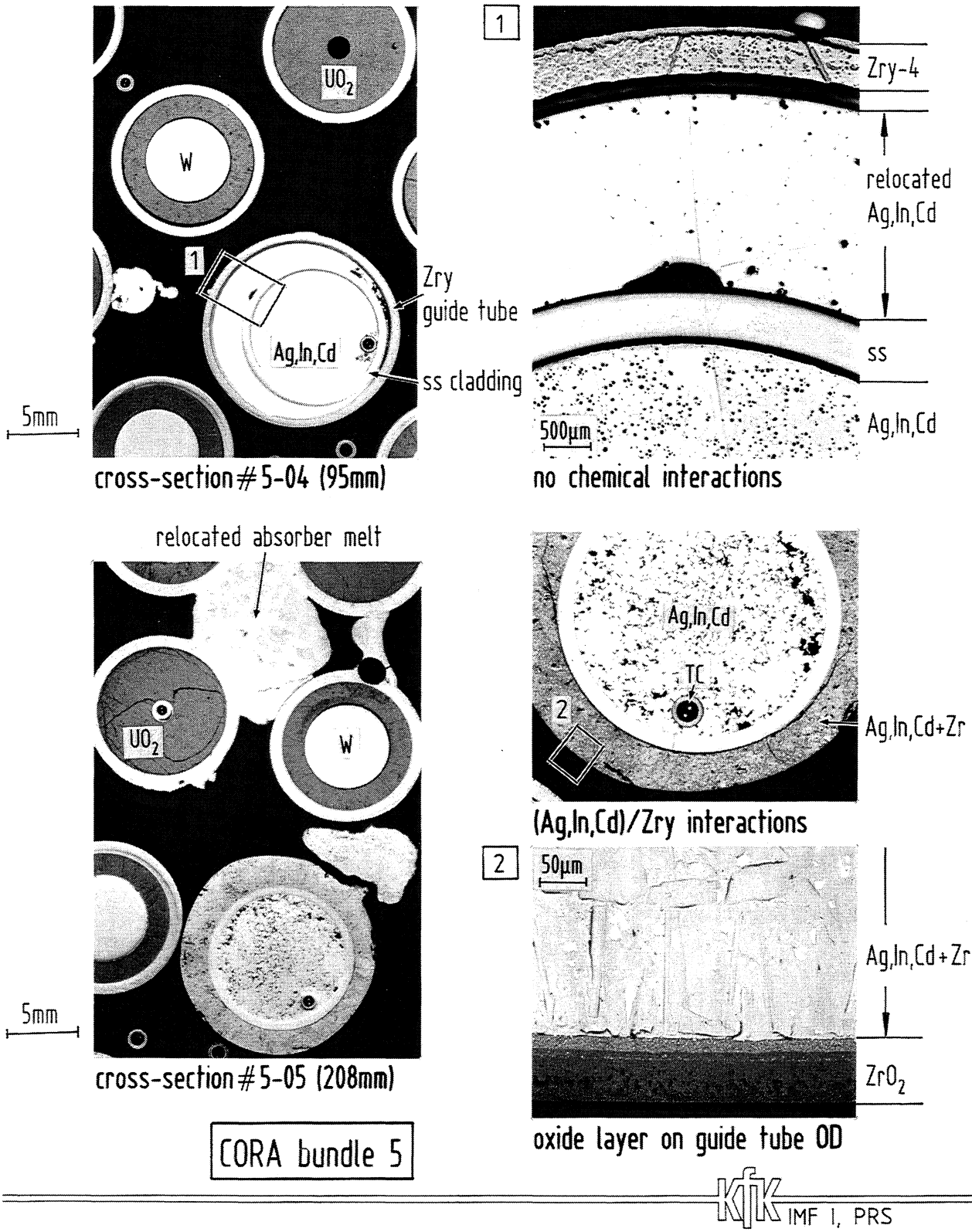

Fig. 64: Microstructures at 95 and 208 mm (CORA-5)

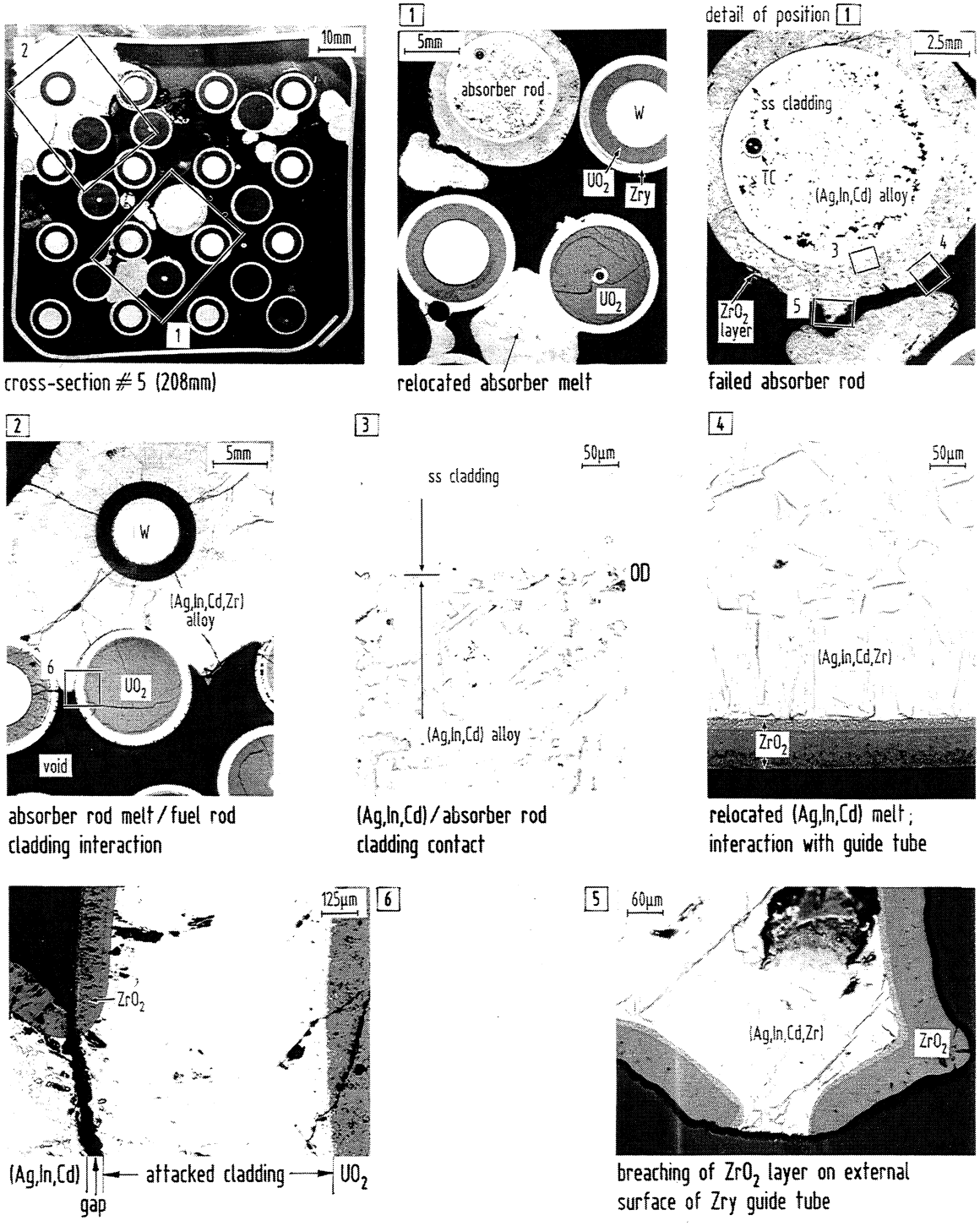

Fig. 65: Macro and microstructures in the cross section at 208 mm elevation of test CORA-5

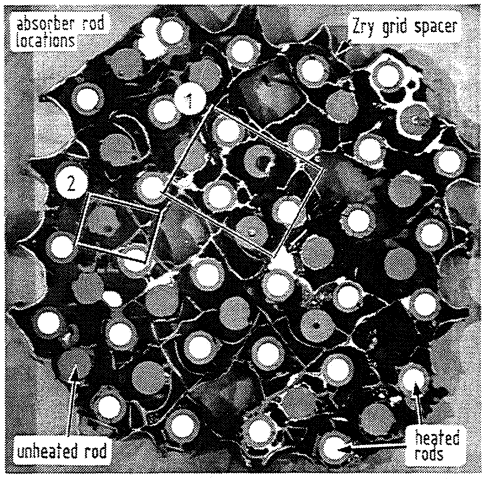

cross-section CORA 7-07 (863mm)

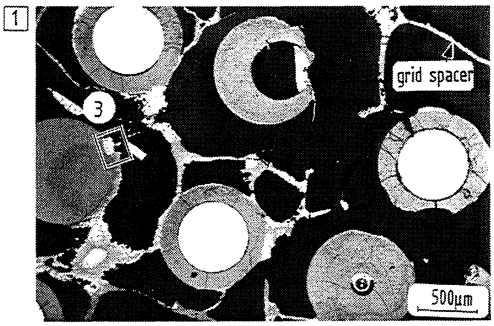

declad UO_2 fuel pellets

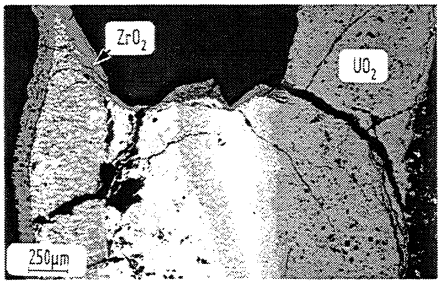

molten Zircaloy/UO_2 interaction

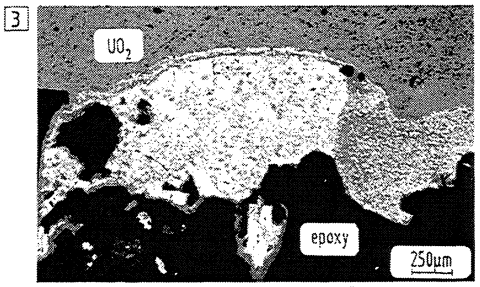

localized UO_2 attack by molten Zry

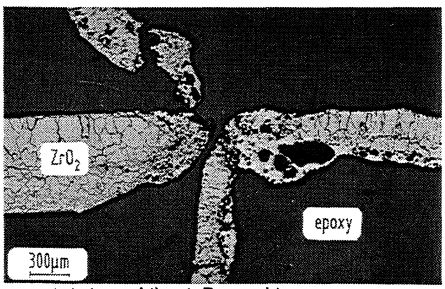

completely oxidized Zry grid spacer

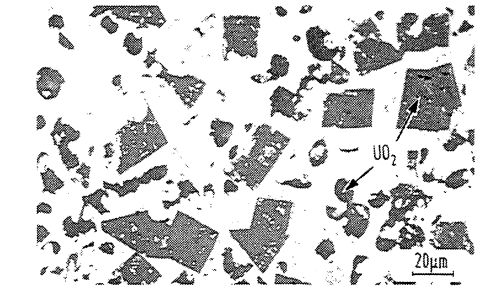

metallic melt with ceramic precipitations

accumulation of solid fragments

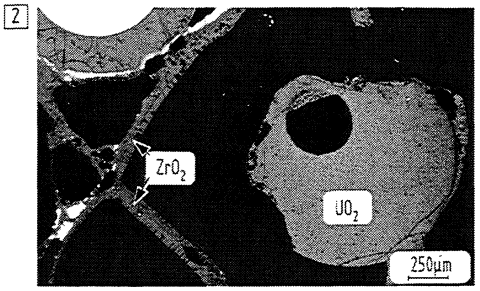

partially dissolved UO_2 pellet

Fig. 66: Microstructures of cross section CORA-7-07 (863 mm)

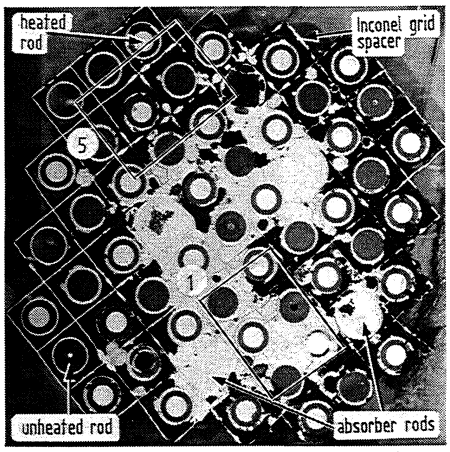

cross-section CORA 7-04 (480mm)

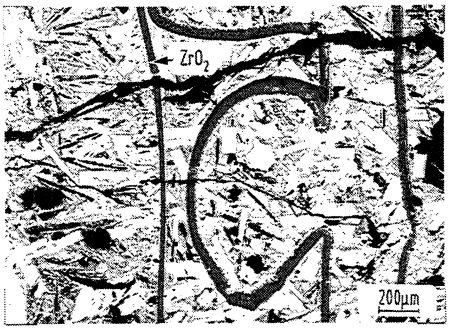

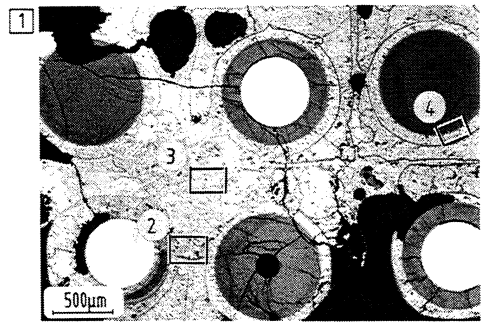

relocated solidified metallic melt

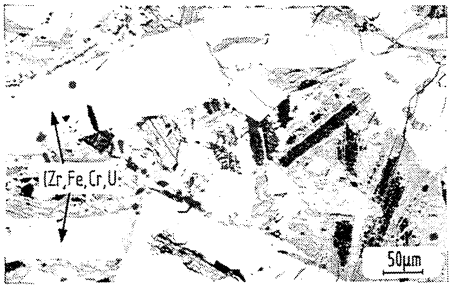

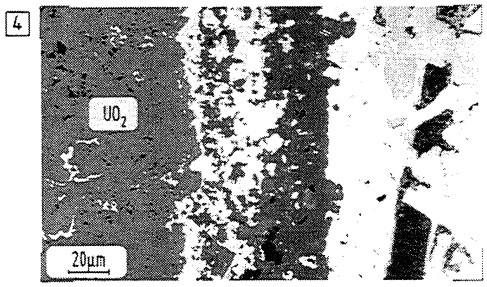

chemical attack of UO_2 pellet

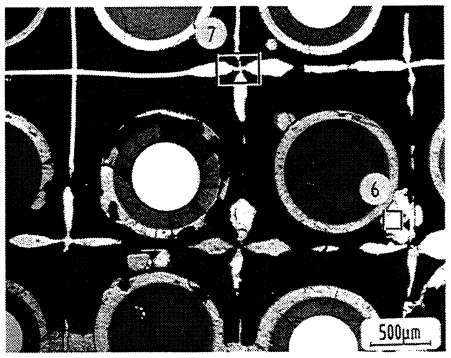

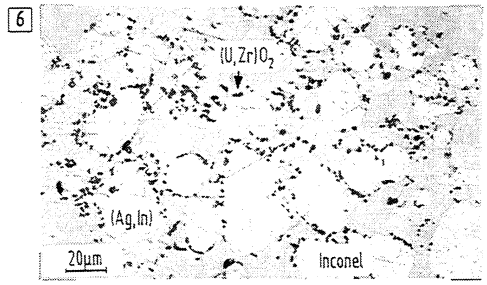

precipitations in relocated solidified metallic melt

partially oxidized Inconel grid spacer

Fig. 67: Microstructures of cross section CORA-7-04 (480 mm)

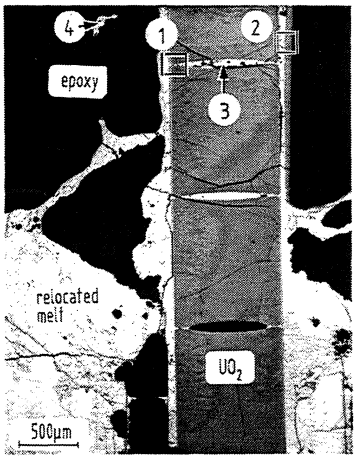

detail of longitudinal section CORA 7-f

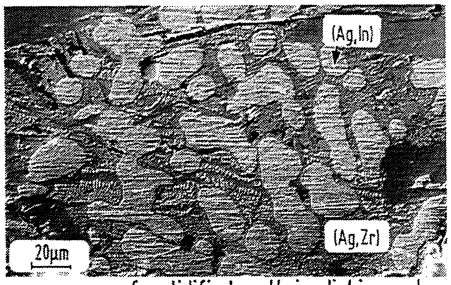

appearance of solidified melt in dishing volume (interference contrast)

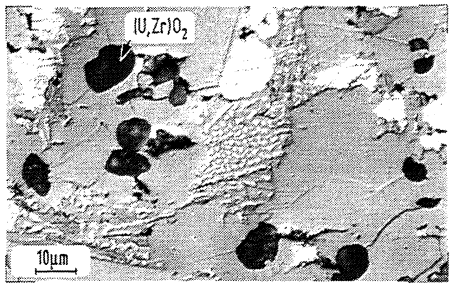

relocated solidified metallic melt (interference contrast)

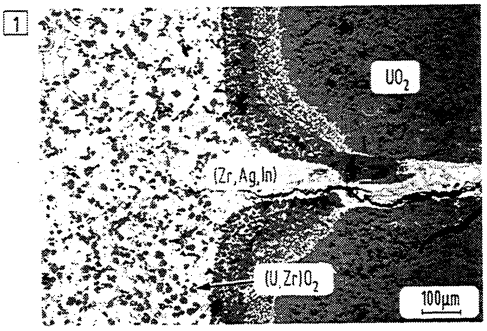

UO_2 dissolution by molten Zircaloy

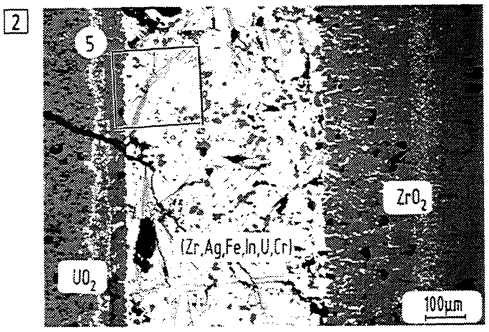

UO_2 and ZrO_2 attack by molten Zry

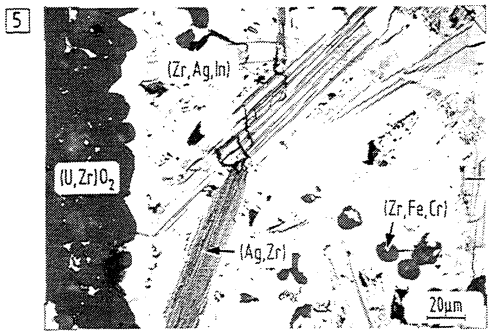

(Ag,Zr) precipitations in metallic melt

Fig. 68: Microstructures of the vertical cross section CORA-7-f (482 - 622 mm)

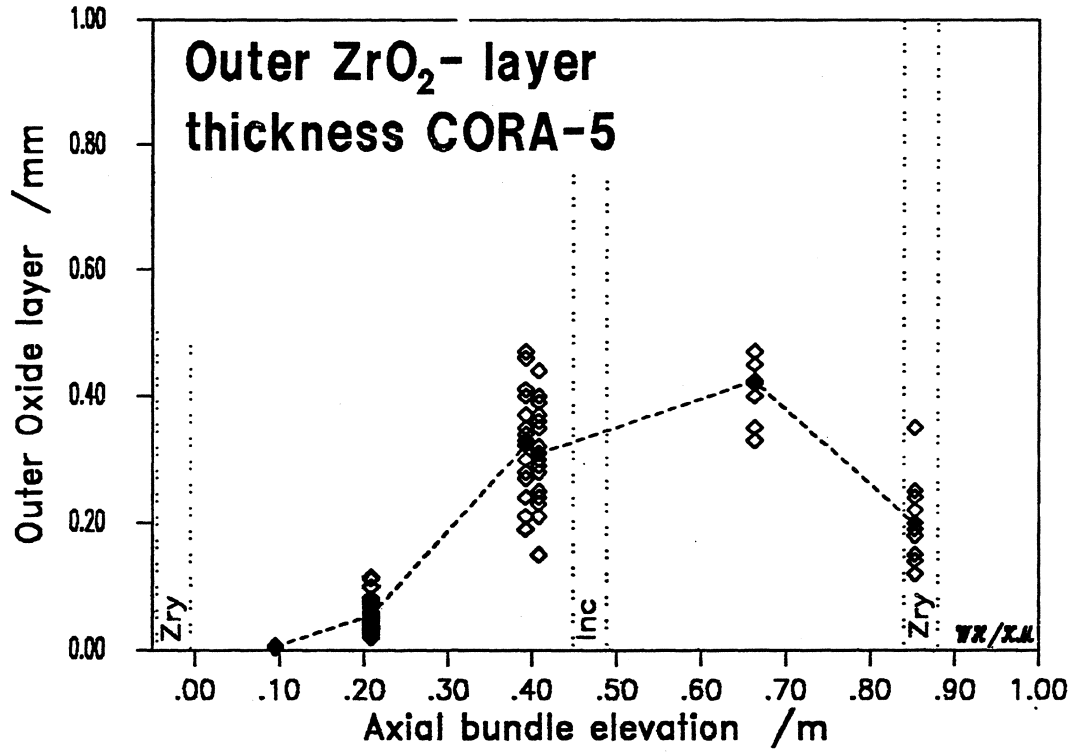

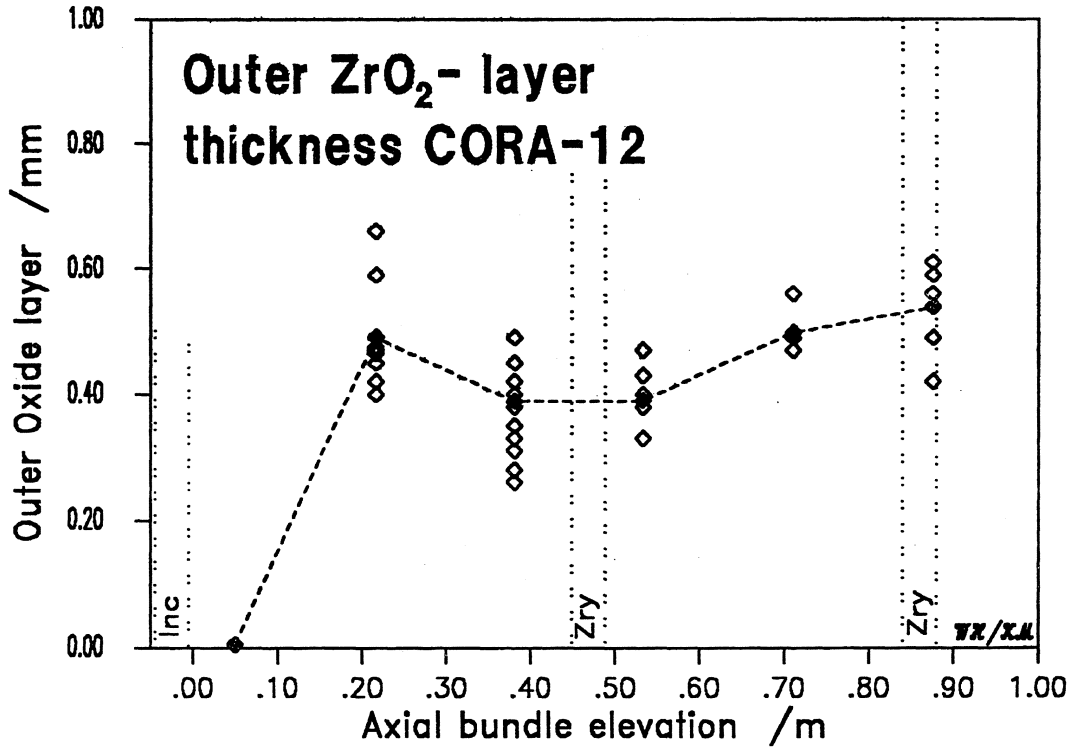

Fig. 69: Oxide layer thickness evaluated from tests CORA-5 and CORA-12

Appendix

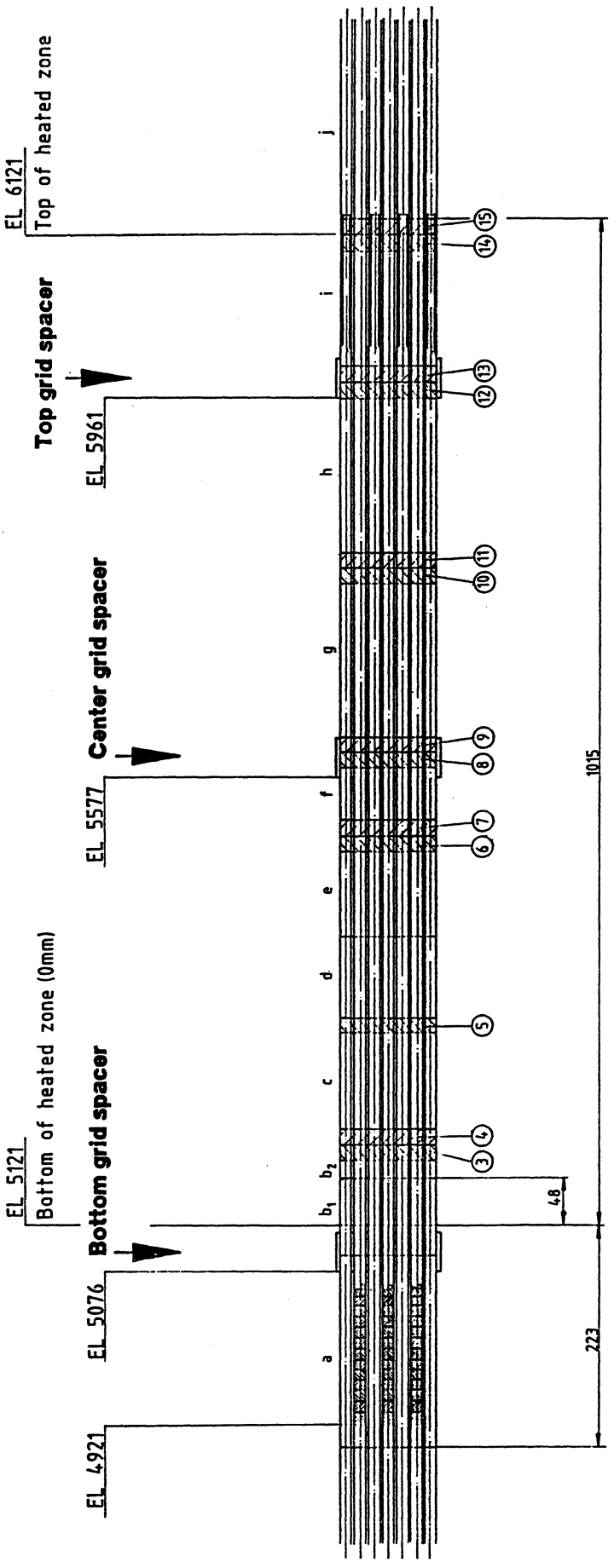

Fig.A1: CORA-5; Bundle sectioning

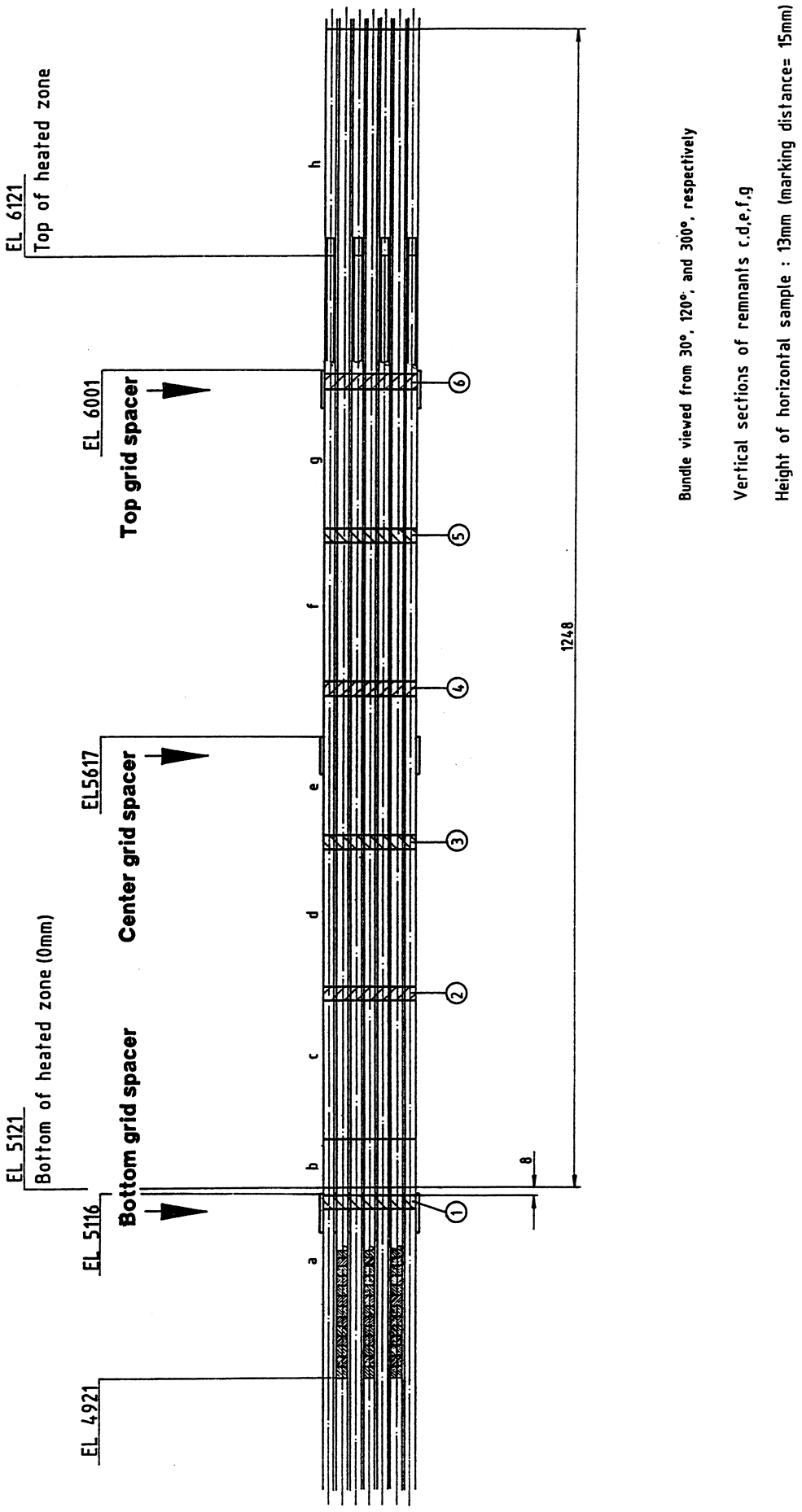

Fig.A2: CORA-12; Bundle sectioning

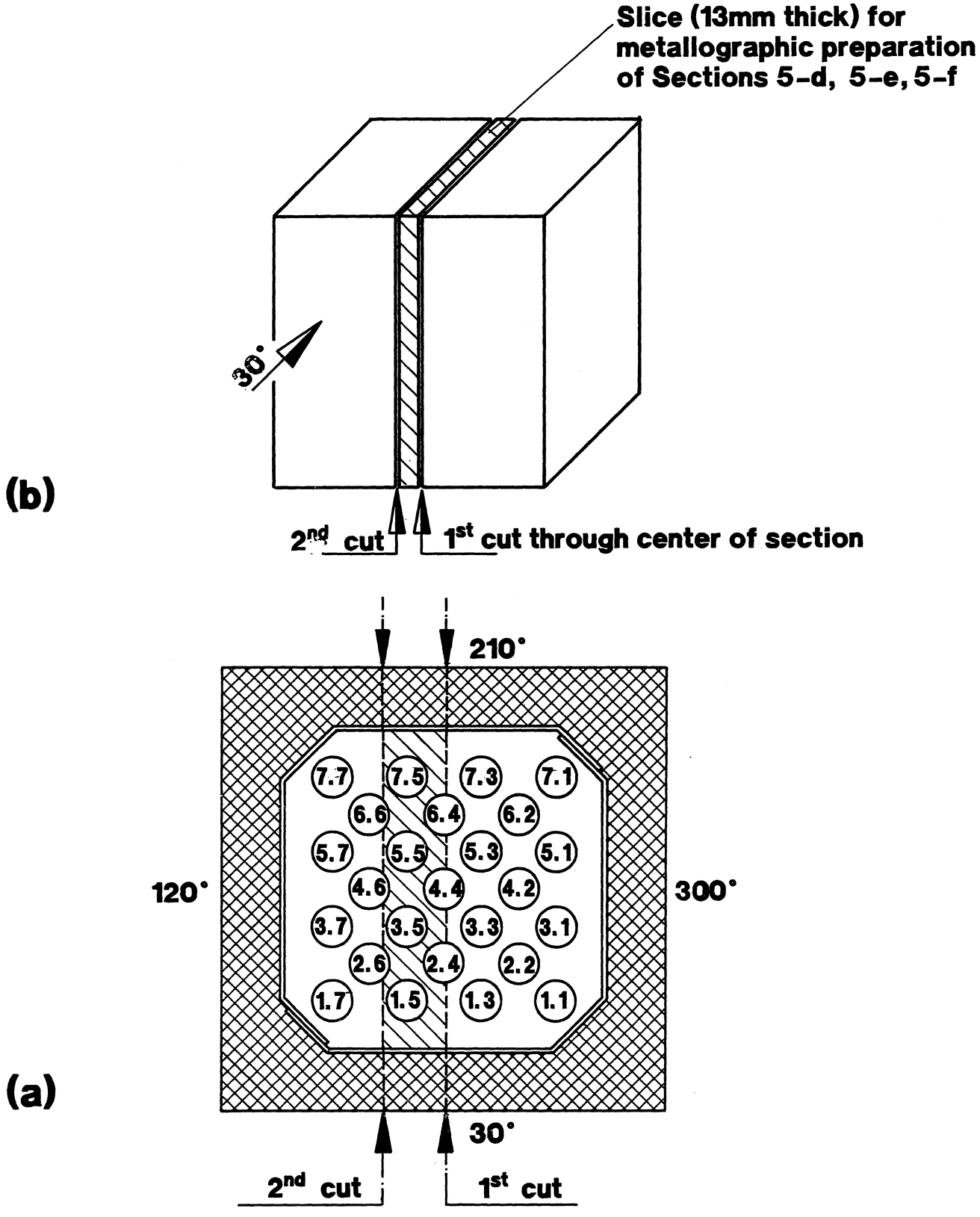

Fig. A3: CORA-5; Locations of vertical cuts through sections 5-c, 5-d, 5-e, 5-f, 5-g, 5-h, 5-i ; (a) top view, (b) viewed from 30 degree

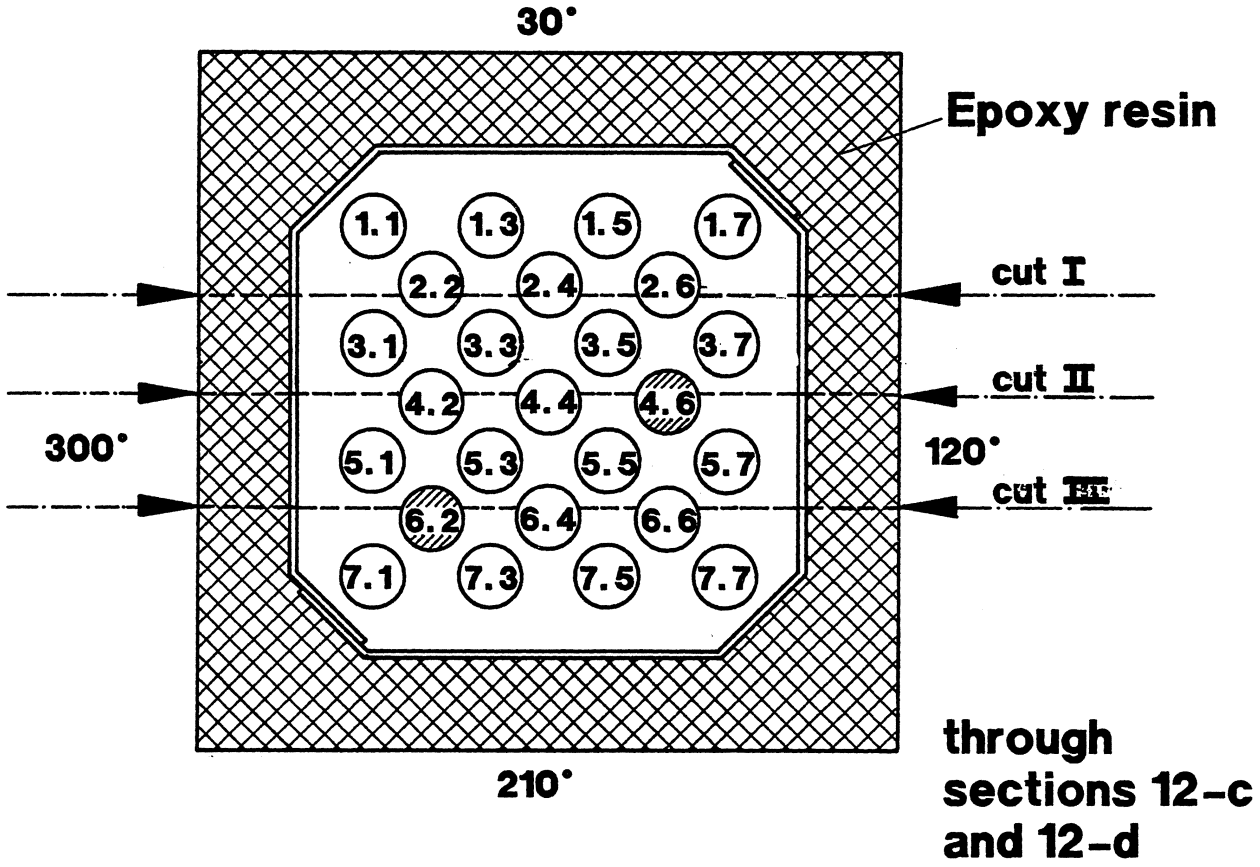

Fig. A4: CORA-12; Locations of vertical cuts through sections 12-c, 12-d (3 cuts), 12-e, 12-f, 12-g, (1st cut only); top view CORA-5, Bundle sectioning

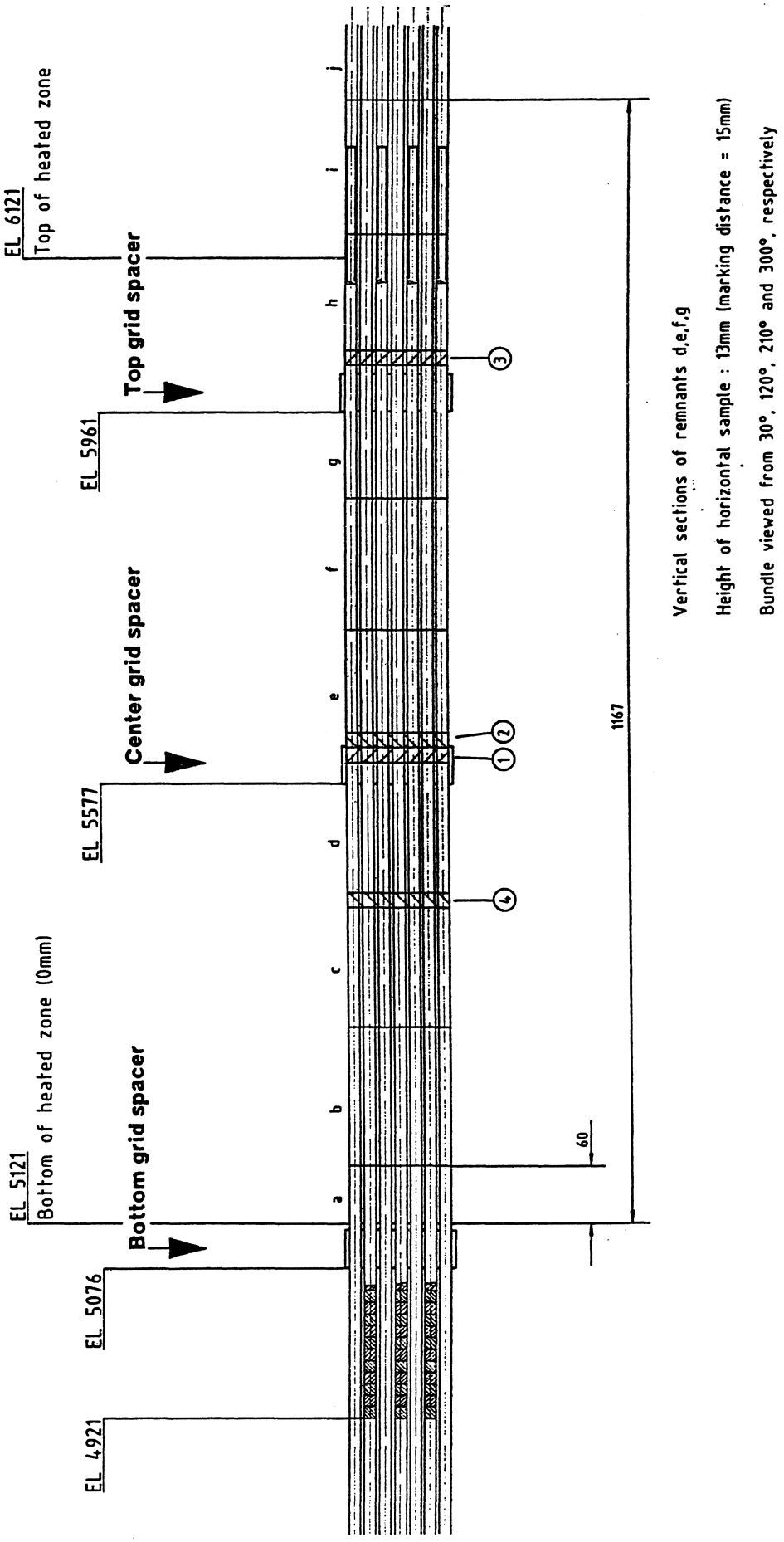

Fig.A5: CORA-15; Bundle sectioning

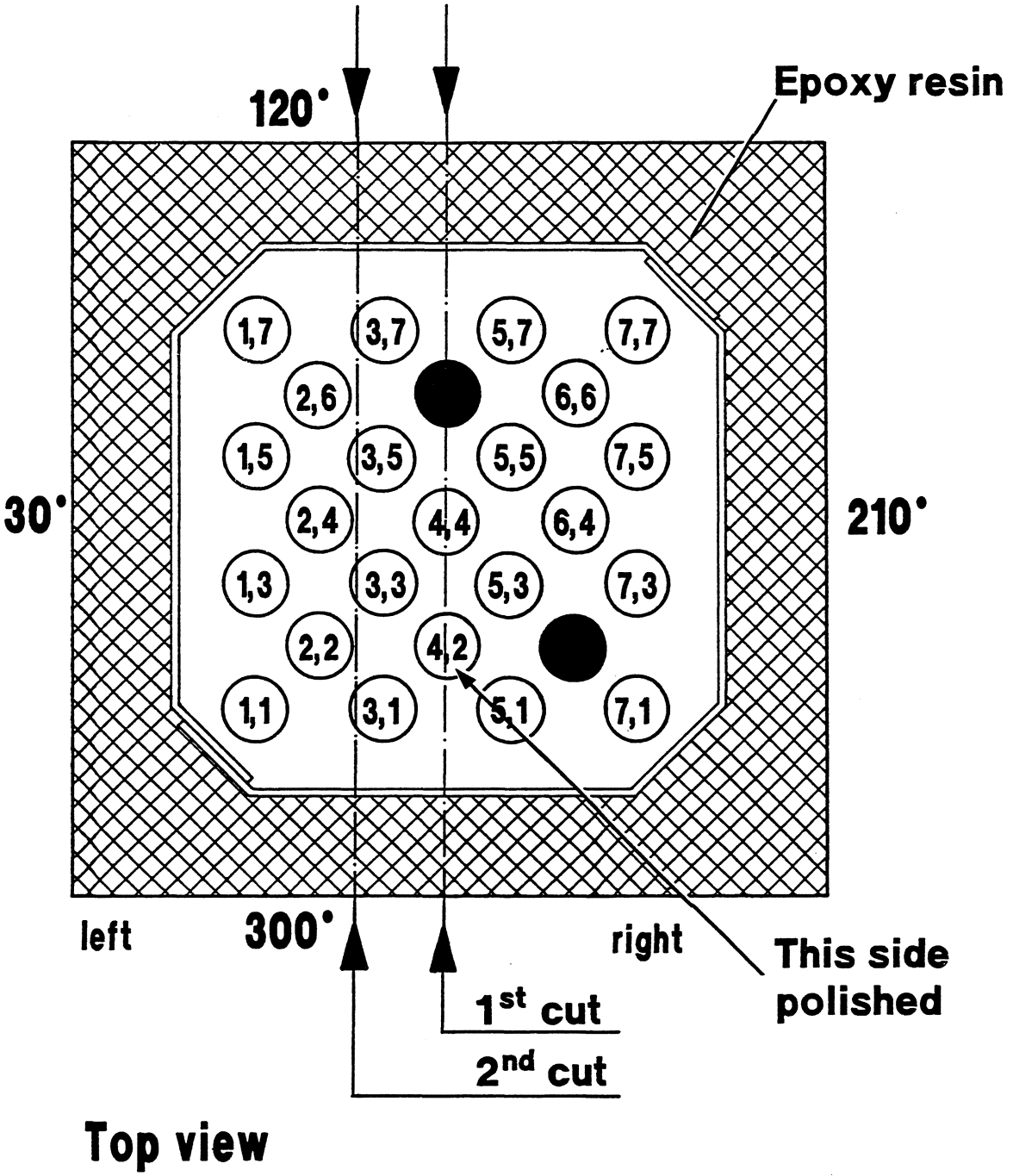

Fig. A6: CORA-15; Locations of vertical cuts through sections 15-d, 15-e, 15-f; top view

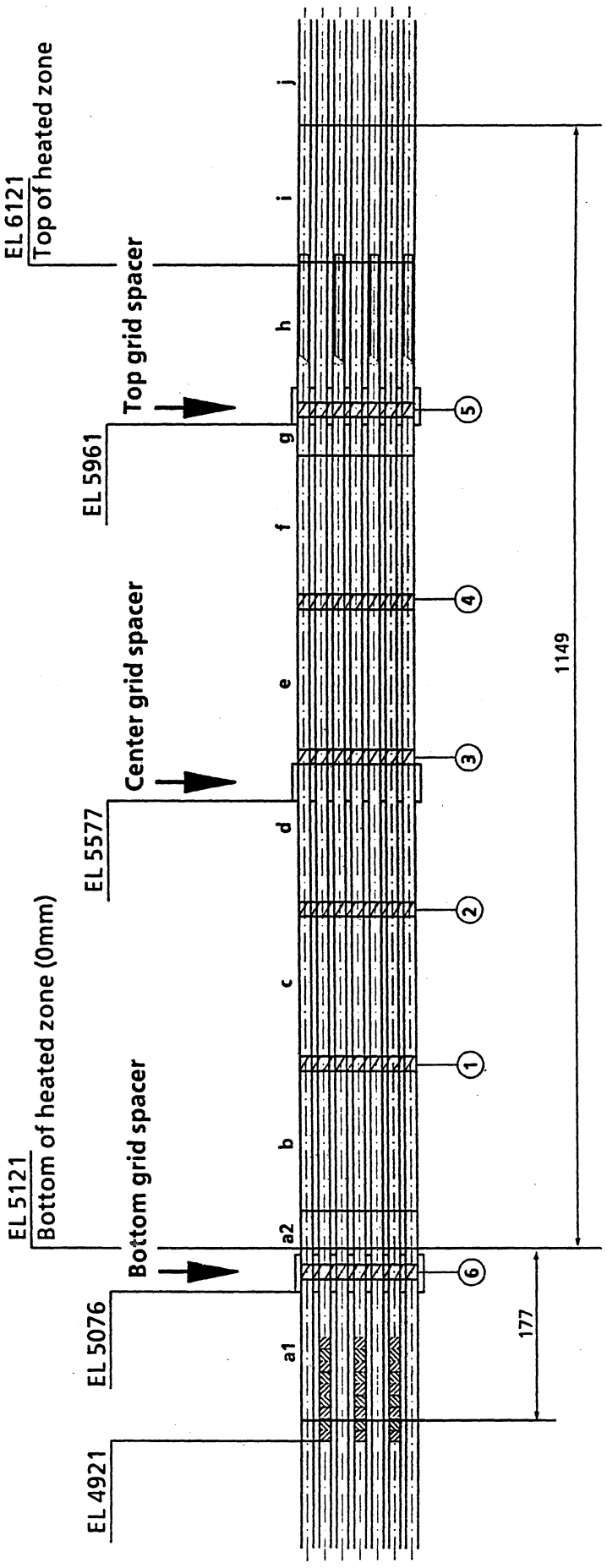

Vertical sections of remnants a1, b,

Height of horizontal sample : 13mm (marking distance = 15mm)

Bundle viewed from 30°, 120°, 210°, and 300°, respectively

Fig.A7: CORA-9; Bundle sectioning

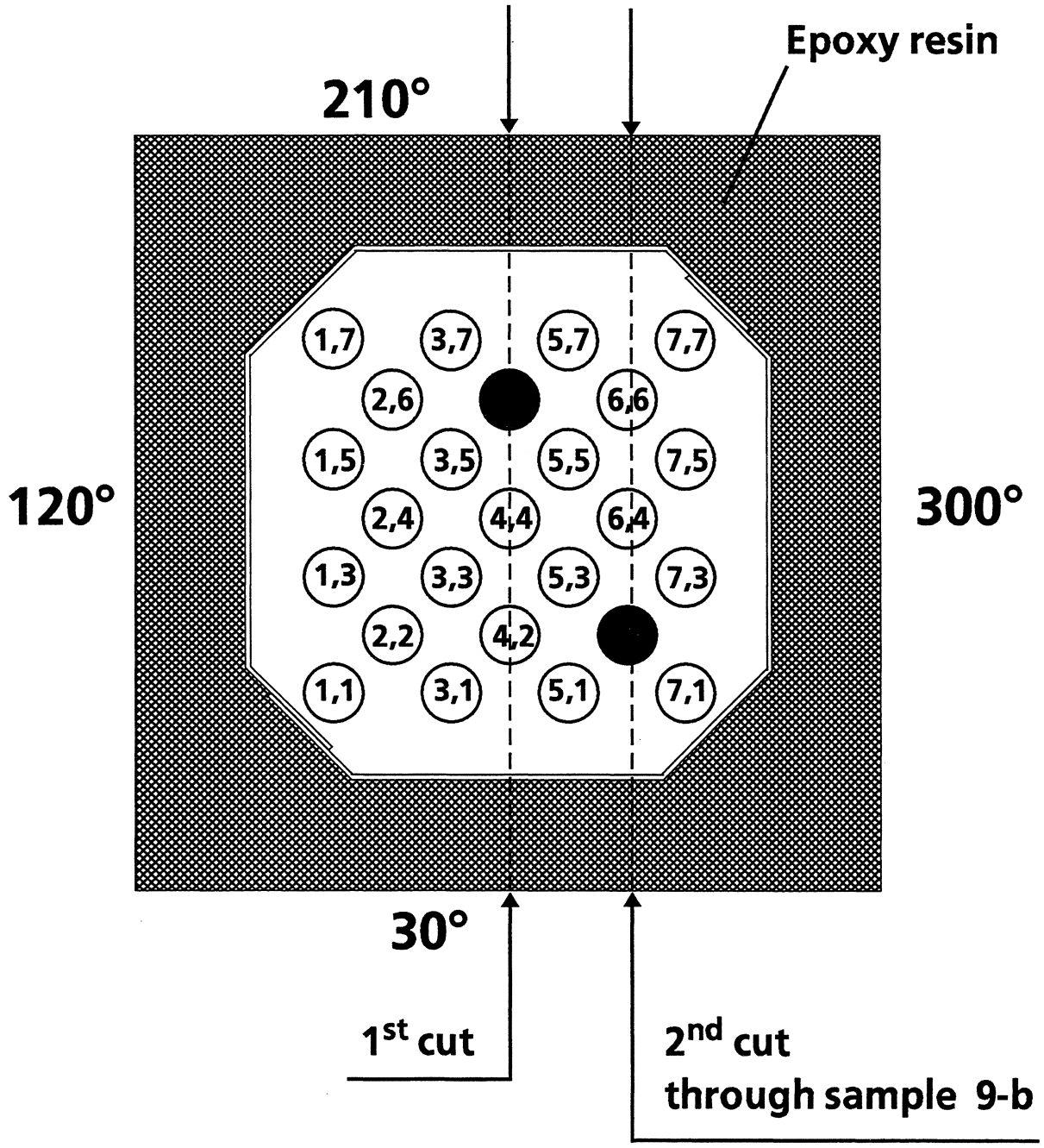

Top view

Fig. A8: CORA-9; Locations of vertical cuts through sections 9-a1, 9-a2, 9-06, and 9-b (1st cut)

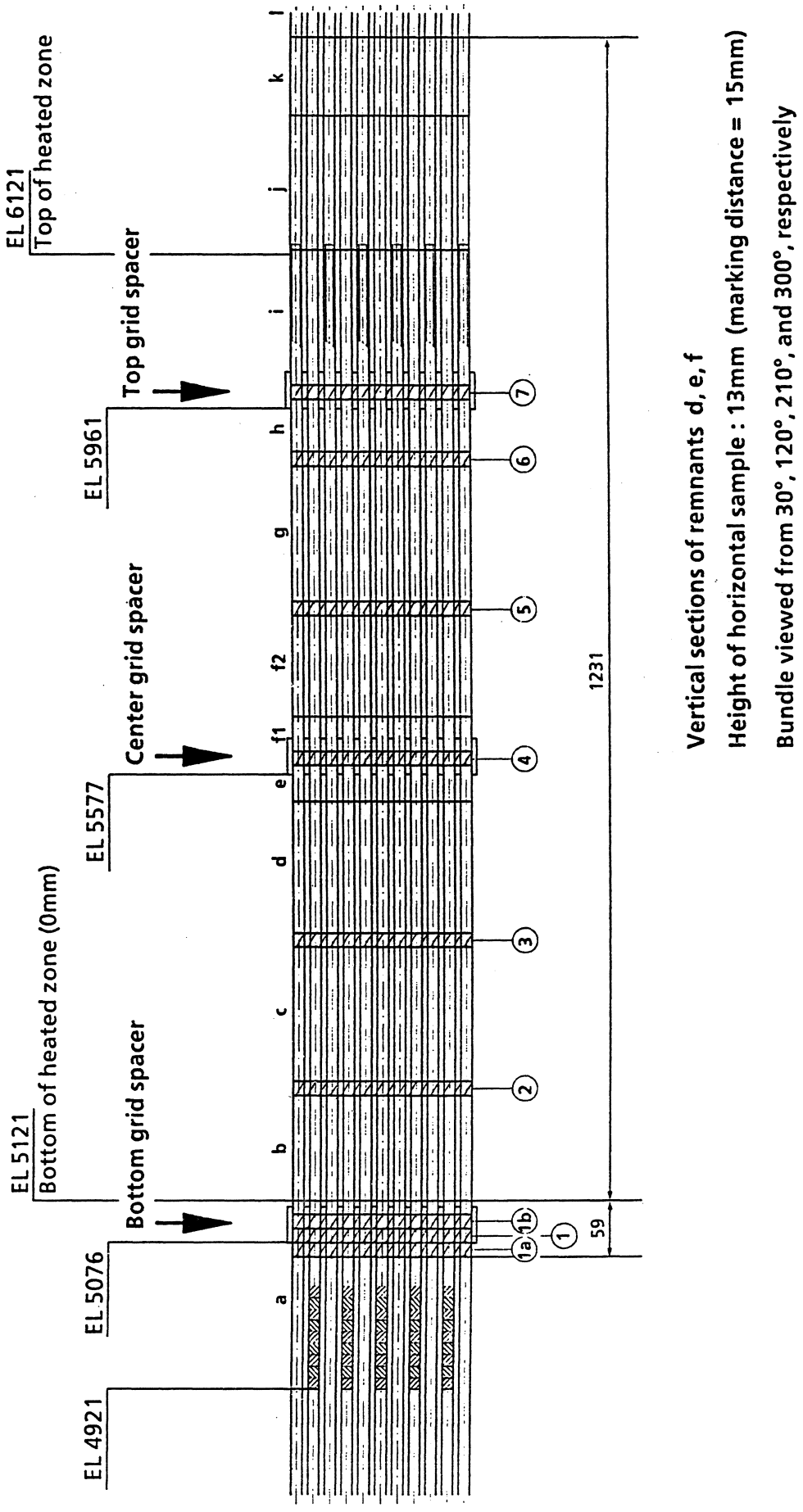

Fig.A9: CORA-7; Bundle sectioning

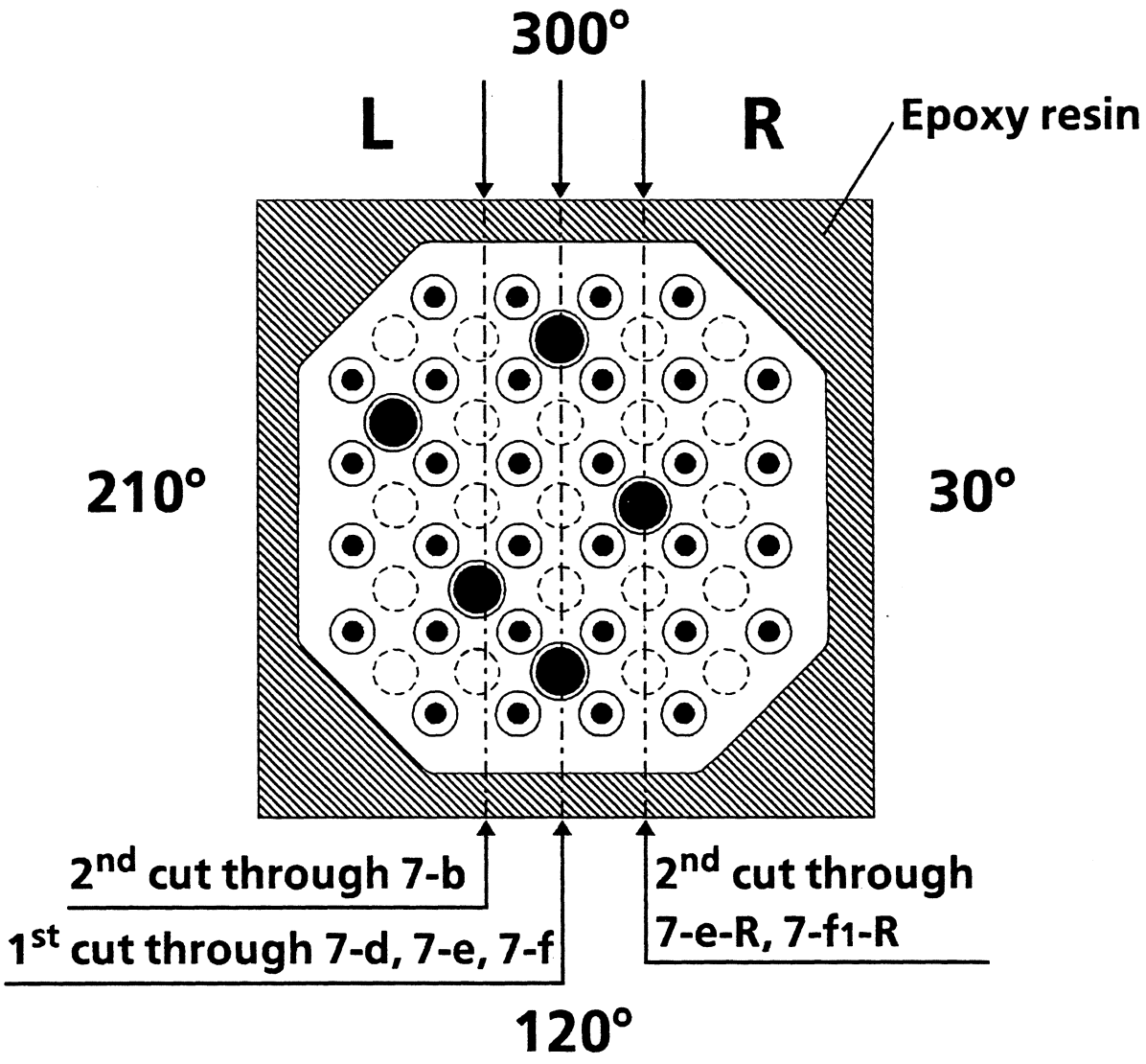

Top view

Fig. A10: CORA-7; Illustration of the vertical cuts through sections of the CORA-7 bundle